AFWL-TR-76-61

AFWL-TR-76-61

LASER-INDUCED DAMAGE AS A FUNCTION OF DIELECTRIC PROPERTIES AT 1.06μm

July 1976

Final Report

Approved for public release; distribution unlimited.

AIR FORCE WEAPONS LABORATORY
Air Force Systems Command
Kirtland Air Force Base, NM 87117

This final report was prepared for the Air Force Weapons Laboratory under Job Order 88091601. Captain Jerry R. Bettis (DRE) was the Laboratory Project Officer-in-Charge.

When US Government drawings, specifications, or other data are used for any purpose other than a definitely related Government procurement operation, the Government thereby incurs no responsibility nor any obligation whatsoever, and the fact that the Government may have formulated, furnished, or in any way supplied the said drawings, specifications, or other data is not to be regarded by implication or otherwise as in any manner licensing the holder or any other person or corporation or conveying any rights or permission to manufacture, use, or sell any patented invention that may in any way be related thereto.

This report has been reviewed by the Information Office (OI) and is releasable to the National Technical Information Service (NTIS). At NTIS, it will be available to the general public, including foreign nations.

This technical report has been reviewed and is approved for publication.

JERRY R. BETTIS
Captain, USAF
Project Officer

FOR THE COMMANDER

DR. ARTHUR H. GUENTHER
Chief Scientist

JOHN S. DEWITT
Lt Colonel, USAF
Chief, Technology Division

DO NOT RETURN THIS COPY. RETAIN OR DESTROY.

UNCLASSIFIED

SECURITY CLASSIFICATION OF THIS PAGE (When Data Entered)

REPORT DOCUMENTATION PAGE	READ INSTRUCTIONS BEFORE COMPLETING FORM
1. REPORT NUMBER (14) AFWL-TR-76-61	2. GOVT ACCESSION NO. / 3. RECIPIENT'S CATALOG NUMBER
4. TITLE (and Subtitle) (6) LASER-INDUCED DAMAGE AS A FUNCTION OF DIELECTRIC PROPERTIES AT 1.06 μm Micrometers.	5. TYPE OF REPORT & PERIOD COVERED (9) Final Report. / 6. PERFORMING ORG. REPORT NUMBER
7. AUTHOR(s) (10) Jerry R. Bettis, Captain, USAF (16) AF-8809	8. CONTRACT OR GRANT NUMBER(s) (17) 880916
9. PERFORMING ORGANIZATION NAME AND ADDRESS Air Force Weapons Laboratory (LRE) Kirtland AFB, NM 87117	10. PROGRAM ELEMENT, PROJECT, TASK AREA & WORK UNIT NUMBERS 62601F; 8809 1601
11. CONTROLLING OFFICE NAME AND ADDRESS Air Force Weapons Laboratory (LRE) Kirtland AFB, NM 87117	12. REPORT DATE (11) Jul [redacted] 76 / 13. NUMBER OF PAGES 98
14. MONITORING AGENCY NAME & ADDRESS (if different from Controlling Office) (12) 100 p.	15. SECURITY CLASS. (of this report) UNCLASSIFIED / 15a. DECLASSIFICATION/DOWNGRADING SCHEDULE

16. DISTRIBUTION STATEMENT (of this Report)

Approved for public release; distribution unlimited.

17. DISTRIBUTION STATEMENT (of the abstract entered in Block 20, if different from Report)

18. SUPPLEMENTARY NOTES

19. KEY WORDS (Continue on reverse side if necessary and identify by block number)

Laser damage; Damage; Laser; Laser-induced; Radiation; Interaction; Fused silica; Fluorides; Windows; Dielectrics

micrometers

TEM sub 00 Nd(+3)

20. ABSTRACT (Continue on reverse side if necessary and identify by block number)

Ten dielectric materials in half-wave optically thick films and eleven uncoated dielectric surfaces were subjected to damaging radiation from a (TEM_{00} Nd^{+3}) in glass laser operating at 1.06 μm. The threshold optical electric field for damage was determined for each thin film and uncoated surface. It was demonstrated that the root mean square surface roughness was important in determining the threshold field for roughness ranging from nearly 1000 Å (rms) to less than 10 Å (rms). The basic relationship between damage threshold and surface

OVER

DD FORM 1 JAN 73 1473 EDITION OF 1 NOV 65 IS OBSOLETE

UNCLASSIFIED

SECURITY CLASSIFICATION OF THIS PAGE (When Data Entered)

013 150 AB

roughness held both for the bare surfaces and for the thin films placed on surfaces with varying roughness. A theoretic-empirical formula was developed which is used to predict threshold fields as a function of material properties, such as refractive index and atomic number density, and surface roughness as well as thin-film material. The relationship holds for a variety of materials in bulk form as well as bare surfaces and thin-film coatings. Agreement between prediction and experiment was generally within 20 percent, the typical experimental accuracy. Previously published results were favorably compared to the predicted values. A new model of laser-induced damage was developed which accounts for material-to-material variation as well as the dependence of the damage threshold on pulse duration and spot size. Threshold fields for silicon dioxide and magnesium fluoride films were shown to vary with the amount of free hydroxyl ion in the coating substrate. The threshold field for film stacks of pairs of coating materials was shown to depend on the design of the film stack and the standing wave generated by reflections. The threshold for magnesium fluoride films was shown to depend on the deposition technique used.

PREFACE

This technical report was originally prepared as a dissertation presented to the faculty of the School of Engineering of the Air Force Institute of Technology, Air University, in partial fulfillment of the requirements for the degree of doctor of philosophy.

This research was made possible through the close cooperation of the Air Force Weapons Laboratory (AFWL) and the Air Force Institute of Technology (AFIT). The author gratefully acknowledges the assistance of the following: Dr. Arthur H. Guenther, Capt. Rickard A. House II, Dr. Donald C. Wunsch, Mr. W. E. Kunzler, Mr. Wayne Wasson, Capt. John Gowan, Mr. Arthur Goodman, Ms. Leonie D. Boehmer, SSgt. Kenneth B. Rowland, Capt. Eric Jumper, and Mrs. Georgiana Hillyer (AFWL); Dr. Jean Bennett and Dr. Hal Bennett (Michelson Laboratory at the Naval Weapons Center); Maj Kenneth Jungling, Dr. Robert Hengehold, and Maj. Carl Case (AFIT); Dr. Norman Boling (Owens-Illinois Corp); Dr. Jane Bruce (Cambridge Research Laboratory); Mr. Russel Austin (Perkin-Elmer Corp); and Dr. John Reichert (Texas Tech University).

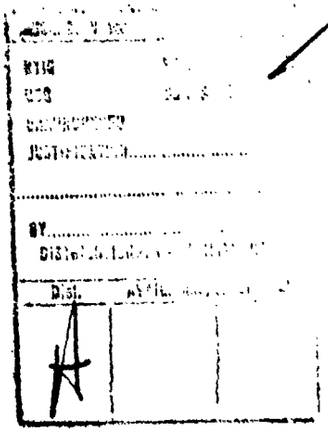

CONTENTS

ILLUSTRATIONS

ILLUSTRATIONS (Continued)

TABLES

SECTION I

INTRODUCTION

Laser-induced damage to transparent optical materials is a process by which optics suffer an observable change upon passage of a laser beam. Laser-induced damage can be divided into four temporal regions: damage involving picosecond pulses, pulses from a few nanoseconds to a few hundred nanoseconds, pulses from a few to about 20 microseconds, and CW laser beams. Over the longer periods, damage is characterized by the cumulative effect of absorption of the laser beam and subsequent distortions or heating of the material to its melting point. In the nanosecond and picosecond time regions the onset of damage is similar to the exponential growth of ionization and resultant plasma formation associated with electrical breakdown. It is in the few tens of nanosecond pulse region with which this report is concerned.

The purpose of this study was to examine the material properties and fabrication techniques which directly bear on the resistance of optical materials to laser-induced damage. In particular the properties and manufacturing techniques of thin films applied to optical substrates were examined. A prime purpose of this study was to correlate the observed behavior with material properties such as refractive index, condition of the surface, and material structure.

In any high-power laser system employing pointing and tracking or beam collimation, lenses, windows, and isolators must intercept the beam before the output can be utilized. With a nominal 4 percent reflection at each surface only 17 surfaces are required to reduce the available power by 50 percent. Since optical systems can easily contain this many surfaces it becomes necessary to place on the bare components antireflective thin-film coatings. The survivability of thin-film coatings to laser beams then is of the utmost importance in the reliability and efficiency of high-power laser systems. By increasing the threshold to laser-induced damage of an optical surface one can reduce the size of that optical component by increasing the power density which it can withstand. Such size reduction and resulting weight reduction are very important to any laser devices which are designed for airborne use.

Because it is presently uncertain what the final design requirements of a laser weapon system will be in terms of output wavelength, the resulting materials problem may not yet be solved. Those materials which are appropriate at one wavelength may be entirely unsuitable at half or twice that wavelength. Because of this uncertainty it is imperative that a fundamental understanding be gained of those material properties and surface finishing techniques as well as thin-film characteristics which affect the surface threshold to laser-induced damage. Due to surface imperfections and contamination it is the surface of materials which generally fail first. Surface thresholds are generally only 0.3 to 0.5 of the bulk damage threshold. Thus not only material properties but the mechanics of surface finishing determine the damage threshold of optical elements and limit the power density which can be accepted by the element without degradation. Thus, it is frequently necessary to expand the beam and optics to lower the incident power density while maintaining the total transmitted power. This causes a multitude of problems. Figuring a 20-inch window to $\lambda/10$ tolerances is more expensive and more difficult to do than a 10-inch window. Cooling problems climb rapidly with diameter and the resulting weight penalties and increased volume requirements may outstrip the ability of a transport vehicle to accommodate it. Thus, it is seen that the phenomenon of laser-induced damage to optical components places constraints in the design of high-power laser systems. By increasing the resistance to laser-induced damage of the materials used in a high-power laser system one can reduce the system in weight and volume, thereby reducing aerodynamic influences. Concomitant gains in operation can be realized since slew rates can be made greater for smaller systems and thus pointing and tracking can be improved. In finding ways to improve the damage resistance of optical materials one must first isolate as much as possible those factors which affect the damage threshold. With the exception of laser-induced damage in the bulk of materials caused by nonlinear self focusing it is the surface of materials which fails first. An important question to be considered in this study is which factors affect the threshold power density for laser-induced surface damage. Since thin-film coatings are used not only as antireflective devices but also to afford a measure of environmental protection for certain materials, it is appropriate to ask why films fail at lower incident laser power densities than do bare surfaces of the same material. In seeking an answer to this question, one is led to study those factors, both intrinsic and extrinsic to the thin-film, which affect damage thresholds. These considerations place a need on identification of the

basic mechanisms involved in laser-induced damage so that functional relationships between material properties and surface treatment and damage threshold levels will allow selection and development of materials which will meet these engineering requirements.

A comprehensive compendium of papers dealing with laser-induced damage would probably serve no useful purpose. The subject is so important that an annual symposium discussing only laser-induced damage and attended by 150 or more scientists to hear over 40 select papers is now in its seventh year. During the initial stages of a new science or the investigation of a new process it is difficult for the experimentalist to identify the important parameters which must be reported to completely specify the experiment. A great number of the early papers on laser-induced damage failed to report such factors as pulse widths, focusing conditions, beam quality, characterization of meaningful material properties and experimental technique. It appears now that each of these is important if one were to attempt to reproduce a given laser damage experiment or attempt a correlation of published data. Omitting these reports, which in light of subsequent developments failed to adequately specify the experiment, and eliminating those which deal with CW systems, picosecond systems (except as relative indicators), and 10.6 μm systems leaves primarily those studies conducted and reported since the inception of the Symposium on Laser-Induced Damage to Optical Components (refs. 1 through 7).

Most publications on laser-induced damage list threshold values in terms of energy density; a few list damage thresholds in terms of incident power density; however, an elegant and simple description by Crisp et al. (ref. 8) has shown that the correct quantity in specifying the damage threshold in the short pulse region is the electric field associated with the laser pulse. This proposal stems from the well-known observation that optical flats exhibited lower damage threshold in terms of energy and power density at the exit face than at the entrance face (ref. 9). Many complex explanations were put forth, but it was Crisp who assumed that the damage threshold depended on the optical electric field and that, upon applying the appropriate Fresnel equations, the effective electric field at the exit face of an optical flat was greater than that at the entrance for a given incident power density in just the right proportion to account for the apparently lower energy threshold. In fact, the threshold electric field at the entrance and exit were the same (ref. 10). As proof, an optical flat was placed in a damaging laser beam at Brewster's angle so that

reflection losses were eliminated; it was observed that the entrance and exit faces failed at the same level of laser density.

In the work of DeShazer et al., and Newman and DeShazer (refs. 11, and 12) further support is found for tying the electric field to laser-induced damage thresholds. Films of TiO_2 in $\lambda/4$, $\lambda/2$, and $3\lambda/4$ thickness were deposited on glass substrates and subjected to damaging laser pulses. The threshold fields were 5.13×10^7, 3.78×10^7 and 3.69×10^7 V/m, respectively. These values are sensibly constant within the quoted experimental uncertainty of ±15 percent. These values are apparently related more closely to an intrinsic property of TiO_2 than are the widely variant incident threshold power densities of 3.45, 0.6, and 1.8 GW/cm^2. This divergence in threshold power densities was enhanced by the wide variation in index between the film (n = 2.28) and glass substrate (n = 1.51). The relationship between refractive index, laser power density, and optical electric field is contained in the formulation of the Poynting Theorem taking Fresnel reflections into account. The Poynting vector, $\vec{S}$(watts/m^2), is related to the electromagnetic components, $\vec{E}$ and $\vec{H}$, of the light wave by

$$\vec{S} = \vec{E} \times \vec{H} \tag{1}$$

The constituent relations yield the ratio between electric and magnetic field amplitudes as

$$\sqrt{\epsilon}\, E = \sqrt{\mu}\, H \tag{2}$$

where ϵ and μ are the dielectric permittivity and permeability, respectively. For a linearly polarized plane wave in a linear, nonmagnetic material the magnitude of the Poynting vector is related to the magnitude of the optical electric field by

$$S = \sqrt{\frac{\epsilon}{\mu_0}}\, E^2 \tag{3}$$

The identities $n^2 = \epsilon/\epsilon_0$ and $c^2 = 1/\epsilon_0\mu_0$, where n and c are the refractive index of the medium and the speed of light in free space, respectively, allows one to rewrite equation (3) as

$$E = \sqrt{\frac{S}{n_o \varepsilon_o c}} \tag{4}$$

Here the refractive index of air, $n_o \approx 1$, has been used to indicate the magnitude of the electric field incident at the air-dielectric interface. The Fresnel relations are now used to calculate the optical electric field at the surface of a bare substrate and at the surface of thin films of $\lambda/4$, $\lambda/2$, and $3\lambda/4$ thicknesses. The optical electric field at the surface of an uncoated material with index n_g is

$$E(V/m) = \frac{19.4}{n_g + 1}\sqrt{S(watts/m^2)} \tag{5}$$

For films of $\lambda/4$ and $3\lambda/4$ optical thickness with index n_f applied to a substrate of index n_g, the optical electric field at the film surfaces are

$$E(V/m) = \frac{2n_g}{n_g + n_f^2}\, 19.4\, \sqrt{S(watts/m^2)} \tag{6}$$

For a film of $\lambda/2$ optical thickness the field is

$$E(V/m) = \frac{2}{1 + n_g}\, 19.4\, \sqrt{S(watts/m^2)} \tag{7}$$

As n_f approaches n_g the expressions given in equations (6) and (7) coalesce and if the field is indeed the threshold quantity one would expect the variation in threshold power density with film thickness to vanish. Correspondingly, we note that for the case of SiO_2 ($n = 1.45$) applied to BSC-2 ($n = 1.51$) the values for threshold field versus incident power density for $\lambda/4$ and $\lambda/2$ films were 1.65, 1.56×10^8 V/m; and 10.5, 9.9 GW/cm^2, respectively.

Two trends apparent from a review of past work are that, in general breakdown, threshold varies inversely with refractive index. From Turners' work (ref. 13), in which he tested 13 quarter wave films at 0.69 μm, it was seen that damage thresholds were lower for high index materials as compared to low index materials. This fact was noted by Austin et al. (ref. 14) when they chose candidate materials to test in vapor-phase mixture films. Their work also displayed the inverse dependence of damage threshold on refractive index.

The thin-film studies of DeShazer et al., and Newman and DeShazer (refs. 11 and 12) displayed a similar trend as did the surface studies on uncoated optics conducted by Boling et al. (ref. 15). Because surface damage studies and thin-film studies involve many more variables than do bulk damage studies the results of Fradin and coworkers (refs. 16 and 17) were taken as more significant of the refractive index trend than were the studies mentioned above. In their experiment they damaged 11 alkali halide crystals by using pulsed lasers with 10.6-μm, 1.06-μm, and 0.69-μm wavelengths and compared the threshold electric field with reported dc dielectric breakdown thresholds. Not only was a definite trend between the damage threshold and refractive index established, but from the close correlation between the dc breakdown fields and the damaging optical fields (being about 1.5 times the dc fields), a confirmation of the importance of the optical electric field in the damage process was evident.

Although not quantified, it was known at least from 1970 (ref. 9) that surface roughness, impurities, and imperfections reduced the threshold of surfaces below that of the bulk. Although the attendent problems of self-focusing and inaccurately known focal volumes in the bulk of materials make the comparison between bulk and surface threshold tenuous, it was generally reported that surface thresholds were only 0.3 to 0.5 times that of the bulk thresholds. This problem was attacked in a paper by Bloembergen (ref. 18) in which he used static field theory to calculate the field enhancement expected in certain dielectric cavities which model surface imperfections. Electric field enhancement by factors of up to the square of the refractive index were attained in cavities of not unreasonable size and shape. This infers a maximum field enhancement of ~2.25 for SiO_2, for example. One main conclusion of his work was that surface features with characteristic dimensions less than about 100 Å (10 nm) would be unimportant in laser-induced damage. Bloembergen argued that diffusion of electrons out of a volume with a 100 Å characteristic dimension would be so rapid that pulses of a few nanoseconds would have to be increased in power density to that of intrinsic threshold levels to compensate for the migration. There have been studies to confirm Bloembergen's basic hypothesis that a surface with a finish which has no irregularities larger than 100 Å will have the same threshold as the bulk. There has also been conjecture that the 100 Å criterion was too stringent. Fradin and Bass (ref. 19) super polished fused silica, sapphire, and BSC-2 glass in an attempt to raise the surface threshold to that of the bulk. With conventional polish the ratio of surface to bulk thresholds ranged from 0.5 for sapphire to 0.77 for BSC-2 and fused silica. After

polishing by a technique which recirculates the polishing slurry (bowl feed polishing), they were able to raise the surface threshold to that of the bulk for BSC-2 and fused silica. The sapphire, notoriously difficult to polish, was not improved by this technique. No other study has claimed to have observed surface threshold equal to that of the bulk.

With this background it was decided to investigate the dependence of the threshold optical electric field for laser-induced damage on such material properties as refractive index, number density, and structure. Realizing the importance of surface finish, very careful finishing procedures and surface measurements were required of the vendor. For the thin-film portion of the study optically half wavelength thick films (at 1.06 μm) were applied to carefully finished flats primarily of fused silica. The substrates were polished as smooth as possible in large batches to minimize variation. Film deposition was carefully controlled as were a number of extrinsic variables such as background pressure in the coating chamber to obtain films as free from structural inhomogeneities as possible.

This report is divided into five sections. Following the introduction are Experiment, Theory, Results, and Conclusions. The general plan of attack was to: (1) obtain a maximally characterized laser beam which exhibited minimal spatial, temporal, and transverse mode variation, (2) use the laser to damage a set of carefully manufactured coated and uncoated optical flats to obtain threshold damage fields versus refractive index, surface structure, film structure to include inhomogeneities, film deposition techniques, and atomic number density, (3) develop theoretical expressions sufficient to explain the observed behavior.

SECTION II

EXPERIMENT

In the experimental phase of this study various optical samples with and without film coatings were subjected to 1.06-μm laser radiation from a Nd^{+3} in glass laser controlled to operate in the TEM_{00} transverse mode. The laser used was a Compagnie General Electric Model VD640 which has normal operating characteristics of 35 nsec pulse width and up to 500 joules output. A greatly reduced version of this system was used to produce the high beam quality required with attendant characteristics of a 30 to 40 nsec pulse width and ~1 joule output. Of the seven stages in the total system only the oscillator and first amplifier were retained. Each consisted of 16-mm diameter rods; the oscillator being 300 mm long and the amplifier 500 mm long. The oscillator, Q-switched by a Pockel's cell, was constrained to the TEM_{00} transverse mode using an intracavity aperture of 1.9-mm diameter placed between the oscillator rod and output mirror. For the plano-plano cavity employed in the oscillator, it is difficult to obtain a reliable calculation for the size aperture necessary to constrain the laser to the TEM_{00} mode. Because of this, a number of apertures ranging from about 1 mm in diameter to about 3 mm in diameter was fabricated, and the proper one was selected on the basis of resulting far-field intensity distributions. This method, although time consuming, indicated a proper selection of 1.9 ± 0.05 mm. The 1.8-mm aperture was no improvement in the expected far-field intensity distribution but provided significantly less than the nominal 80 mj output available from the 1.9-mm aperture.

The oscillator output was amplified by the single stage amplifier to a total output of 380-410 mj. With the 503.5-mm focal length lens used in this experiment the laser radiation was focused to a 147-μm spot size to the e^{-2} power points. The resulting optical electric field was 6.7 MV/cm in air, which is sufficient to damage the surface and bulk of most conventional dielectrics in a 30 to 40 nsec pulse.

The remainder of the equipment was used for diagnostics and parameterization.

Figure 1 is a schematic diagram of the optical test conditions. The laser beam was directed down an optical bench with the aid of two 45°-100 percent

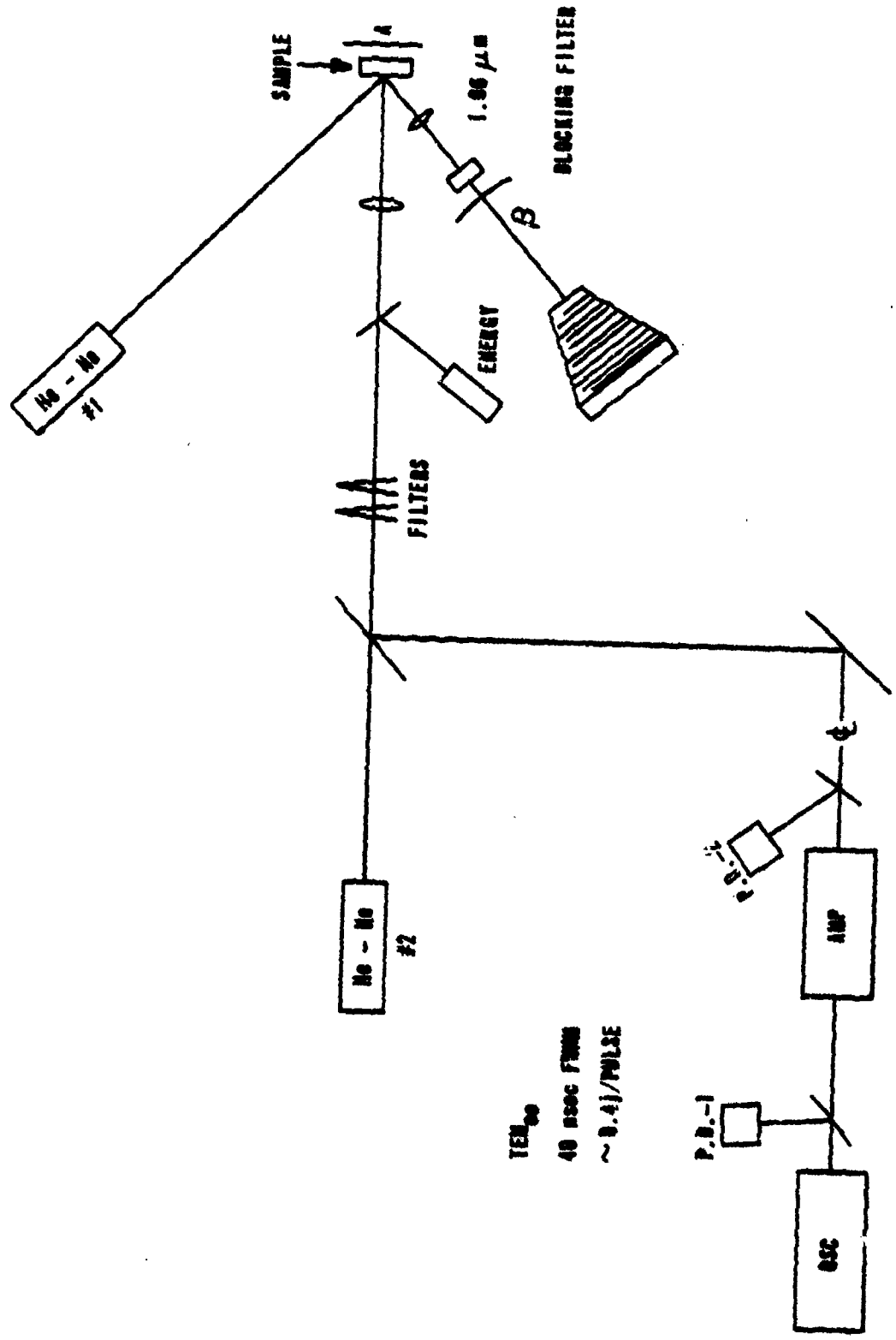

Figure 1. Experimental Arrangement

reflectors. These reflectors were gimbal mounted to facilitate alignment of the system. The samples were held in a translating-rotatable mount approximately 12 meters from the beam waist of the oscillator.

The laser was mounted on 12 cm x 15 cm granite rails to maintain mechanical stability. Due to this arrangement the alignment, checked twice each working day, was remarkably stable. To eliminate fluctuations in ambient conditions, the room in which the test facility was located had its own environmental control system. A separate heating/air conditioning system maintained the temperature to ±2.0 degrees while a humidity control system kept the relative humidity at 45 percent. An air filtration system removed airborne particulate matter. The laser was fitted with a dry nitrogen purge system which aided in keeping the rod faces dust free.

The focusing and beam attenuation systems were mounted on a 2-meter lathe bed optical bench. This bench was rigidly attached to a 4-inch thick honeycomb-backed steel plate for stability.

The focusing lens was a carefully selected biconvex fused silica lens of the highest quality. A startling revelation in the course of this study was that very expensive, supposedly high-quality lenses exhibited large variations from sphericity. The lens chosen, 503.5 mm focal length, was tested along with a couple of dozen other candidates with a Foucault knife-edge device. The chosen lens alone showed excellent sphericity.

The laser was operated at constant input energy to maintain the temporal and spatial quality of the output beam. The energy delivered on target was controlled by attenuating the main beam with 5 mm x 5 mm nonsaturable Schott optical filters. These filters were placed in the beam at a 6° angle to the normal to prevent regenerative feedback. This necessitated using the filters in sets of two or four to minimize steering of the laser beam. The maximum transmission needed in this study was 35 percent and the minimum was 4.5×10^{-2} percent. The set of 64 filters provided variation between these ranges in steps separated in total transmission by 10 percent.

The 3.8-cm diameter samples were held in a mount with 6 degrees of freedom. The samples were canted 5 degrees from the axis of the laser beam to prevent feedback into the laser. Even with this precaution when high-transmission pulses caused dense, bright plasmas, the reflection from these plasmas was enough to

generate post-lasing in the conventional mode, and a great deal of care was taken to identify and prevent this situation from arising.

In a past damage symposium (ref. 20), it was noted that the plasma associated with laser damage disrupted the surface of an optical sample to several diameters of the damaging beam. And indeed, one needs only to condense water vapor on the surface of a damaged sample to clearly and incontrovertibly identify each damage site and the surrounding area which was disrupted by the plasma (more on this to follow). To confine this disrupting influence to the vicinity of each separate damage site, a face-plate aperture mask was fabricated and installed on each sample prior to testing. The mask was drilled with fifty-four 2.0-mm diameter holes to allow passage of the damaging 147-μm diameter laser beam. The center 1.25 cm was drilled to accommodate a metallic coating used in the characterization of each surface. Each 2.0-mm aperture was surrounded by an annulus of circuit board layout tape which, when pressed onto the face of the sample, prevented leakage of the plasma and leakage of ultraviolet radiation to surrounding damage sites. Examination of damaged samples confirmed the confinement.

A spot size of approximately 150 μm in diameter was chosen to obviate erroneous results due to the spot size dependence of laser induced damage observed by DeShazer et al., (ref. 11). In their study of laser-induced damage to thin films, they noted that increasing the spot size decreased the damage threshold until a spot size greater than about 150 μm was reached. Above ~150 μm diameter there was no spot size dependence. The result was explained on the basis of an increased probability for hitting a defect when using a larger spot size. Diagnostics equipment was mounted rigidly either to the optical bench, steel plate, or granite rails. The diagnostic tools were of two categories: active and parametric.

1. ACTIVE DIAGNOSTICS

The energy and temporal shape of the laser pulse was constantly monitored by two biplanar photodiodes with S-1 photocathodes and by a calibrated pyroelectric energy meter. The temporal characteristics of the oscillator pulse were monitored by photodiode PD-1 shown in figure 1. The output of this photodiode was displayed on a Tektronix Model 519 oscilloscope and, through the first 3000 shots, was recorded for each event by a Polaroid scope camera. Due to the minute variation in this pulse shape, during the last 2800 shots only every fifth shot was so recorded. Figure 2 is a trace typical of the oscillator

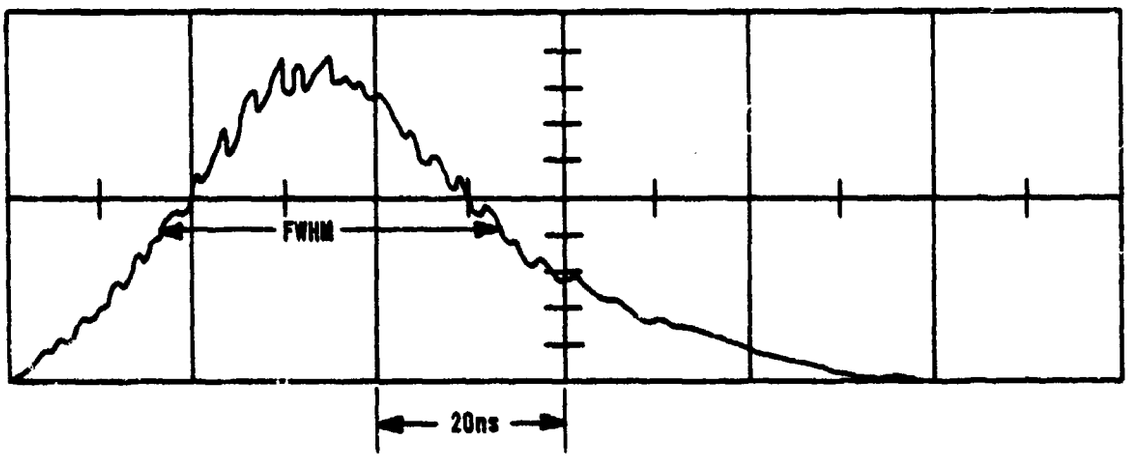

Figure 2. Typical Oscillator Pulse

pulse. The amplifier output was monitored by a second photodiode also shown in figure 1. In addition to the temporal response, this photodiode contained an integrating circuit which detected pre- and post-lasing and gave a measure of the total output energy. Because conventional lasing of microsecond duration prior to the giant pulse (pre-lase) or following the giant pulse (post-lase) is not detectable on the fast-sweep oscilloscope used to record the giant pulse, it is necessary to monitor these conditions separately. To monitor both the giant pulse (tens of nanoseconds) and the conventional lasing (microseconds), it is necessary to incorporate an integrating network with an R-C time constant of about 200 μsec. On a typical sweep rate of 200 μsec/cm, a giant pulse appears as a step (see figure 3) while the conventional mode lasing (μsec pulses for about 0.5 millisecond) builds steadily with time. Any regenerative feedback caused by reflections from optical elements downstream from the final amplifier can be amplified in the active medium. Such feedback, when coupled into the oscillator, can damage the optical elements in the oscillator. The feedback can only be amplified when the gain is sufficient and the Pockel's cell is open. It appears as post-lasing on the integrated photodiode. Constant monitoring of the output of the integrating photodiode gave notice of this condition at which time downstream optical elements were slightly misaligned to prevent subsequent feedback. Because the step function is an integrated record of the light intensity in the giant pulse, it also served as a crude energy monitor.

The energy incident on target was monitored by a pyroelectric detector placed after the beam attenuating filters and before the focusing lens. It

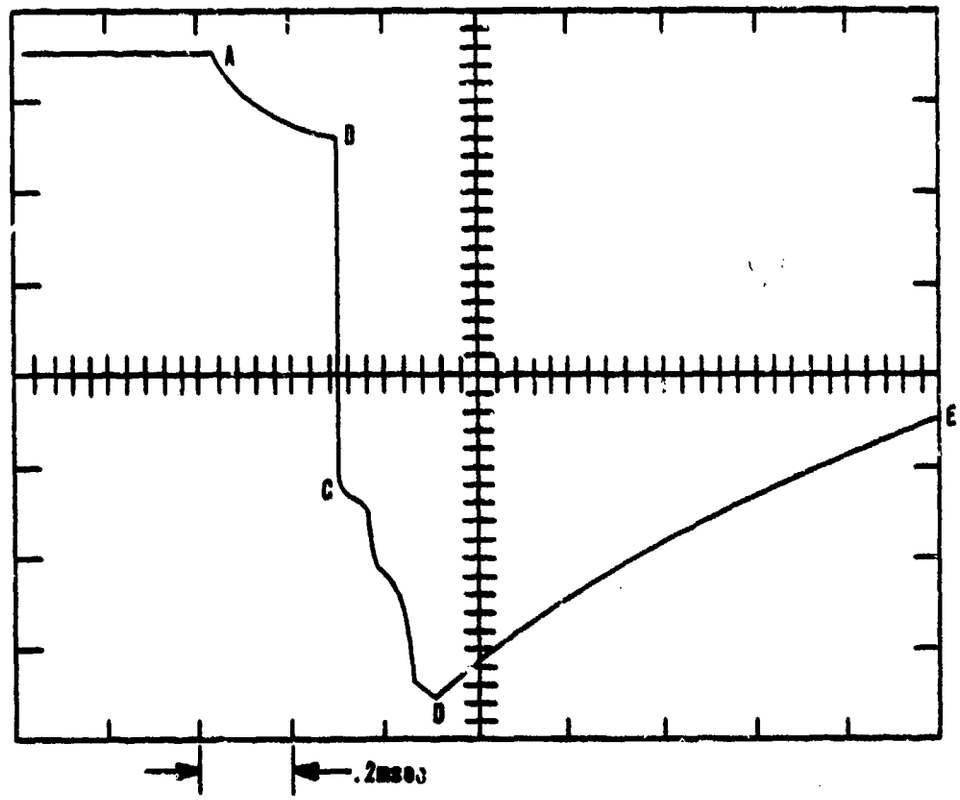

Figure 3. Integrated Photodiode Trace Exhibiting Pre- and Post-Lasing

has a dynamic range from 1 joule full scale to 20 microjoules full scale. Readings as low as 5 percent of full scale were reliable to ±4 percent of full scale. Through beam splitting, attenuation at the detector head, and reflection losses, the device recorded 0.51 percent of the energy on target. On the two samples which exhibited the lowest threshold for damage, it was necessary to change this ratio to record these lower energy pulses. The detector, a Laser Precision model Rk 3230, was compared to a separate Rk 3230 and they were found to track to a precision of ±4 percent. The detector was calibrated against two separate carbon cone thermal calorimeters (TRG Model 117) which have an accuracy of ±10 percent compared to a silver sphere calorimeter. The rest of the active diagnostics were used to define the occurrence of damage.

For the purpose of this study we have defined damage as any irreversible change indicated by one of four detection techniques: (1) visible plasma formation, (2) laser-induced scattering, (3) phase-contrast microscopy, and (4) breath-fogging.

Referring to figure 1, two observers were positioned behind 1.06-μm blocking filters at positions A and B. They actively observed each event for the appearance of the bright plasma which usually accompanies the occurrence of laser-induced damage. In about 98 percent of the events this observation was sufficient to positively identify damage. For the two low index materials, ZnS and ZnSe, there were several events that (even in a darkened room) failed to produce a visible plasma during a damaging event. In these cases a general brightening was usually observed on the surface by one or both observers. Because of the qualitative nature of this visual observation of damage, it was reinforced by the three other techniques, although in the great majority of tests the detection of a plasma proved effective as a damage indicator.

The appearance of observable scatter from a He-Ne laser incident on the damage site was used as a secondary indicator. The forward scatter of He-Ne No. 1 at position B was used as well as the scatter of He-Ne No. 2 observed at position A. Since the latter was focused on the front surface of the sample, any change in the pattern viewed on a screen placed behind position A afforded a method for distinguishing between front surface damage, back surface damage, and low-lying (i.e., near the front surface) bulk damage sites. The diffraction pattern from front surface damage was quite distinctive. Although this technique proved useful in many cases, the final determination of surface damage was made by the most sensitive method described later, i.e., breath-fogging.

A third detection scheme involved an adaptation of Zernike phase contrast microscopy (ref. 21). Briefly stated, when a coherent beam of light is reflected from a scattering surface the specular background component is brought to focus by a lens. This light is insensitive to the gross nature of the surface. That light which is scattered out of the background contains components of higher spatial frequency and is not generally brought to a sharp focus by the lens. By suitably altering the phase of the central order, it is possible to transform the phase change introduced by a scattering site into an intensity variation of the scattered beam. The damage sites produced by near-threshold laser pulses are not discernible in ordinary room light. They absorbed little or no light and as such are largely transparent. When light passes through or

is reflected from one of these small damage sites, the predominant effect is the introduction of a spatially varying phase shift which, since ordinary optics responds to changes in light intensity, is not directly observable. Zernike proposed a phase contrast technique which not only increases the contrast and hence the visibility of such phase objects, but under certain circumstances the observed intensity varies linearly with the phase. To understand this process, assume that a damage site introduces a phase shift $\phi(x,y)$ into coherent light transmitted through it. In the physical layout of this technique the coherent light was reflected from the site, but this merely introduces a reflection coefficient into what follows and was dropped for simplicity. Following Goodman (ref. 21) the light transmitted through the site then has an electric field amplitude based on unit input of

$$u(x,y) = \exp[j\phi(x,y)] \tag{8}$$

For small variations in phase this becomes

$$u(x,y) \approx 1 + j\phi(x,y) \tag{9}$$

neglecting terms of order ϕ^2 and higher. The first term in equation (9) is just the field that one would observe if the damage site were not present, while the second term generates weaker diffracted light that is scattered out from the axis of the system.

The intensity $I(x,y)$ then is

$$I(x,y) = | u(x,y) |^2 \approx | 1 + j\phi(x,y) |^2 \approx 1 \tag{10}$$

or just the input intensity. Since the background, corresponding to the unperturbed input wave, is brought to a sharp focus while the diffracted light introduced by the phase change of the damage site and containing higher spatial frequencies is spread away from the focal point, it is possible to adjust the phase of the central order so that it interferes with the diffracted light.

By introducing a phase shift of $\pi/2$ radians into the focused background, one obtains

$$I(x,y) = | \exp(j\pi/2) + j\phi |^2 = | j(1+\phi) |^2 \approx 1 + 2\phi \tag{11}$$

Thus the intensity has become linearly related to the phase shift ϕ. The required phase shift was introduced by depositing a $\lambda/4$ optically thick transparent dielectric dot on a glass substrate so that the dot just intercepted the focused background radiation. It was hoped that this technique could be used to provide a quantitative measure of the radial extent and depths of the disruptions at each site to be able to compare the amount of material removed with the incident energy density. To this end, a comparison was made between the information inferred from the phase contrast method and physical measurements of selected craters using a Talystep weighted stylus surface profiler. A positive correlation was obtained, which did not lend itself readily to quantitative analysis. Figure 4 is one scan done by the Talystep on a laser-produced crater in SF-12 glass. The different materials exhibited crater profiles more or less characteristic of the material. Note the difference in figure 5, which is a Talystep done on a crater in fused silica. Here the sides do not drop abruptly from the average surface but gently slope for several radii of the central crater. Finally figure 6 depicts the ring structure typical of damage in ED-2 and BK-7 glasses. These craters were produced by laser pulses with power densities generally well above threshold but were impossible to locate without the final damage detection scheme.

The final technique, which proved the most sensitive, was used only after the sample was removed from the holder. It has been noted (ref. 20) that condensing water vapor on the damaged surface of an optical sample clearly indicated the extent of the damage site. It has also been noted (ref. 20) and mentioned above that the plasma associated with laser-induced damage alters the surface surrounding the damage site. During the course of this study these two observations were tied together. Upon receipt of samples which had been ion polished, a cleaning procedure was instigated which included as one step rinsing in water. On the ion-polished samples the water would not wet the surface but beaded up and was removed readily by agitation. The phenomenon, whatever it is, must account for the efficacy of the breath-fogging technique. Plasmas associated with damaging laser irradiation, in effect, cause ion bombardment of the surface in the vicinity of the interaction zone. When one blows his breath across the sample, the first places that the condensed water vapor escapes from are the plasma-polished damage sites. When viewed in oblique white light, the damage sites clearly show up. Whenever there was a doubt about whether a site had sustained damage, the fogging technique was employed. Care must be taken when employing this technique to ensure that no

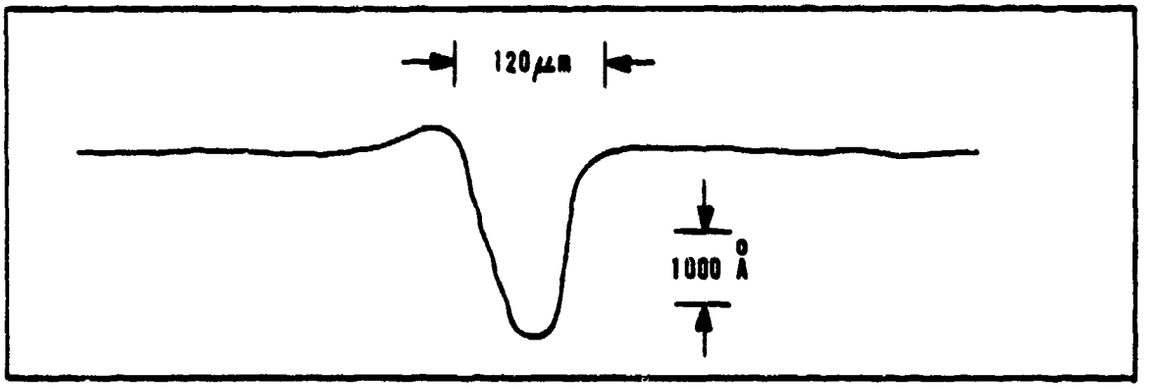

Figure 4. Talystep of Laser-Produced Crater in SF-12 Glass

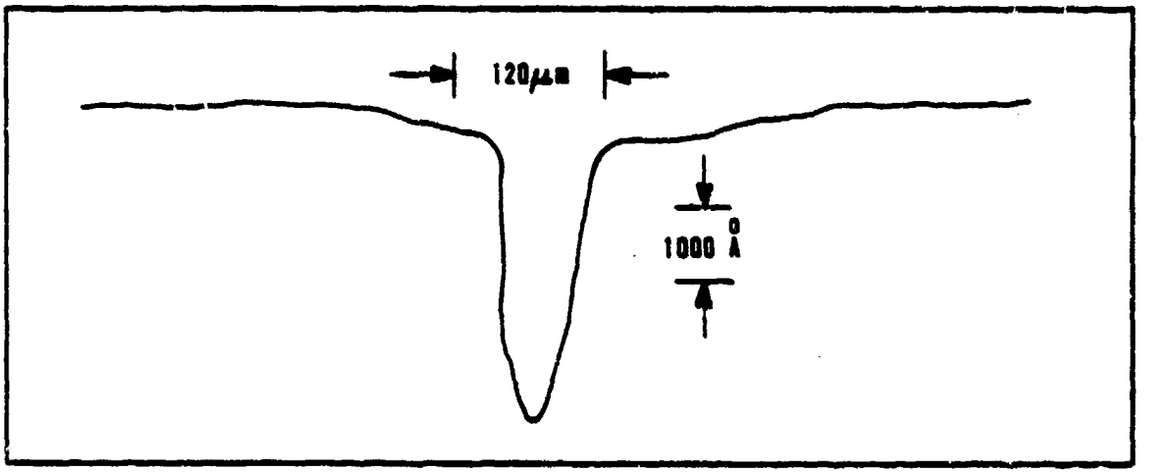

Figure 5. Talystep of Laser-Produced Crater in Fused Silica

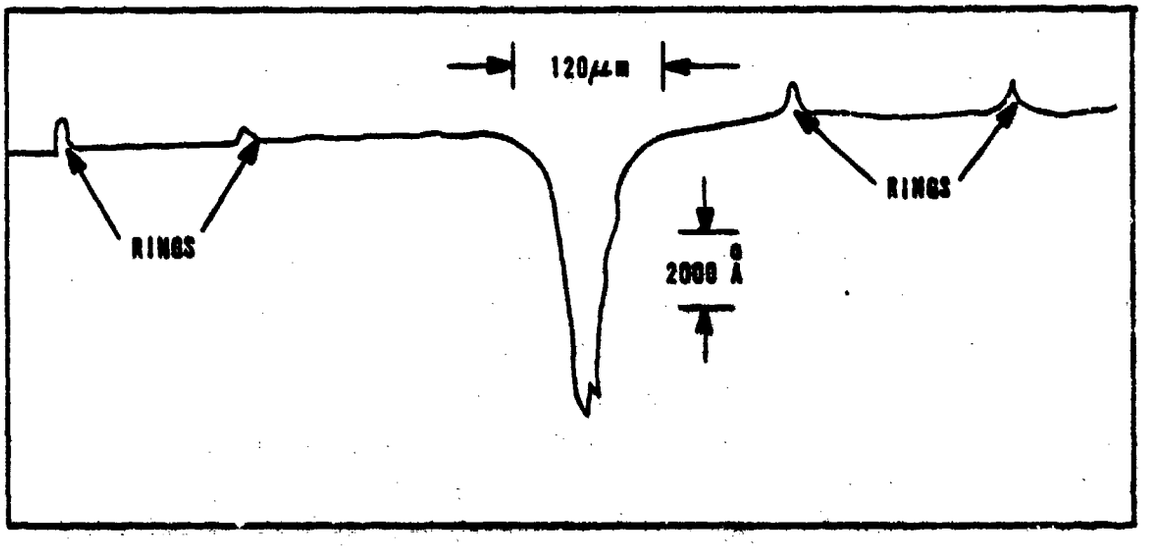

Figure 6. Talystep of Laser-Produced Crater in BK-7 Glass Showing Ring Structure

damage testing is attempted subsequent to fogging the sample. The surface threshold is markedly reduced after the surface has been fogged. It proved to be the most sensitive of the techniques. The alteration of the surface by the plasma appears to be permanent since samples damaged more than a year ago still reveal their sites by breath-fogging.

2. PARAMETERIZATION

It has been the general opinion in recent years that a TEM_{00} laser was essential in the study of laser-induced damage. It was argued (ref. 22) that filamentary hot spots in the beam contained a fraction of the total energy sufficient to cause damage yet was contained in such a small area that actual energy density on target due to this filament could be an order of magnitude greater than the average energy density. Recently, however, argument has been made (ref. 23) that a TEM_{00} beam is not necessary because filamentary structure in a laser beam is focused to a spot size too small to contribute to damage. Real-world lasers are not always operated in the TEM_{00} mode, and thus a certain justification for using multimode lasers in damage studies is made. However, to understand the processes and assign meaningful numbers such as threshold optical electric fields to damage tests, it is necessary to employ a well-defined beam with constant spatial pattern. To this end, a TEM_{00} mode laser was used in this study. To check on the TEM_{00} nature of the beam a near-field scan at 10 m from the oscillator waist and a far-field scan at the focal plane of both a 1.9-m lens and the 503.5-mm lens used in the surface damage experiment was performed. Since the fundamental mode is a Gaussian plane wave in the far field (i.e., at a position where the Fraunhofer approximation is valid), the intensity profile will be Gaussian in spatial extent. A measure of this spatial profile was obtained in two ways. In the first arrangement shown in figure 7, a photodiode was used as a receiver for the total laser pulse. A 130-μm diameter pin hole supplied by A. Owyoung (ref. 24) was used to sample the focused beam across its approximately 4-mm diameter. The temporal shape of the sampled pulse was compared to that of the full beam as revealed by photodiode number 1 and no variations were found. The deflection of the oscilloscope trace from the photodiode used to observe the sampled beam was ratioed to the deflection of the oscilloscope trace from the photodiode used to observe the whole beam. The variation of this ratio as the pinhole was stepped across the output beam gave a measure of the radial intensity distribution of the beam. Beam center was located and both a vertical and horizontal scan were made. By

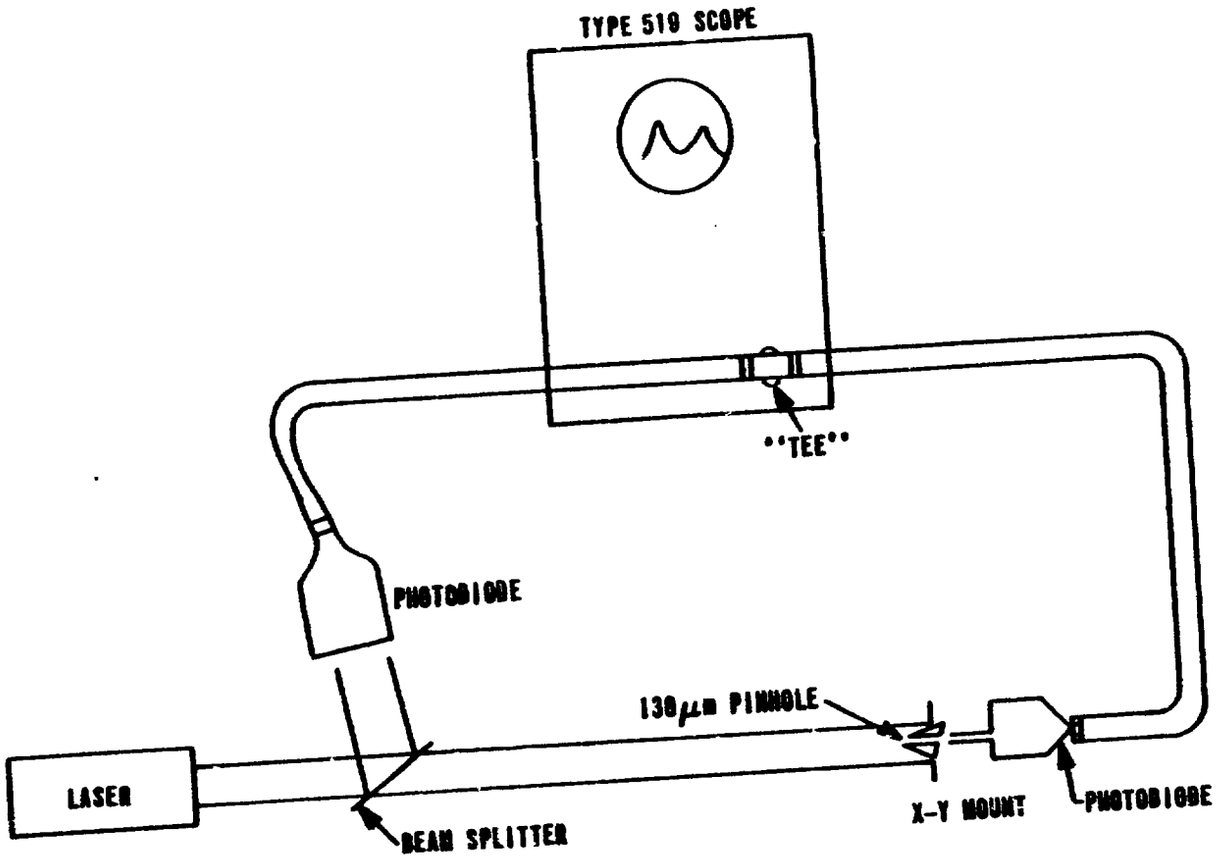

Figure 7. Experimental Arrangement for Profiling the Intensity Distribution of the Laser Beam

placing a lens a distance of one focal length in front of the pinhole, the half power diameter was found and related to the full angle beam divergence by $d = f\theta$, where f is the focal length of the lens used (ref. 25). For a transmission of 99 percent of a Gaussian beam through an aperture, one requires $d = 3w$ where w is the Gaussian spot size and d is the diameter of the aperture. The aperture used was 1.9 mm, thus the full-angle beam divergence becomes 1.07 mrad. The measured beam divergence of 1.34 to 1.58 mrad agrees within experimental accuracy to the expected value of 1.38 times diffraction limited beam divergence. This fact, coupled with the Gaussian fit to the intensity of 13 to 17 percent supports the claim of TEM_{00} mode operation. The procedure was repeated using the 503.3-mm lens and replacing the receiver photodiode with the Rk 3230 energy detector. The results in figure 8 are plotted against a Gaussian for comparison. For the 1.9-m lens the fit was ±13.6 percent while for the 503.5 mm lens the fit was ±17 percent. In the latter, the beam divergence was calculated to be 1.09 mrad.

It was necessary to know the focused spot diameter of the laser beam since the surface of the optical sample was placed not at the focal plane of the 503.5 mm but at the focus of 530.3 mm from the midplane of the lens. Since a Gaussian beam remains a Gaussian under propagation, it was necessary to measure the Gaussian spot size at the focus. The method, illustrated in figure 9, consists of using specially treated dark paper* which bleaches upon receiving a specific incident energy density threshold of ≈ 2 j/cm^2. The beam was successively attenuated as the laser was fired on separate sites. For a Gaussian beam the intensity varies as $I(r)$ as $I_0 e^{-r^2/w^2}$, thus a plot of (I/I_0) versus r^2 gives a relationship which readily identifies the spot size, w. By this method it was found that the spot size to the e^{-2} power point was 147 μm. A number of these determinations throughout the course of the study agreed to better than 10 percent.

3. SURFACE CHARACTERIZATION

One of the prime reasons for conducting this study was to determine those characteristics of surface finish and film deposition which materially affect the laser-induced surface threshold. It was imperative, therefore, to fully characterize the surfaces of both the uncoated samples and the thin-film coatings.

*Hadron Inc. Laser Footprint Report

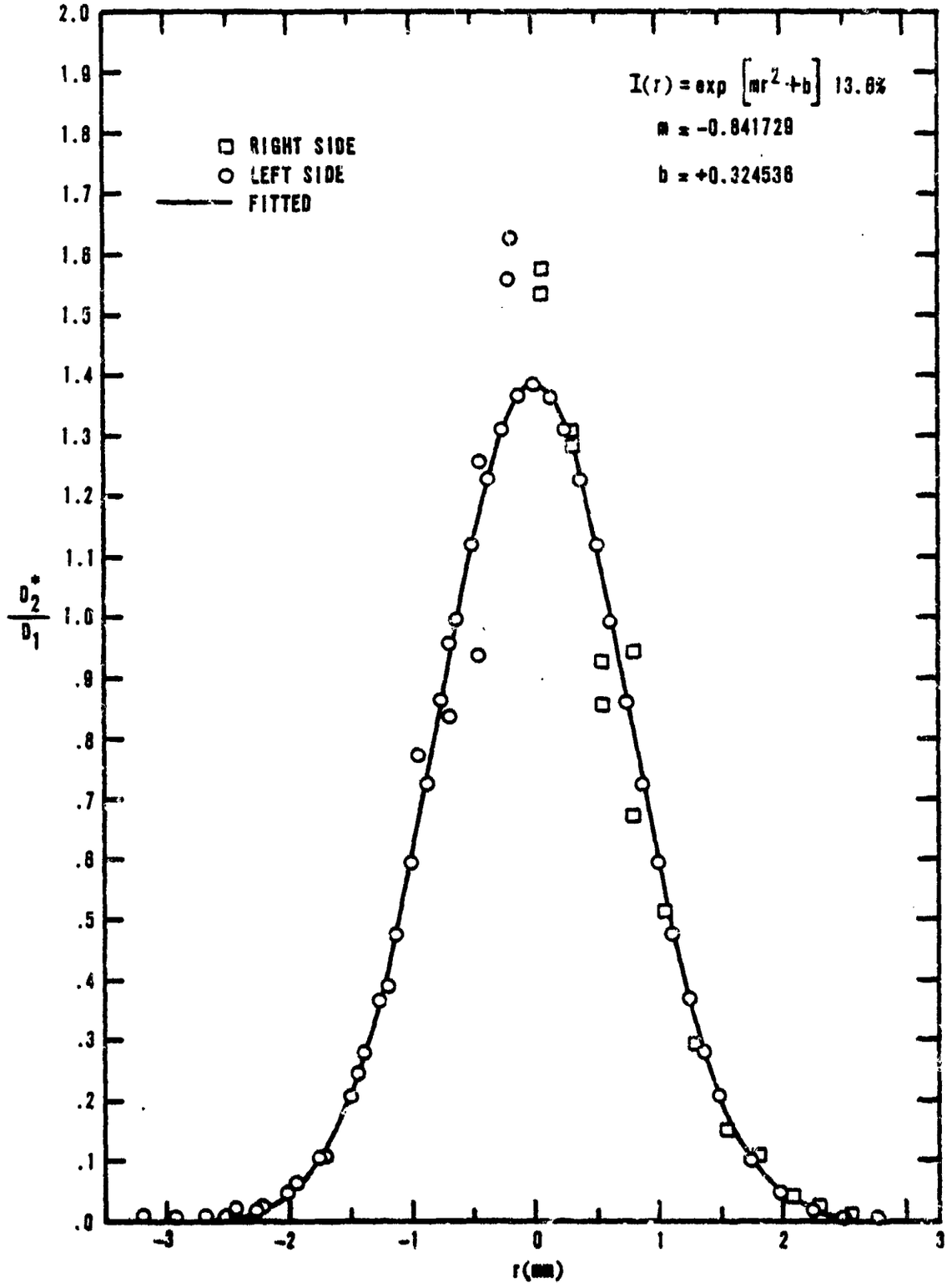

Figure 8. Experimentally Determined Intensity Profile at the Focal Plane of a 503.3-mm Lens

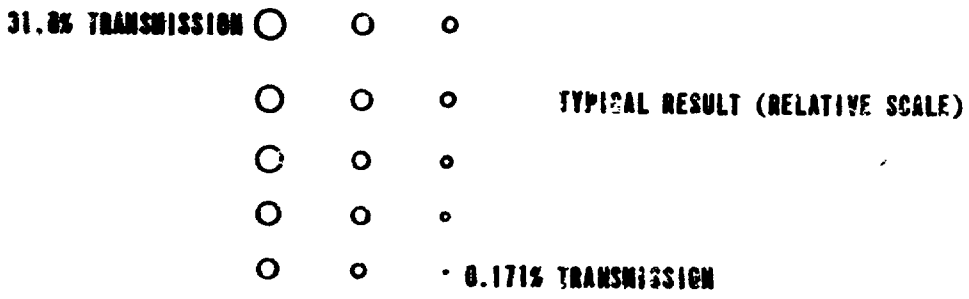

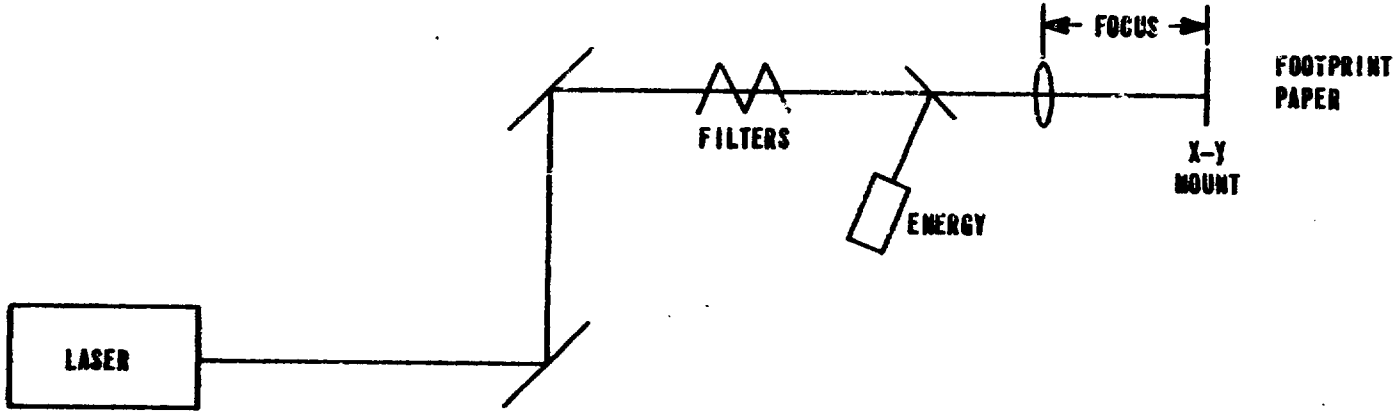

Figure 9. Method Used to Determine Focused Spot Size

The surfaces were measured for roughness by three methods: fringes of equal chromatic order (FECO), total integrated scatter (TIS), and Talystep depth profiling. FECO was the prime indicator of surface roughness while the total integrated scatter and Talystep were used only as auxiliary measurements. For a flat surface the roughness is defined as the root mean square deviation of surface heights from the average surface. Thus on a surface with a specified rms roughness, surface features as large as twice that in depth are not uncommon.

FECO interferometry is a technique shown schematically in figure 10. Both a reference flat and the surface to be measured are partially silvered. The sample and flat are brought to within a wavelength or so of each other and parallel. A portion of the two plates is imaged by lens L_2 onto the slit of a spectroscope. As the distance between the flat and sample varies due to surface roughness, the spectroscope passes only those wavelengths which satisfy $2d = m\lambda$ (m an integer). Since m is constant along any one fringe, d/λ is constant. The fringes, referred to as fringes of equal chromatic order, reveal the topographical features of the surface of the sample imaged on the slit of the spectroscope (refs. 26 and 27).

Total integrated scatter, from a discussion by Porteus (ref. 28), is a technique which relates the scatter from the reflection of a laser beam incident on a surface to the surface roughness. The sample is normally located tangent to one port of a hollow, diffuse reflecting sphere. Laser light enters another port and the nonspectral reflected light enters a detector after being totally integrated by the sphere (figure 11). Surface roughness is given by

$$\sigma = \frac{\lambda}{4\pi} \sqrt{-\ell n(1-TIS)} \qquad (12)$$

where λ is the wavelength of the test laser and TIS is the fraction of the test beam scattered outside the prime spectral reflection. The technique also affords a method for determining scatter of imperfections in thin-film coatings.

The Talystep device uses a weighted stylus and electronic amplification of its vertical motion to topographically scan the surface of the sample. For hard films it can also be used to mechanically measure the physical thickness of the film. It was also used in this study to measure a few of the damage craters (figures 4, 5, and 6). The final method was reliable for surfaces with values of $\sigma > \sim 50 - 75$ Å rms, but the diameter of the tip of the stylus precluded

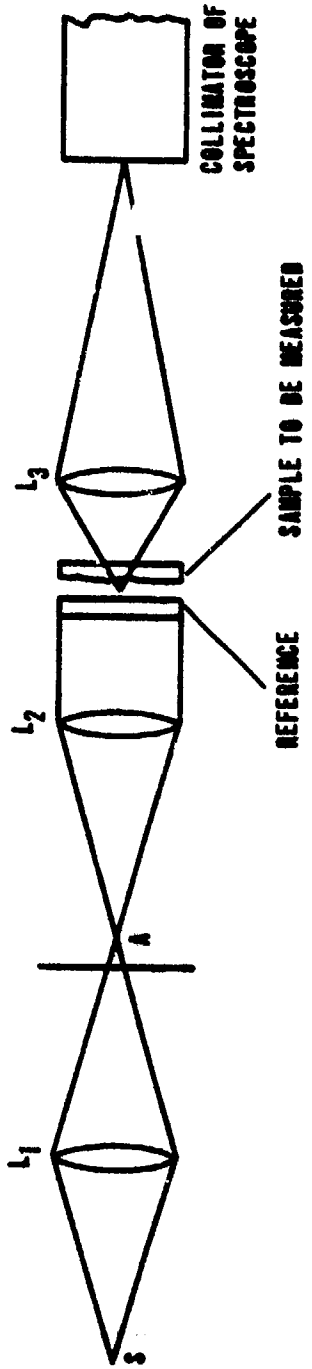

Figure 10. Schematic Representation of Fringes of Equal Chromatic Order (FECO) Interferometric Method for Determining Surface Roughness

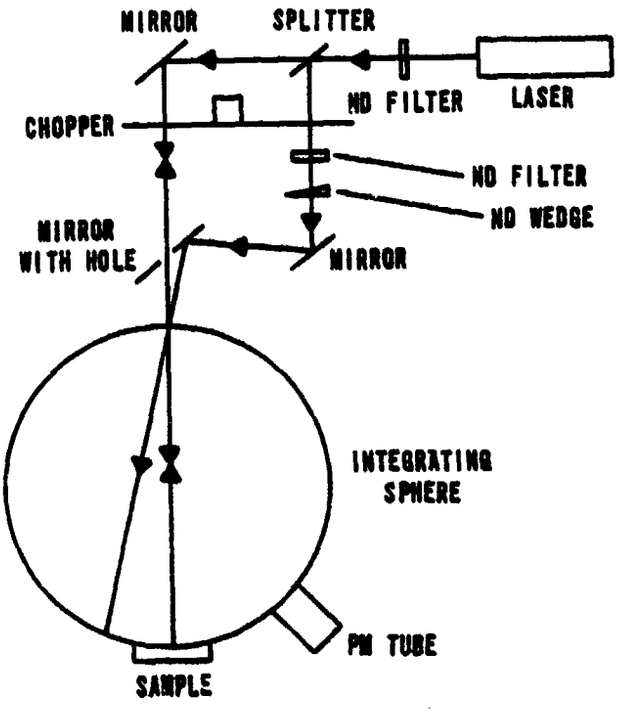

Figure . Schematic Representation of the Total Integrated Scatter (TIS) Method for Determining Surface Roughness

the me ement of very small features and gave uniformly too low readings on the smo er samples. The smallest stylus radius was 1.0 μm. To obtain an rms surface ghness by Talystep, a one-dimensional scan of 2 mm in length is obtained at several representative locations. For each scan of the topography of the surfa e the surface height is measured from a baseline at regular intervals to det rmine an average surface height. The deviation of the surface height from the average is then measured at regular intervals and the root mean square deviation is calculated. It is this deviation which is termed surface roughness.

From the results of surface roughness measurements performed by the vendor, the author, and the Optical Evaluation Facility at the Naval Weapons Center, China Lake, California, the striking conclusion was the lack of correlation between the measurements. For example, sample 800-7169-080 was supplied by the vendor with a roughness of 42 Å rms as determined by the most accurate technique, FECO. Accompanying that reading was the total integrated scatter of 0.11 percent, which indicates an equivalent roughness of 16.7 Å rms. The same sample was measured at China Lake by TIS at 16.5 Å and by the author by

Talystep at 27 Å. It would appear that the state of the art in surface measurements still allows for a great deal of uncertainty in surface roughness determinations. Industry sources (ref. 29) indicate that the FECO measurement is the most reliable, although very time consuming and difficult to perform and analyze. For this reason the FECO measurement was used in calculations involving surface roughness.

The refractive indexes of the bare samples and films were measured by ellipsometry. Number densities and nearest neighbor separations were calculated or obtained from standard references.

Of major concern in the study of the thin films was the homogeneity of the film throughout its depth. The spectral reflectivity is a reliable indicator of this parameter. A Carey 14 spectrophotometer was used in the double pass reflection mode to obtain the spectral reflectivity of the films. Figure 12 is the spectral response of two $\lambda/2$ ThF_4 and ZrO_2 films. These two films are examples of the excellence of a film coater's art in being able to produce homogeneous coatings. Since both films were specified as half wave at 1.06 μm, a perfect film would have the reflectance of the substrate at 1.06 μm. Since ThF_4 at n = 1.49, matches index more closely with the fused silica substrate index at 1.449 than does the ZrO_2 at n = 2.0, the reflectance of the ThF_4 film versus wavelength is not very different from the substrate. In fact, the maximum reflectance of the ThF_4 film on SiO_2 at 2.12 μm, where the film is a quarter wavelength thick, is only 4.15 percent compared to 3.36 percent for the substrate, while for the ZrO_2 film the maximum is 22.3 percent at 2.12 μm. Conversely figure 13 reveals the spectral response of LiF and MgF_2. These films display a markedly inhomogeneous character with an index apparently increasing outward from the substrate. Since they both have refractive indexes less than that of the substrate, their reflectance should increase toward and match that of the substrate at 1.06 μm. These two films along with BaF_2 exhibited the most inhomogeneity in this respect. The author will call attention to this fact during the discussion of the thin-film results.

To appreciate the magnitude and nature of the inhomogeneity, a computer program designed by Capt John Loomis (ref. 30) was used in an attempt to model the observed behavior of these films. The program was designed to accept up to 50 film layers of varying thickness, absorptance, and refractive index and to compute the angular and wavelength dependence of the reflectance. The parameters used included the total physical thickness of the film as measured by

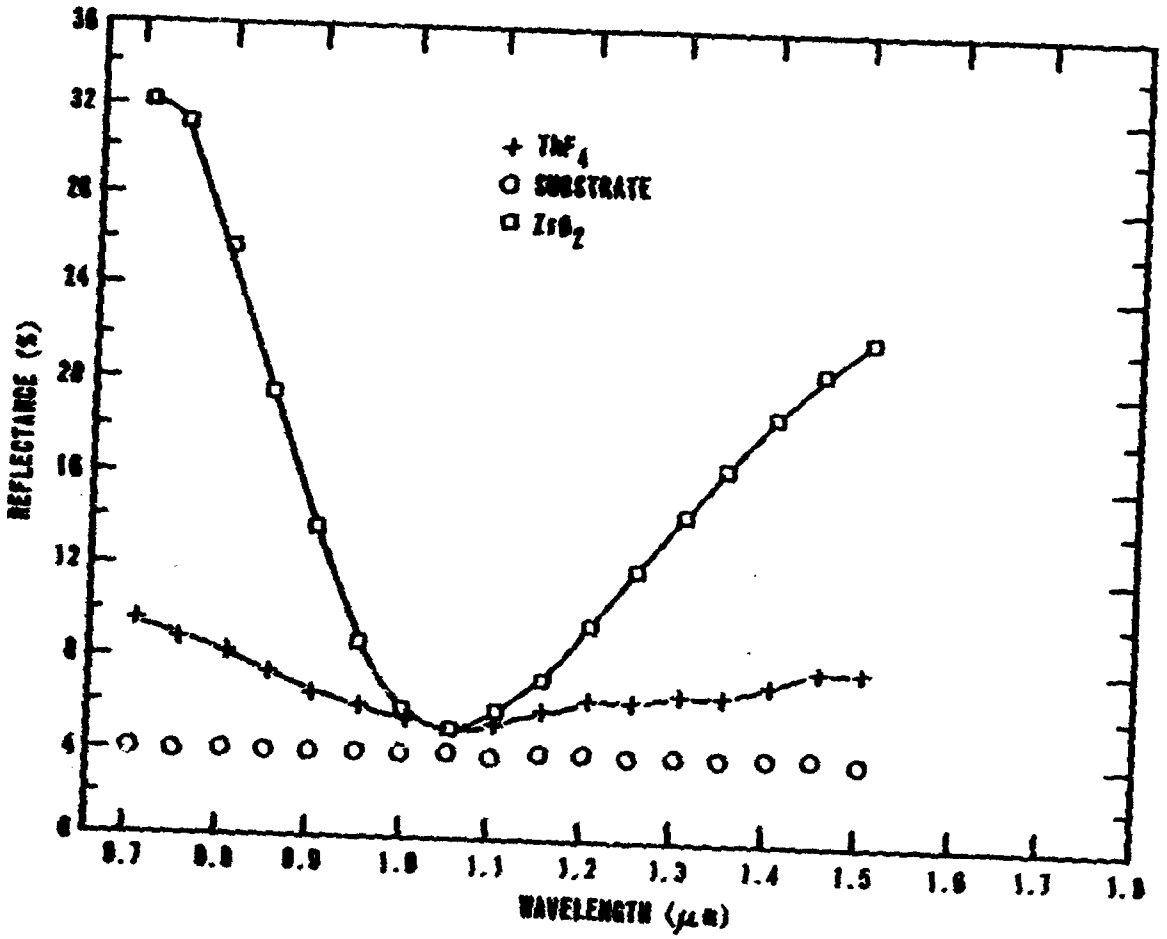

Figure 12. Reflection Spectra of Two Half-Wave Homogeneous Films Compared to the Fused Silica Substrate (Reflectance is on a relative scale)

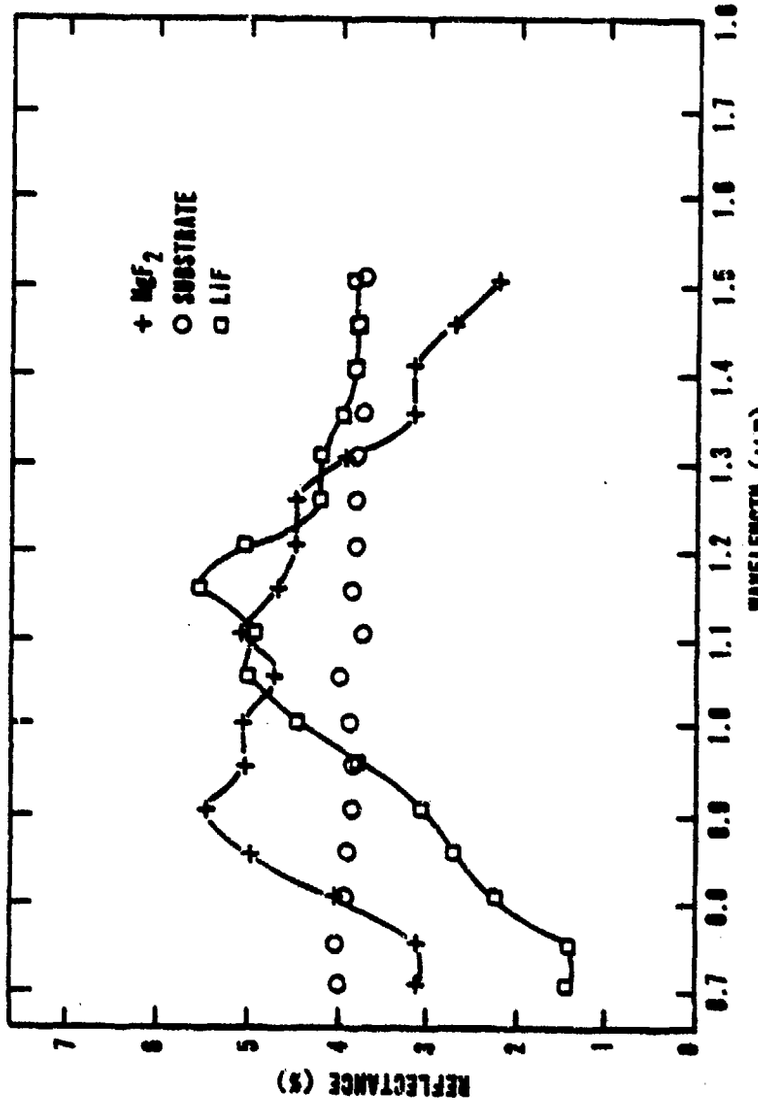

Figure 13. Reflection Spectra of Two Half-Wave Inhomogeneous Films Compared to the Fused Silica Substrate (Reflectance is on a relative scale)

Talystep, the refractive index of the substrate, and the measured refractive index at the surface of the film. The inhomogeneous film with varying index was discretized into a stack of from four to eight films with refractive index and thickness the variable parameters. It was found that a variation in the refractive index of about 7 percent (1.28 at the substrate to 1.38 at the film surface) produced a spectral response quite suggestive of the measured spectral response. One result has been reproduced as figure 14 which should be compared to figure 13.

If one assumes that fused silica is invariant, independent of the source, a comparison of the absorption and transmission spectra for various fused silica blanks will quickly dispel that notion. While the major portion of this effort used fused silica supplied by the Amersil Corporation under the trade name Optosil I, an ancillary study involved fused silica substrates supplied by a variety of manufacturers. During the coating process absorption spectra are routinely taken. From these spectra varying amounts of hydroxyl ion was identified in the different fused silica types. This observation formed the basis for an unexpected conclusion which at first seemed to be anomalous behavior. This result will be discussed in detail later. This last measurement was mentioned to indicate that in thin-film coatings it is not at all entirely obvious what deposition conditions, techniques, and properties of films lead to high damage threshold films.

4. SAMPLE PREPARATION

The test samples for this study required surface finishes of two types: (1) bare surfaces and substrate surfaces for film depositions with the lowest practical surface roughness and (2) bare surfaces and substrate surfaces for film depositions with a controlled range of surface roughnesses. The latter category was designed to test the influence of surface roughness on the laser-induced damage threshold and whether thin-film thresholds are affected by the surface roughness of the substrate. Both the smooth and rough surfaces were created by variations of the process of controlled grinding.

The effect of the grinding process in the preparation of optical surfaces extends below the surface. A layer of subsurface disorder in the form of microcracks and fissures develops when an optical surface is ground. A commonly accepted rule in the optical industry (ref. 31) is that subsurface disorder extends to a depth roughly three times the diameter of the grit used in the grinding process. Controlled grinding is a technique for minimizing the

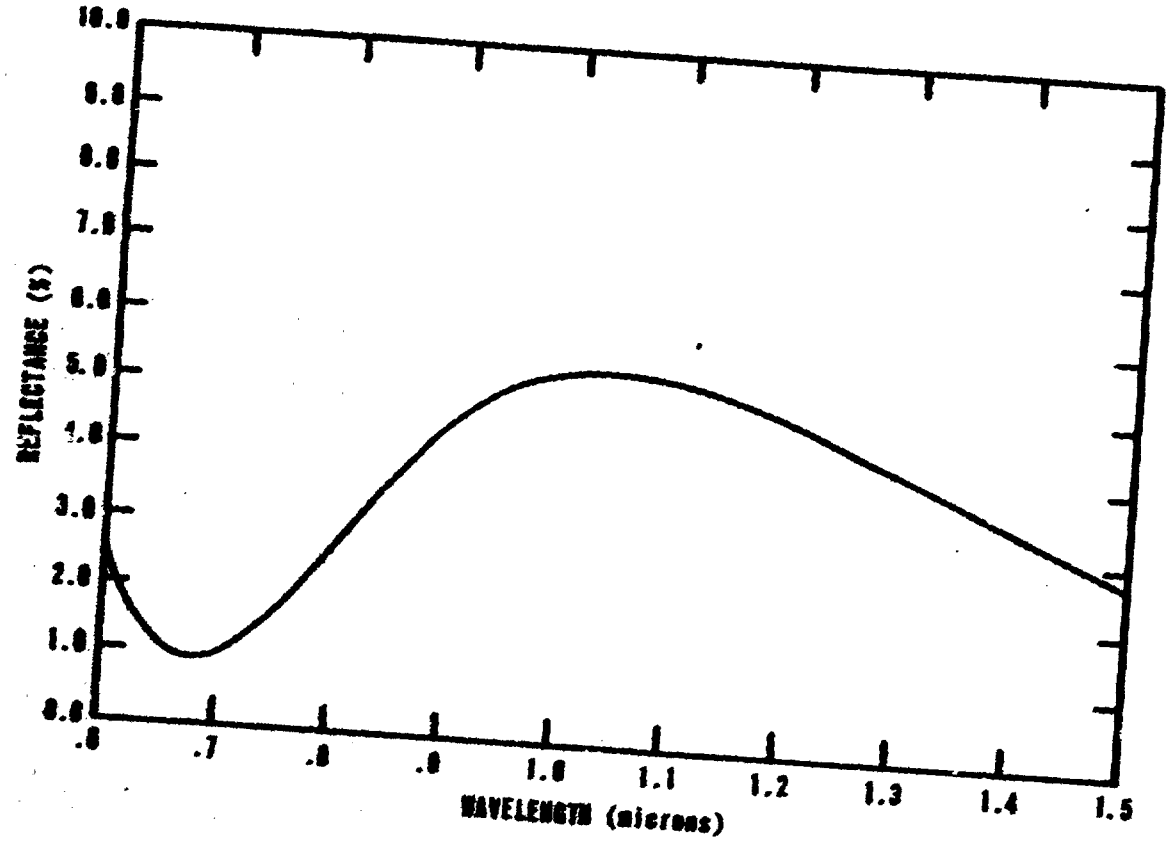

Figure 14. Computed Reflectance Spectrum of a Four-Film, Half-Wave Stack with Indexes 1.28, 1.32, 1.36, and 1.38 Increasing Outward from a 1.45 Index Substrate

subsurface disorder. The controlled grinding process used to obtain the "best finish" surface proceeds as follows: A 30-μm grit is used to rough in the surface finish. Since this process introduces a subsurface disorder to a depth of ~90 μm the next stage, employing 20-μm grit, proceeds until ~100 μm of the material is removed, thus eliminating the disorderly effect of the 30-μm grit. This process continues through 12-, 5-, and 3-μm diameter alumina grit, each stage removing material to a depth about three times the diameter of the previous grit. The surface is then polished, which removes about 10 μm of material and gives the final finish. The final roughness values varied from about 10 Å rms for fused silica to about 40 to 50 Å rms for sapphire and ZnS.

The roughness samples were created by interrupting the polishing at selected total polish times. Samples in the 300 Å(rms) range were polished for about 30 minutes. Forty minutes of polishing time gave a 150 Å(rms) surface, while 10 to 20 hours gave 40 to 50 Å(rms), and best finish (less than 20 Å(rms)) required 40 hours polishing time.

The dielectric films were deposited by one of three frequently employed techniques: rf sputtering, electron beam heating, and thermal-evaporation. A set of MgF_2 samples were prepared by each of the three deposition techniques. The MgF_2 films applied to substrates on which the substrate roughness was varied were deposited by thermal evaporation. The remainder of the films were applied by electron beam heating.

Each dielectric film was specified to be a half wave in optical thickness at the 1.06-μm wavelength used in the study. This parameter was monitored by observing the reflectance of the film-substrate system as the film was being applied. For films whose index is greater than the substrate index, a minimum in reflectance is obtained when a half-wave optical thickness is reached. For homogeneous films this minimum corresponds to the reflectance of the bare substrate. The half-wave thickness was chosen because this assured that the electric field at the substrate-film interface was the same as the optical electric field at the film-air interface. It was also the thickness which gave the least variation in the electric field of a standing wave pattern for slight variations in the thickness. For films whose index is less than the index of the substrate, a reflectance maximum is obtained when a half-wave optical thickness is reached. For films whose index was the same as or very near the index of the substrate, it is necessary to use a separate witness plate with a sufficiently different refractive index to accurately monitor the thickness.

The materials covered in figures 12 and 13 make it apparent that the most sensitive variation of reflectance about the extremum was provided by the ZrO_2 ($n = 2.0$) on fused silica ($n = 1.449$). Thus to obtain the most sensitivity in the thickness determination requires the use of a witness plate whose index varies from that of the film as much as possible.

SECTION III

THEORY

Pulsed laser-induced damage in solid dielectrics is intimately linked with the study of the dc breakdown of solid dielectrics. This assertion follows from the electric field view of laser-induced damage which now has wide acceptance for the reasons noted in the introduction of this report. It is not reasonable to claim that there is a one-to-one correspondence between the two processes. Laser-induced damage does not involve electrodes with their associated influences nor is the damage region, therefore the total energy drop, as localized in dc breakdown studies as it is in laser damage situations. It is appropriate to argue, however, that certain of the electric-field related processes are similar between the two phenomena. For this reason a brief background of the current theories of dc breakdown of solid dielectrics will be given, followed by a review of current thought on laser-induced damage to solid dielectrics, and finally a proposed model and theory.

1. DC BREAKDOWN OF SOLID DIELECTRICS

A. von Hippel (ref. 32) in an attempt to reconcile the accepted theory of dc gas breakdown to solids proposed that an energy balance must be maintained for any electron in the conduction band of a solid. A sufficient alteration from this equilibrium energy balance (e.g., by applying a large enough electric field) leads to an increase in the energy of every free electron and subsequent dielectric breakdown. Under the influence of an electric field, E, the z component of momentum will obey

$$\left(\frac{dp_z}{dt}\right)_E = -qE \tag{13}$$

However, the motion of the electron is retarded due to electron-phonon collisions

$$\left(\frac{dp_z}{dt}\right)_L = \frac{p_z}{\tau(E)} \tag{14}$$

where $\tau(E)$, the relaxation time, is assumed to be a function of the electron energy. In a steady state when

$$\left(\frac{dp_z}{dt}\right)_E + \left(\frac{dp_z}{dt}\right)_L = 0 \tag{15}$$

the electron drifts in the field direction with velocity

$$\frac{p_z}{m} = -\left(\frac{q_e}{m}\right)\tau(E)E = -\mu(E)E \tag{16}$$

where m is the electron mass and $\mu(E)$ is the mobility of the electron. This drift velocity is superimposed on the random thermal motion. This will be seen to be of importance later when we consider the calculations of Seitz (ref. 33). To determine the total energy of the electron, one must balance the gain, A, experienced from the applied field against the losses to the lattice, B. Energy gain is given by

$$A(E,E,T_o) = q_e\mu(E)E^2 = \frac{q_e^2E^2\tau(E)}{m} \tag{17}$$

where T_o is the lattice temperature. Electron-phonon interactions involve the absorption or emission of a phonon of energy $\hbar\omega$. The ratio of the probability of emission versus absorption is given in elementary quantum theory as $(N_\omega+1)/N_\omega$ where N_ω is the average number of lattice quanta with energy $\hbar\omega$, that is

$$N_\omega = \left[1 + \exp\left(\frac{\hbar\omega}{dT_o}\right)\right]^{-1} \tag{18}$$

The rate at which energy is lost, $B(E,T_o)$, is obtained by observing that a net loss occurs in only one of $(2N_\omega + 1)$ collisions so that

$$B(E,T_o) = \frac{\hbar\omega}{\tau_t(E)(2N_\omega+1)}\left(1 - \frac{kT_o}{E}\right) \tag{19}$$

where $\tau_t(E)$ is the mean time between collisions and is equal to $\tau(E)$ if the electron scattering is isotropic and varies from it slightly if it is anisotropic. The factor $1 - kT_0/E$ is a scaling factor to ensure that no energy is lost for electrons with energy kT_0. For a steady state then,

$$A(E,E,T_0) = B(E,T_0) \tag{20}$$

so that

$$E^2 = \frac{m}{q_e^2} \frac{B(E,T_0)}{\tau(E)} \approx \frac{m}{q_e^2} \frac{\hbar\omega}{\tau\tau_t(2N_\omega+1)} \left(1 - \frac{kT_0}{E}\right) \tag{21}$$

This relationship, with appropriate values of $\tau(E)$ and $\hbar\omega$ is depicted graphically in figure 15. Note in figure 15, for low values of electric field equation (21) is satisfied for two values of the electron energy. For field E_1 consider an electron with energy E such that $E < E_1$. Under the action of the field the energy would increase to E_1. Similarly, for $E_1 < E < E_2$ the losses predominate until the electron energy is reduced to E_1. For fields greater than E_H, A is always greater than B and the energy of the electron will increase continuously under the applied field. This view, which treats electrons whose energy does not lie to the right of the intersection of curves A and B, is referred to as the von Hippel low energy criteria and the field E_H is the breakdown field. However, Frölich (ref. 34) raised objection to this treatment because it fails to properly account for the possibility of initially present high energy electrons.

Frölich argues that when $E > E_2$ for $E = E_2$, then A is greater than B and this high energy electron will continuously gain energy from the field. This being the case, E_H has no significance as a breakdown field. To prevent such a runaway condition, which due to the shape of electron distributions can occur at any field no matter how small, additional loss mechanisms must be introduced. The proponents of collective breakdown introduce free-free electron collisions, while proponents of avalanche breakdown introduce free-bound electron collisions.

Stratton (ref. 35) discussed collective breakdown by observing that at sufficiently high free electron densities, free-free collisions will have a moderating effect on electrons which have energies which exceed the Frölich

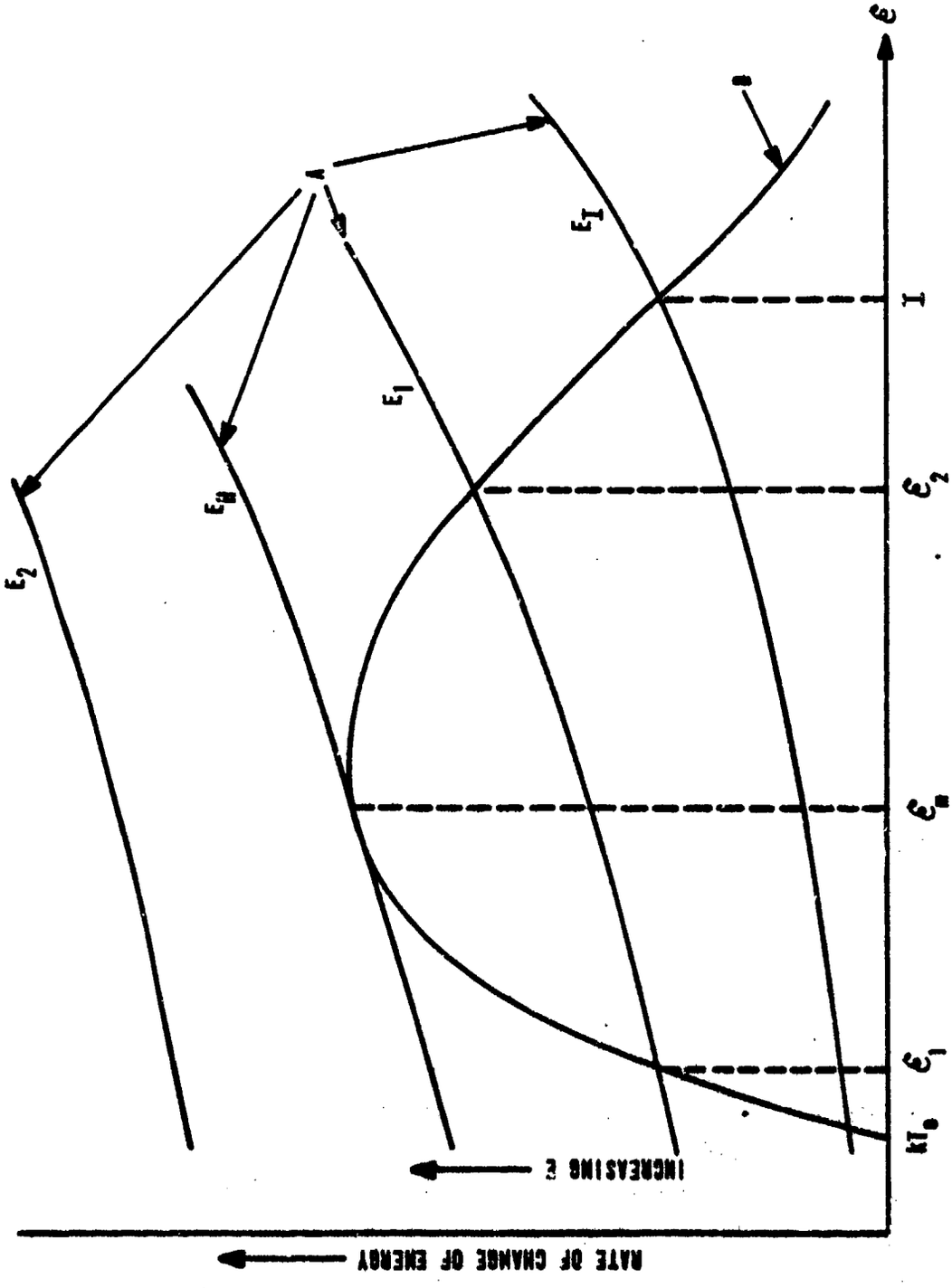

Figure 15. Schematic Construction of von Hipple's Low Energy and Frölich's High Energy Criteria (after reference 35)

objection. He states that if the free-free collisions exceed the occurrence of electron-phonon collisions, the electron distribution in the steady state will be Maxwellian with a temperature T greater than the lattice temperature T_o. Equation (20) is thus replaced by

$$\bar{A}(E,T,T_o) = \bar{B}(T,T_o) \tag{22}$$

where the bar denotes average values. $\bar{A}$ and $\bar{B}$ behave qualitatively the same as A and B so that there will be a critical field E_c which corresponds to the electron temperature T_c. E_c is similar to, though a bit less than von Hippel's E_H. The theory is only applicable for electron densities sufficiently great so that the rate of energy loss by the electron to the lattice is less than the rate of energy loss by free-free interactions given by Pines (ref. 36) as

$$B_e \approx \frac{4\pi N q^{*4}}{p} \tag{23}$$

where q* is an effective charge such that $(q^*/q_e)^2 \approx 1\sqrt{\varepsilon}$ where $\bar{\varepsilon}$ is a dielectric constant which depends on the velocity of the electron. Thus the electron density for collective breakdown must exceed

$$N_c \approx \frac{p\varepsilon^{-2}}{4\pi q_e^4} B(E,T_o) \approx \frac{p\varepsilon^{-2}}{4\pi q_e^4} \frac{\hbar\omega}{\tau_t(E)(2N_\omega+1)} \tag{24}$$

Stratton further shows that the critical electron density is of the order of 10^{18} cm^{-3}.†

It has been well established in gas breakdown (especially in the photographs of Raether) (ref. 37) that ionization proceeds by accelerating electrons to ionizing potentials so that collisions with neutral atoms frees an electron, which provides additional low energy electrons to start the process over. Thus Frölich assumed that for densities below N_c, electron-neutral atom ionizing collisions would be important in solids. Electrons of energy E_2 greater than the ionizing energy, I, (see figure 15) can ionize lattice atoms and produce

†This particular number appears in many of the theoretical and experimental studies of dc and laser-induced breakdown.

two low energy electrons per ionizing collisions. In steady state this process is balanced by the reverse process of recombination in which two free electrons produce a bound electron and a high energy electron. For electrons whose energy satisfies $E_2 < E < I$ they can only increase in energy until they reach or surpass I. Thus a steady state is realized only when $E_2 = I$ and equation (21) then becomes

$$E_I^2 = \frac{m}{q_e^2} \frac{B(I,T_o)}{\tau(I)} \approx \frac{m}{q_e^2} \frac{\hbar\omega}{\tau(I)\tau_t(I)(2N_\omega+1)} \tag{25}$$

This is referred to as the Frölich high energy criterion. Stratton states that once electrons achieve energies in excess of E_2, they are rapidly accelerated ($A > B$) up to energies of the order I. E_I is then a lower limit for fields which give appreciable ionization while the actual breakdown field ($>E_I$) is determined by the amount of ionization which is required to give avalanche breakdown.

In an electron avalanche in the simplest medium (i.e., gas) for a given field E, one electron will produce α electrons by collisional ionization per centimeter of travel. The Townsend ionization coefficient, α, is related to the reduced field in the gap, E/p, where p is the pressure as

$$\alpha/p = (E/p)^m \tag{26}$$

where m is material dependent. It has a value of 9.2 for air as reported by Meek and Craggs (ref. 38). The growth of ionization is governed by

$$\frac{dN}{dx} = N\alpha \tag{27}$$

which for an initial concentration of free electrons N_o gives the number N after the avalanche has traveled a distance d as

$$N = N_o e^{\alpha d} \tag{28}$$

Breakdown occurs when N reaches a critical value, N_c, and from the form of equation (26) it is easy to see why a small increase in the electric field

near the breakdown field leads to a rapid onset of breakdown. Much the same view of the avalanche process is held by those who support the avalanche theory of dc breakdown in solid dielectrics. The first problem encountered is that there does not exist a Townsend ionization coefficient for solids which exhibits the simple form of equation (20) but rather one with a very complicated dependence on electric field which cannot be reduced to quadratures. For solids Seitz (ref. 33) has given an estimate of the critical electron density necessary to produce a discharge. He argues that in a field of 1 MV/cm an electron drifting with the field 1 centimeter while executing random thermal motion about the direction of drift sweeps out a volume of $\approx 3 \times 10^{-6}$ cm^3 and that it seems safe to assume that breakdown will occur if each primary electron produces one electron for each 10^5 atoms in the drift tube. Thus when an electron density of $\approx 10^{18}$ cm^{-3} is reached, breakdown will occur. The total number of electrons in this example is $\approx 10^{12}$ and since each ionizing collision produces two electrons, it takes i generations to produce $2^i = 10^{12}$ electrons. Since i here must be 40, this is the basis of the Seitz 40 generation model.

The mean energy of an electron E_1 (figure 15) must be raised to I before an ionizing collision can occur. Under the action of the field if the electron experiences no collisions, it would be accelerated to an energy I in time

$$t_I = \frac{m(v_I - v_1)}{qE} \tag{29}$$

or after moving a distance

$$\ell_I = \frac{I - E_1}{qE} \tag{30}$$

in the direction of the field. Typical values of 6 eV for ionization energy and 1.0 MV/cm in equation (29) yield an ionization time of about 8×10^{-14} sec or about 23 full cycles of 1.06-μm radiation.

If $P(t_I)$ the probability that the electron makes no collision for a time t_I and $\tau_t(E_1)$ is the mean time between collisions, then the mean rate of ionization per unit time is

$$W = \frac{P(t_I)}{\tau_t(E_1)}$$

the ionization rate per unit path length is thus

$$\alpha = \frac{W}{\mu(E_1)E} = \frac{P(t_I)}{\tau_t(E_1)\mu(E_1)E} \tag{31}$$

Breakdown then occurs when $\alpha L = 1$ where L is the thickness of the sample. Upon using equation (31),

$$1 = \frac{P(t_I)L}{\tau_t(E_1)\mu(E_1)E} \tag{32}$$

A formula for $P(t_I)$ can be obtained by calculating the probability that there is no collision between t and t + dt.

$$P(t + dt) = P(t)(1 - dt/\tau) \tag{33}$$

which yields

$$P(t_I) = \exp\left[-\int_0^{t_I} \frac{dt}{\tau}\right] = \exp\left[-\frac{m}{qE}\int_{V_1}^{V_I} \frac{dv}{\tau(E)}\right] \tag{34}$$

or

$$P(t_I) = \exp(-H/E) \tag{35}$$

where H is a constant field. The breakdown field can then be determined as

$$E_B = \frac{H}{\ln[L/E_B\mu(E_1)\tau_t(E_1)]} \tag{36}$$

Here one observes that the breakdown field depends on sample thickness while in collective breakdown it does not.

Thermal breakdown theories share the final stage of each of the previously described processes. Obviously, the existence of an electron density of 10^{18} cm^{-3} is not reason in itself for damage in a solid. Good conductors routinely have electron densities at room temperature several orders of magnitude above

10^{18} cm^{-3} with no detrimental effects (ref. 39). Rather it is the increased conductivity of the dielectric which couples with the breakdown field (~ 1 MV/cm) through joule heating to locally melt the dielectric. Thermal breakdown theories assume that the small conductivity of a dielectric allows some joule heating at the large fields of interest in breakdown studies. The joule heating raises the lattice temperature which raises the temperature dependent conductivity (probably through increases in the number of electrons in the conduction band as well as increases in mobility) and this spiraling process culminates in localized melting and dielectric failure.

Any calculation of the thermal breakdown field starts with the basic heat flow equation

$$C_v \frac{dT_o}{dt} = \sigma E^2 - \text{div}(\kappa \text{ grad } T_o) \qquad (37)$$

but its solution is very difficult since T_o is a function of position and the electrical conductivity σ is a complicated function of T_o. κ is the thermal conductivity. Usual attempts at solution are the steady state in which $dT_o/dt = 0$ or the short time solution in which thermal conduction is ignored.

The conclusions of thermal breakdown theories are generally valid at high temperatures where the ratio of electrical to thermal conductivity is large. This is also true for large electron densities such as might be generated by any of the other competing mechanisms.

Before considering theories of laser-induced breakdown a few thoughts drawn from Stratton (ref. 35) seem appropriate. He states that the collective breakdown theory of Frölich and Paranjape (ref. 35) provides a straightforward method for calculating a well defined critical dielectric breakdown field. Their theory is free from objections if the initial assumptions of a Maxwellian electron energy distribution is valid. Calculations based on collective breakdown strongly suggest the theory is valid for alkali halides.

Stratton further states that the theory of avalanche breakdown is based on so many assumptions, some of which are difficult to justify, that no great confidence can be attached to the results. He finally states that it is possible that avalanche multiplication in dielectrics, with a low initial electron density, will produce electron densities in excess of the critical density N_c for collective breakdown before avalanche breakdown takes place.

2. LASER-INDUCED BREAKDOWN

Theories of laser-induced breakdown of solid dielectrics have attempted to explain: (1) the mechanism for initiating primary electrons, (2) the mechanisms responsible for creating electron densities of sufficient magnitude to cause damage, (3) the close correlation between dc breakdown results and laser-induced results, (4) the pulse width dependence of laser-induced damage, (5) the statistical fluctuations in the breakdown field values, and (6) the frequency dependence of laser-induced damage. Proposed mechanisms include inverse bremsstrahlung, collective ion oscillation, and various multiphoton schemes. Basically, the current status of the theory of laser-induced breakdown involves those who confirm electron avalanche as the breakdown mechanism and those who claim that electron avalanche is too improbable to be operative.

Bloembergen (ref. 40) gives the rate of increase in the electron density N during low-frequency breakdown (i.e., below a frequency at which multiphoton processes are probable) as

$$\frac{\partial N}{\partial t} = \alpha(E)N + \left(\frac{\partial N}{\partial t}\right)_{\text{tunnel}} - \left(\frac{\partial N}{\partial t}\right)_{\text{loss}} \tag{38}$$

The first term on the right side of the equation represents the familiar avalanche multiplication where $\alpha(E)$ is the probability per unit time that an electron in field E will have an ionizing collision. For the high frequency limit the tunneling term becomes the same as the multiphoton ionization process (ref. 40). It is this term which Bloembergen claims, in the absence of initial electrons, initiates the breakdown process. Neglecting the final term in the short pulse lengths of interest and assuming an initial electron density N_o of $10^8 - 10^{10}$ cm^{-3}, one can neglect the second term and the result is the familiar

$$N = N_o \exp\left[\int_o^{t_p} \alpha(EIt')dt'\right] = M_c(t_p) \tag{39}$$

Bloembergen then states that at electron densities greater than 10^{18} cm^{-3} the energy deposition rate by absorption of the laser beam becomes so high that the temperature rise of the lattice is sufficient to cause damage even in picosecond pulses.

Fradin et al., (ref. 17) further refined Bloembergen's argument by stating that the process of electron avalanche involves energy exchange between the field and electrons which is governed by the formula for ac conductivity

$$\frac{dE}{dt} = \frac{Nq_e^2\tau}{m(1+\omega^2\tau^2)} E^2 \tag{40}$$

and, since the details of energy input determine the energy distribution and thence N, that threshold field scales with frequency as

$$E^2 \sim 1 + \omega^2\tau^2 \tag{41}$$

where τ is the electron-phonon collision relaxation time. Equation (41) is used to explain the observed factor of 1.5 between dc and optical frequency breakdown fields.

Bass and Barrett (ref. 41) propose a probabalistic view of laser-induced damage based on (cf. equation (35))

$$P_1 \propto \exp(-K/E) \tag{42}$$

as the probability that a single pulse will produce damage at the given field E. The avalanche theory is modified to account for the possibility that an electron will suffer only lucky collisions; that is, collisions which reverse the momentum of the electron just as the electric field reverses. Such collisions are necessary to increase the energy of a free electron in an alternating field since the momentum of the electron in an alternating field and the phase of the electric field are always opposed.

The pulse length dependence was treated by Fradin (ref. 16) using equation (39). Assuming an initial electron density of 10^6, required a multiplication M_c by avalanche of 10^{10}. Then the ionization constant is taken as

$$\alpha(E) = \frac{1}{t_p} \ell n M_c \simeq 18/t_p \tag{43}$$

where t_p is the pulse duration.

Without belaboring the subject, this review will be concluded by citing the highly readable paper by Sparks (ref. 42) on his objections to the current avalanche theories of laser-induced breakdown. Sparks shows that the avalanche multiplication constant is too small by tens of orders of magnitudes in some cases to explain damage results even when initial electron densities as high as 10^{10} cm^{-3} are assumed. The proposed frequency dependence of the breakdown field $E_B^2 \sim 1+\omega^2\tau^2$ disagrees with experimental results. The explanation in terms of an anomalously small electron relaxation time was shown to be inconsistent with the value of τ required to explain the magnitude of E_B with calculated values of τ and with the difference between the dc and 1.06-μm breakdown results. Sparks further shows that the temperature dependence of E_B is incorrect and that values of N_o in the range 10^8-10^{10} cm^{-3} would place the alkali halides in the semiconductor class of materials. Further, densities of this magnitude are inconsistent with photoconductivity measurements and, in fact, limits on N_o set by conductivity arguments estimate the probability of finding even one electron in the focal volume of typical laser experiments as being less than 10^{-6}. The lucky electron theory was considered and even with overgenerous estimates of the probability of backscattering into phase with the field yielded a probability of the success of an electron reaching an ionizing energy of $\sim 10^{-52}$. Sparks then proposes a preliminary new theory involving Holstein processes (photon-electron-phonon) and avalanche mechanisms.

With these remarks as background, a new approach to laser-induced damage utilizing direct-field ionization will be proposed.

3. AN ALTERNATIVE TO AVALANCHE BREAKDOWN

Because of the objections to an avalanche theory of solid dielectric breakdown voiced by Stratton and the equally vigorous objections to an avalanche theory of laser-induced damage raised by Sparks it does not appear fruitful to give here yet another attempt at a modification of basic avalanche theory. Rather a simpler theory of direct-field ionization will be proposed which has the advantage over the more complicated theory in that it is predictive. The model and basic assumptions will provide a basis for the mathematical treatment to follow.

a. Assumptions

One of the few threads common to nearly all theories of dc breakdown and laser-induced damage to solid dielectrics is that an electron density of the

order of 10^{18} cm^{-3} is required before energy conversion to the lattice through absorption by the electrons is sufficient to damage the lattice. David et al., (ref. 43) measured electron densities of ~10^{18} cm^{-3} required to effectively begin to absorb laser energy. Guenther and Pendleton (ref. 44) reported densities of 10^{18} cm^{-3} at visible plasma thresholds in deuterium gas. Recently Alyassini and Parks (ref. 45) calculated the electron density at surface damage threshold using the observed change in refractive index. The values they report are ~10^{18} cm^{-3}. Thus a basic assumption is that if electron densities of the order of 10^{18} cm^{-3} can be provided by the laser pulse, damage will follow by the subsequent absorption of the remainder of the pulse.

The other basic assumption around which the theory is devised is that a semiclassical description of the field-atom interactions can provide the requisite electron density.

b. The Model

The author proposes here a model which explains the salient features of pulsed, laser-induced damage to transparent dielectrics. The laser beam liberates electrons from the atoms in the region of interaction between the laser beam and the material. As has been stated previously, it is not the liberation of electrons which damages the dielectric but rather the deposition of the energy of the laser beam in the electronic plasma which heats the lattice and causes damage. The behavior observed by Milam, et al., (ref. 46) supports this conjecture. Milam determined the starting times of damage events by observing the attenuation of the laser pulse which was transmitted by the dielectric. The majority of starting times occurred at or before the peak laser intensity. A few damage events occurred after the peak of the laser pulse, but in no case did damage occur in the final third of the laser pulse duration. One explanation of these observations is that once a critical electron number density is reached, sufficient to initiate absorption of the laser beam, damage will occur only if a significant portion of the energy in the laser beam is available for absorption and subsequent heating of the lattice to localized destruction. A heuristic argument can be given here for the observed increase in threshold damage fields with decreasing laser pulse length (ref. 47). If one assumes that a constant heat input is necessary to induce damage in a given material, then the heating rate must vary inversely with the duration of the pulse. Since the heating rate is proportional to the input power density, the power density and thus the threshold field will also exhibit an inverse pulse length dependence. It is also

possible to suggest that there is a maximum pulse length for which the inverse pulse length dependence is valid. For pulse lengths greater than electron recombination times, an increase in the energy of the laser pulse is necessary to overcome the losses in the electron density due to electron recombinations. Thus one would expect, if not a leveling off, at least a decrease in the inverse pulse length dependence.

Finally, although the tacit assumption has been made that linear absorption can be neglected, the proposed model can be used to indicate the expected behavior of threshold fields on linear absorption. Quite simply, the linear absorption of the laser beam by the dielectric enters directly into the heating rate of the lattice. Thus one would expect that an increase in linear absorption would result in a decrease in the threshold field for laser-induced damage.

c. Alternative Theory

Consider a collection of N atoms per cubic centimeter. Let an electric field $E = E_o e^{j\omega t}$ be incident upon the material. Further consider the interaction of this field with an average optical electron on a typical atom in the collection. The motion, in the classical charged particle on a spring model, of the electron is given by solution of the phenomenological equation of motion

$$m(\ddot{x} + \gamma\dot{x} + \omega_o^2 x) = F = q_e E_\ell \tag{44}$$

where γ is an effective damping or friction coefficient, ω_o is the natural oscillation frequency, x is the displacement, the dot denotes differentiation with respect to time, F is the applied force, and the subscript ℓ denotes local field at the atom. Since E varies sinusoidally the displacement will oscillate at the driven frequency and substituting $x = x_o e^{j\omega t}$ into equation (35) yields

$$x = \frac{q_e/m}{-\omega^2 + j\gamma\omega + \omega_o^2} E_\ell \tag{45}$$

The induced dipole moment of an atom $\vec{p}$ is $q_e\vec{x}$ thus

$$\vec{p} = \frac{q_e^2/m}{-\omega^2 + j\gamma\omega + \omega_o^2} \vec{E}_\ell \tag{46}$$

For linear, isotropic media the polarization is proportional to the applied field with constant of proportionality $\alpha(\omega)$, the atomic polarizability. Thus we write

$$\vec{p} = \varepsilon_0 \alpha(\omega) \vec{E}_\ell \tag{47}$$

Then using equation (46) we obtain

$$\alpha(\omega) = \frac{q_e^2/m\ \varepsilon_0}{-\omega^2 + j\gamma\omega + \omega_0^2} \tag{48}$$

This simple expression is quite close to the rigorous expression obtained from quantum mechanical considerations and, in fact, can be transformed by only a few modifications into the more correct form. The differences in the classical approach and the quantum mechanical are that each atom has not one natural frequency of oscillation but several natural frequencies ω_k each of which responds to the field with a different damping coefficient γ_k and a different oscillator strength f_k. Equation (48) is transformed by these notions into

$$\alpha(\omega) = \frac{q_e^2}{\varepsilon_0 m} \sum_k \frac{f_k}{-\omega^2 + j\gamma_k \omega + \omega_k^2} \tag{49}$$

The volume polarizability is

$$P = N\alpha(\omega)\varepsilon_0 E_\ell \tag{50}$$

and was used in the formulation of Lorentz as reported by Jackson (ref. 48) to obtain the effective local field, E_ℓ, of an atom imbedded in an isotropic medium where a macroscopic field E exists. For fields whose wavelength is much longer than the spacing between atoms the local field of the atom in an isotropic medium is

$$E_\ell = E + \frac{P}{3\varepsilon_0} \tag{51}$$

Combining equations (50) and (51) results in the Clausius-Mosotti or Lorentz-Lorenz formula

$$3\,\frac{n^2-1}{n^2+2} = N\alpha(\omega) \tag{52}$$

where n is the macroscopically averaged quantity, the refractive index.

Now equation (45) can be rewritten as

$$x = \frac{\varepsilon_o \alpha(\omega)\, E_\ell}{q_e} \tag{53}$$

or by using equation (52) this becomes

$$x = \frac{n^2-1}{n^2+2}\,\frac{3(\varepsilon_o)}{Nq_e}\,E_\ell \tag{54}$$

as the relationship between the displacement of an electron and the local field E_ℓ.

Rewriting this expression in terms of the macroscopic field by the Lorentz local field correction yields

$$E = \frac{N}{n^2-1}\,\frac{q_e}{\varepsilon_o}\,x \tag{55}$$

To obtain the threshold for laser-induced damage, one must account for the fact that a critical free electron density of N_c cm^{-3} must be obtained by the field acting on the atoms and one must decide a reasonable critical displacement, x_{cr} beyond which the electron is "freed" from the atom.

If a given total energy is required to ionize every atom in the focal region then only a portion $N_c/N(cm^{-3})$ will be required to ionize N_c cm^{-3}. Since the optical electric field scales as the square root of the total energy, equation (55) becomes

$$E_{th} = \frac{N}{n^2-1}\,\frac{q_e}{\varepsilon_o}\,x_{cr}\sqrt{\frac{N_c}{N}}. \tag{56}$$

Physical arguments can now be used to obtain an order of magnitude estimate for the critical displacement x_{cr}. A lower limit can be obtained from the arguments of Wunsch (ref. 49). He shows that the electric dipole moment of an atom under the action of an applied field does not saturate until the electron is displaced 0.75 - 1.0 Å for most optical materials. Physically this implies that the restoring force assumed in deriving equation (55) through the electric dipole interaction is valid until saturation occurs and thus that the electron is still intimately attached to the atom. An upper limit for x_{cr} can be obtained by observing that on the average an atom in a solid is separated from its nearest neighbor by a distance

$$\sigma_s = N^{-1/3} \tag{57}$$

For ordinary materials this distance corresponds to 2 to 3 Å. It is not therefore unreasonable to assume that when an electron is half way between two atoms it is essentially liberated. Thus the critical distance becomes

$$x_{cr} \approx \frac{\sigma_s}{2} \tag{58}$$

which is consistent with the lower limit described above.

The final expression for the threshold electric field in terms of material properties then becomes

$$E_{th} = \frac{N}{n^2-1} \frac{q_e}{\varepsilon_o} \frac{N^{-1/3}}{2} N^{-1/2} \cdot \sqrt{N_c\ m^{-3}}\ \text{V/m} \tag{59}$$

or combining terms

$$E_{th} = \frac{N^{1/6}}{n^2-1} \frac{q_e}{3\varepsilon_o} \cdot \sqrt{N_c\ m^{-3}}\ \text{V/m} \tag{60}$$

It will prove instructive later to write equation (60) in terms of the average separation as

$$E_{th} = \frac{\sigma_s^{-1/2}}{n^2-1} \frac{q_e}{2\varepsilon_o} \sqrt{N_c\ m^{-3}}\ \text{V/m} \tag{61}$$

To obtain an order of magnitude value for the predicted threshold field the quantity 10^{18} cm^{-3} (10^{24} m^{-3}) is substituted for the critical electron density N_c in equation (61) to obtain

$$E_{th} = \frac{9.05 \times 10^3}{\sqrt{\sigma_s}\,(n^2-1)} \text{ MV/cm} \qquad (62)$$

As will be shown below, equation (62) adequately models the behavior of a variety of materials subjected to damaging laser irradiation. Equation (62), however, was developed to explain laser-induced damage in the bulk of materials. Because the experimental portion of this study dealt with surfaces of materials, additional considerations must be taken into account to make equation (62) directly applicable to this report.

Surfaces introduce additional features such as contamination, surface finish, and roughness. A basic assumption in applying equation (62) to surfaces is that the process of laser-induced damage is the same for surface and bulk regions of dielectrics. For a perfect surface the average atomic spacing and the surface roughness should correspond directly. In such an event, one would expect that the surface and bulk threshold fields would be the same. Thus, equation (62) is directly applicable for perfect surfaces. Equation (62) is still of use--lacking perfection but possessing similarity. If, indeed, the process of laser-induced damage is the same for surfaces and bulk, then a set of different materials with identical physically realizable surface finishes (in terms of roughness and freedom from contamination) will still scale in damage threshold with equation (62). One would expect imperfect surfaces to exhibit damage thresholds less than those of the corresponding bulk materials, but the relative values between materials should still hold. The problem encountered is one of a lack of similarity. That is, the surface of the several materials tested in this study were not identical.

In a study of laser-induced damage as a function of surface roughness House (ref. 50) showed that for a given material the threshold electric field for laser-induced damage scaled with surface roughness, σ, as

$$\sqrt{\sigma}\, E_{th} = \text{constant} \qquad (63)$$

Then for two samples with surfaces roughness σ_1 and σ_2, the threshold fields E_1 and E_2 are related by

$$\sqrt{\frac{\sigma^2}{\sigma_1}}\, E_1 = E_2 \tag{64}$$

House found that this relationship held for the ratio of the surface threshold of a material with roughness σ to the bulk threshold of that material with average atomic spacing σ_s as

$$\sqrt{\frac{\sigma}{\sigma_s}}\; E_{surface} = E_{bulk} \tag{65}$$

Then to compare materials with different surface roughnessas, one chooses a standard roughness value, σ_{STAND} and multiplies the measured threshold field by the square root of the roughness ratio

$$\sqrt{\frac{\sigma}{\sigma_{STAND}}}\, E = E_{STAND} \tag{66}$$

where E, σ are the measured threshold field and surface roughness, and E_{STAND} is the threshold field for a sample with the standard roughness. Thus the material-to-material variation of the threshold electric field can be isolated by comparing the various materials at an equivalent standard roughness.

As a final topic consider the pulse length, spot size, and laser frequency dependence of laser-induced damage. These are contained in the details of the plasma heating by the laser pulse. To calculate the heating rate of a plasma, suppose that laser power density S is incident upon a plasma of thickness dx with absorption coefficient K. Then by Beer's Law the power density after traversing the plasma is $S\, e^{-Kdx}$. The absorbed energy then is

$$dE = \Delta S A dt = (S - Se^{-Kdx})Adt \tag{67}$$

where A is the area of the laser beam, ΔS is the change in S in traversing a distance dx of the plasma, and dt is a differential element of time. Expanding the exponential for small Kdx yields

$$dE = S[1 - (1 + Kdx + \ldots)]Adt \tag{68}$$

or

$$dE \approx KS\ dx\ Adt \tag{69}$$

Then the heating rate is given by

$$\frac{dQ}{dt} = \frac{dE}{dt} = Adz\ K\ S \tag{70}$$

A given material will fail when the total heat input to the lattice is sufficient to cause localized melting. For a given material then the total heating is a constant and equation (70) yields

$$t_p \frac{dQ}{dt} = \text{constant} = t_p\ Adx\ K\ S \tag{71}$$

If the thickness of the plasma, dx, is constant at threshold for a specific material, then equation (71) can be used to investigate the pulse length and spot size dependence of laser-induced damage. The absorption in electronic plasmas is governed by the free-free or inverse Bremsstrahlung process which has an absorption coefficient given by Johnston and Dawson (ref. 51) of

$$K = \frac{3.08 \times 10^{-7}\ Z\ N_e^2\ \ell n\Lambda(\omega)}{\omega^2\ (kT_e)^{3/2}} \frac{1}{(1 - \omega_p^2/\omega^2)^{1/2}} \tag{72}$$

where kT_e is in eV, $\Lambda(\omega) = V_T/\omega_p\ p_{min}$. Here, Zq_e is the ionic charge, T_e is the electron temperature, N_e is the electron number density, V_T is the thermal velocity of the electrons, p_{min} is the minimum impact parameter for electron-ion collisions [$p_{min} \simeq$ maximum of Zq_e^2/kT or $(\hbar/mkT)^{1/2}$].

To quantify equation (72) it was shown by David et al., (ref. 43) that both N_e and T_e obeyed a power-law dependence with laser flux. Fauguignon and Floux (ref. 52) calculated and experimentally verified that $T_e \sim S^{2/3}$. Boland et al., (ref. 53) showed that the expanding plasma obeyed an adiabatic expansion law and verified experimentally that

$$T_e = \text{const } N_e^{2/3} \tag{73}$$

Then

$$\frac{N_e^2}{T_e^{3/2}} \sim S \tag{74}$$

For a given material at a fixed laser frequency and constant spot size, equations (71) and (74) can be used to write

$$t_p S^2 = \text{const} \tag{75}$$

or

$$E = \text{const } t_p^{-1/4} \tag{76}$$

Thus, the threshold electric field varies inversely with the fourth root of the pulse length.

For a given material at a fixed laser frequency and constant pulse duration equations (71) and (74) can be used to write

$$A S^2 = \text{const} \tag{77}$$

or

$$E = \frac{\text{const}}{\sqrt{d}} \tag{78}$$

where d is the diameter of the focal spot of the laser. The limits on the applicability of equations (76) and (78) will now be considered.

There are probably a lower and upper limit on the pulse duration for which equation (76) is expected to hold. Laser frequencies are of the order of $10^{14} - 10^{15}$ sec^{-1}. Such atomic processes as tunneling require about 10^{-14} sec. Thus, equation (76) will probably not hold for pulse durations less than the order of 10^{-14} sec. This is about two orders of magnitude less than the shortest pulse durations currently available, and thus the conjecture cannot now be

tested. Because equation (76) was derived by ignoring losses, it is clear that loss mechanisms will invalidate the predicted behavior. A principle loss mechanism is electron recombination. Since recombination times are of the order of microseconds, equation (76) is not expected to hold for pulse durations much greater than a few microseconds. Thus, the lower time limit would appear to be process dominated while the upper time limit is loss dominated.

The spot size dependence will also exhibit a range of applicability. For small spot sizes, losses due to thermal diffusion become important. The heat added to the lattice diffuses out of the focal volume in a time on the order of $t_d = r^2/D$, where D is the thermal diffusivity and r is the radius of the focal spot. Losses by diffusion then become important when the pulse length, t_p, is of the order of the diffusion time. For a 40-nsec pulse duration and a typical diffusivity of 1 to 10 cm^2/sec, this implies that when the spot diameter is less than about 1 micrometer thermal diffusion losses begin to negate the dependence given in equation (76). Furthermore, when the spot size becomes large enough a minimum laser intensity is reached such that further decreases in the intensity are not possible while still maintaining a damaging level of irradiation. Thus, there is a minimum laser intensity which is necessary to produce a critical number density of free electrons sufficient to initiate damage. For an estimate of the maximum spot size for which equation (78) holds, consider that an intensity level typical of damage in the absence of absorption (~10^9 $watts/cm^2$) is the minimum intensity level sufficient to produce about 10^{18} $electrons/cm^3$. A level of 10^{17} $electrons/cm^3$ is probably too low to initiate intrinsic damage, thus an increase in the typical 100 μm spot size by a factor of 10 to 1 mm will probably result in little decrease in threshold intensity.

SECTION IV

RESULTS

Internal consistency is lacking in the many published reports on laser-induced damage. One of the major causes is the many ways in which the raw data collected by the investigators is reduced to the final form. To obviate the possibility that this report will contain irreproducible results, the collection and transformation of the raw data into final form will now be discussed.

1. RAW DATA

For this study the variables of interest included laser energy, laser pulse duration, focal spot size, and whether damage occurred on a given shot. The first and last of these has been discussed above under active diagnostics and will not be rediscussed here except to note that on each irradiation either a "damage" or a "no damage" was recorded along with the total energy incident upon the target. The focal spot size was measured using the technique described in section II.2, Parameterization. This parameter was rechecked periodically throughout the study and was found consistent to within ±3.5 percent. The temporal shape of the laser pulse was recorded on a fast-sweep oscilloscope,* and the pulse duration was taken as the time separation between the trace at half the maximum deflection.

2. DATA REDUCTION: THE ENERGY THRESHOLD

A method for determining the energy which, for a given sample, can be reported as the energy threshold was developed. It is a method which does not rely on subjective judgement, and thus it must therefore remove one of the largest uncertainties in experimental work. Before the final method to be described here was decided on, a total of 1438 shots were taken on 20 samples to assist in the determination of an objective method for obtaining a damaging energy threshold value for each sample. It should be mentioned here that there is a body of evidence collected by Bass and Barrett (ref. 41), principally, and Milam and co-workers (ref. 46) that suggest that a damage threshold does not exist but that the damage process is entirely probabalistic. Their view is

*Tektronix Model 519

not unrealistic and in fact the damage thresholds reported here should correspond roughly to their P(0.5) point or the energy at which the probability is 0.5 that damage will occur on a single shot. Figure 16 illustrates the method used in determining energy threshold. Each shot is represented by an energy and a +1 or -1 corresponding to damage or no damage, respectively. The highest energy event which did not cause damage is then connected with a line to the lowest energy event which did cause damage and the energy at which the line crosses the zero axis is defined to be the energy threshold. This method removes subjective judgement from the report of the damage threshold. By effectively averaging the highest no-damage and the lowest damage, the effect of either taken singly is moderated. There are those who use a similar method but report only the highest energy which did not cause damage as the threshold, but this is much more sensitive to the unusual endpoint than is the averaging method espoused here. The number of shots which one would need to take to use only the highest no-damage would have to be many times the 25 shots on each sample used in this study. In the 1438 shots in 20 samples alluded to above, it became apparent that 150 shots per sample would not enable one to select a damage threshold with more accuracy than the 25 shots used here and was thus not economically justified. However, very different results were possible if less than 20 shots were used. In particular 15 and 12 shots could vary from the results of 25 to 150 shots by 25 to 30 percent.

The ratio R was computed as the lowest damage event divided by the highest no-damage event. This ratio was used as a measure of the uncertainty in the result by computing

$$\frac{1 - R}{2} = \% \text{ uncertainty} \tag{79}$$

In most cases the uncertainty in energy threshold ranged from ±15 percent to ±20 percent, reflecting the fact that the energy at which the sample will damage on the first shot every time is usually at least twice the energy at which the sample will never damage. Thus, unless one can take the several thousand shots per sample needed to accurately map the probability to damage versus energy, there does not seem to be a better method for determining a "damage threshold."

3. DATA REDUCTION: THE ELECTRIC FIELD THRESHOLD

In this report the threshold values which are listed are the optical electric field thresholds. From equation (4) we see that the average electric

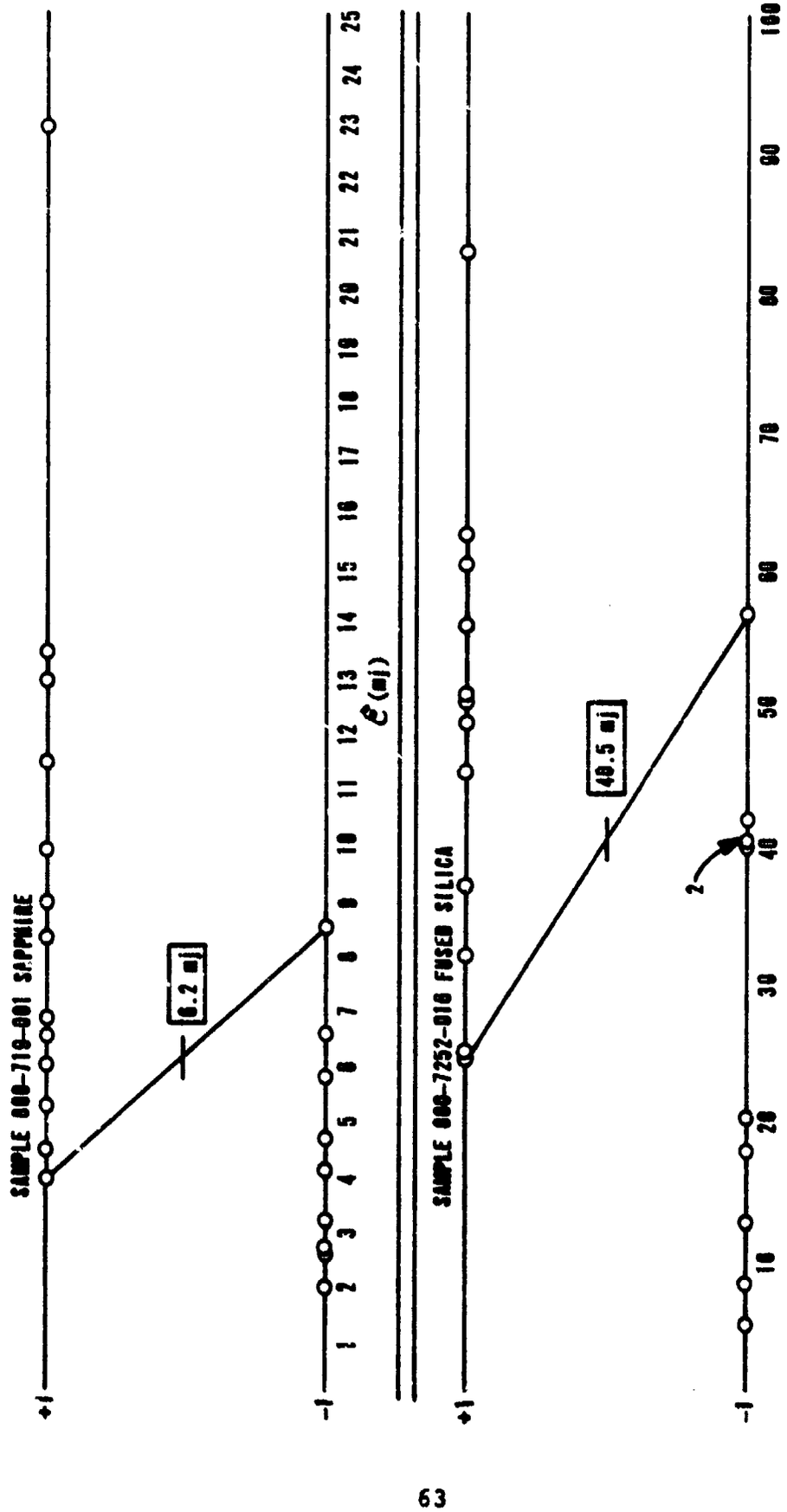

Figure 16. Method Used to Determine Energy Threshold for Damage

field is related to the average power density which, for a Gaussian temporal pulse, is given by

$$S = \frac{E}{t_p \cdot \text{area}} \tag{80}$$

where E is total energy, t_p is the full pulse width at half maximum intensity and the area of the focal spot was taken as that lying within a radius at which the intensity fell to half the maximum intensity. For this study the half-power point had a diameter of 104 μm. Although the optical electric field is reported, it was the energy threshold which was experimentally determined. The electric field was then obtained using the average pulse width (measured for the particular sample) to calculate the average power density from equation (80) and the field from equation (4). The pulse length variation was ±5 percent. Shots which had overly long pulse widths were discounted and not included in the data reduction. Less than 2 percent of the total shots were retaken because of temporal pulse width variation. Variation of the pulse duration usually indicated a slight misalignment. Realignment brought pulse duration back to normal.

From the continuity of the tangential electric field the expression

$$E = \frac{2n}{n+1} 19.4 \sqrt{S} \tag{81}$$

gives the field at the surface of a dielectric with refractive index n. This also is the field at the surface of a nonlossy dielectric film placed on the surface in integral multiples of a half wavelength optical thickness. Except in the case in which a film has a lower refractive index than the substrate, it also represents the peak electric field in half-wave films such as tested in this study. It is this calculated field which is reported as the threshold values in this report.

4. DATA REDUCTION: ACCURACY OF RESULTS

The measured energy has an uncertainty of ±7 percent due to the 4 percent uncertainty in the pyroelectric detector and the ±5.5 percent uncertainty in the calorimeter used to calibrate the pyroelectric detector. The average uncertainty in threshold energy was ±19 percent. With a pulse width uncertainty of 5 percent and an uncertainty in the focal spot diameter of 3.5 percent the electric field

was known for a given shot to ±9.5 percent. Folding in the 19 percent for the threshold energy results in a total uncertainty in the threshold electric field of ±13.4 percent.

5. TEST OF THEORY VERSUS PREVIOUS RESULTS

Sufficient information is contained in the papers by Smith (ref. 54), DeShazer et al., (refs. 11, 15) Austin et al., (ref. 14), and Fradin et al., (ref. 17) to enable one to compare their experimental results against theoretical predictions from equations (55), (62), (76), and (78). For a given laser with fixed frequency and pulse width, equations (55) and (62) should give the relative damage thresholds for various materials. It is desirable to compare the two theoretical expressions in an attempt to identify the major contribution to the expected behavior. In so doing, the critical displacement x_{cr} in equation (55) is simply taken as a constant and the experimentally determined threshold fields are then compared to N/n^2-1. For the full expression given in equation (62), the average atomic spacing, σ_s, is just the cube root of the inverse of the atomic number density.

The experimental study detailed in this report employed a laser with a 40-nsec pulse width. However, it is interesting to compare the pulse length dependence predicted by equation (76) with electric field thresholds experimentally determined at five different pulse lengths. To this end, it will be demonstrated that the process of laser-induced damage at 30 psec is essentially the same as the process at 40-nsec pulse durations. The validity of equation (76) will then be tested directly for NaCℓ at five pulse durations from 15 psec to 10 nsec.

The spot size dependence of laser-induced damage will be considered as the final comparison of the theory with previously published results.

In the tables and graphs which follow, the field is the threshold optical field for laser-induced damage.

First consider the data gathered by DeShazer and co-workers. They placed various thin films on BSC-2 glass substrates. The data have been collected in table 1. These data are plotted in figures 17 and 18. The least square fit to the data has a root mean square variation of ±20.8 percent for E_{th} compared to the full expression and ±29.9 percent when compared to only N/n^2-1. Note that the thicker films fail at lower fields, a result attributable to slight

absorption in the thin films according to an industry source (ref. 29) but absorption which has not been quantified.

Table 1

DAMAGE THRESHOLDS FOR FILM
(adapted from reference 11)

Material	Thickness	Index	Field (MV/cm)	$\frac{N}{n^2-1}$ (10^{28} m^{-3})	$\frac{9.05 \times 10^3}{\sqrt{\sigma_s}(n^2-1)}$ (MV/cm)
Zns	$\lambda/4$	2.35	0.208	1.12	1.22
TiO_2	$\lambda/4$	2.28	0.513	2.07	1.43
ZrO_2	$\lambda/4$	1.975	0.569	2.78	2.05
SiO_2	$\lambda/4$	1.449	1.656	6.02	5.23
TiO_2	$\lambda/2$	2.28	0.378	2.07	1.43
ZrO_2	$\lambda/2$	1.975	0.454	2.78	2.05
SiO_2	$\lambda/2$	1.449	1.54	6.02	5.23
TiO_2	$3\lambda/4$	2.28	0.369	2.07	1.43

The data collected by Putman (ref. 56) and presented by Austin et al., (ref. 14) are presented next. The material consisted of half wavelength (at 1.06 μm) thick films comprised of vapor-phase mixtures of ThF_4 and ZnS. The da are collected in table 2 indicating the percentage of each constituent in the mixture.

Table 2

DAMAGE THRESHOLDS FOR VAPOR-PHASE MIXTURES
(adapted from reference 14)

Zns:	ThF_4	Index	Field (MV/cm)	$\frac{N}{n^2-1}$ (10^{28} m^{-3})	$\frac{9.05 \times 10^3}{\sqrt{\sigma_s}(n^2-1)}$ MV/cm
0:	100	1.5	0.65	4.92	4.55
23:	77	1.59	0.429	3.86	3.69
31:	69	1.72	0.406	2.97	2.88
50:	50	1.91	0.34	2.12	2.12
80:	20	2.15	0.223	1.46	1.53
90:	10	2.33	0.223	1.17	1.25
100	0	2.36	0.175	1.11	1.21

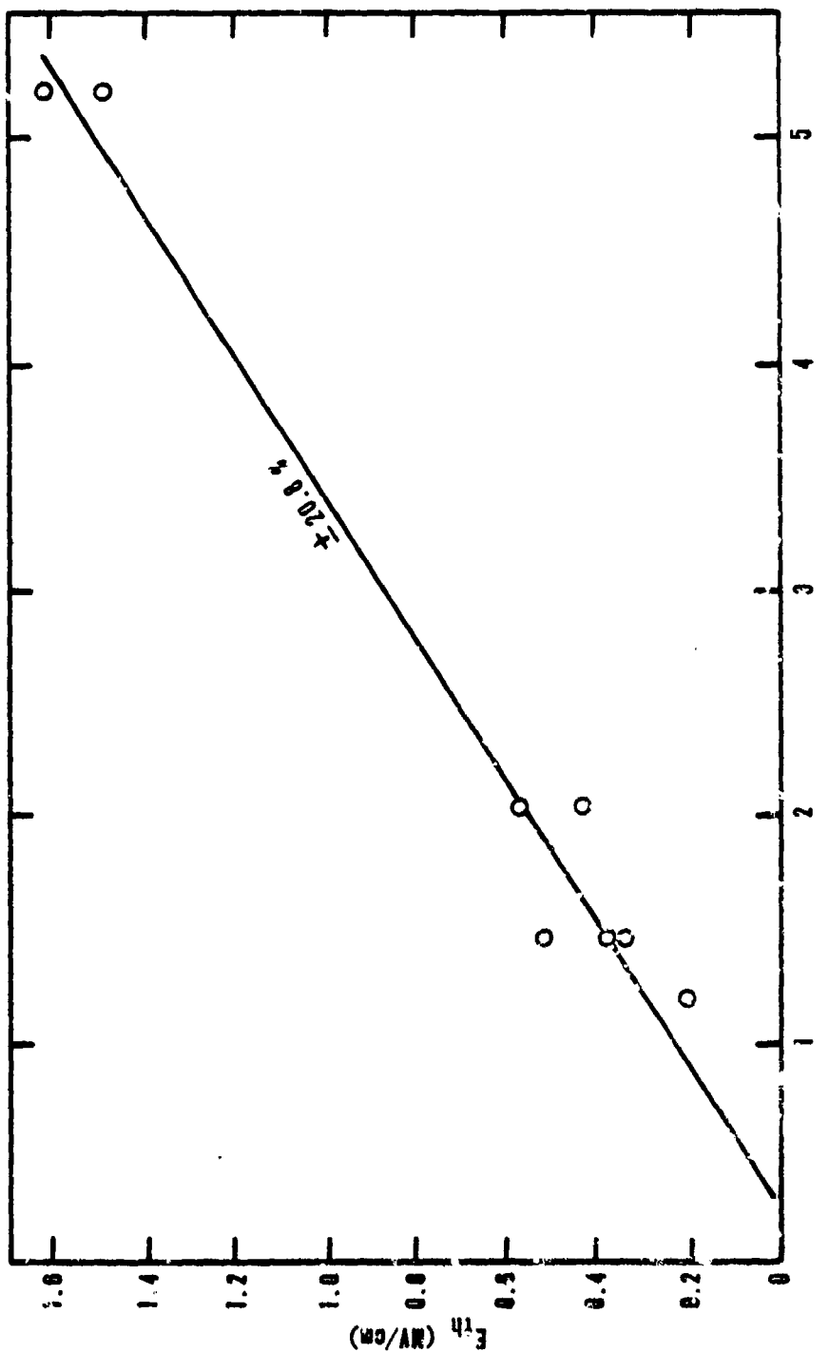

Figure 17 Experimental Threshold Field versus Predicted Threshold Field for Films of Differing Thickness

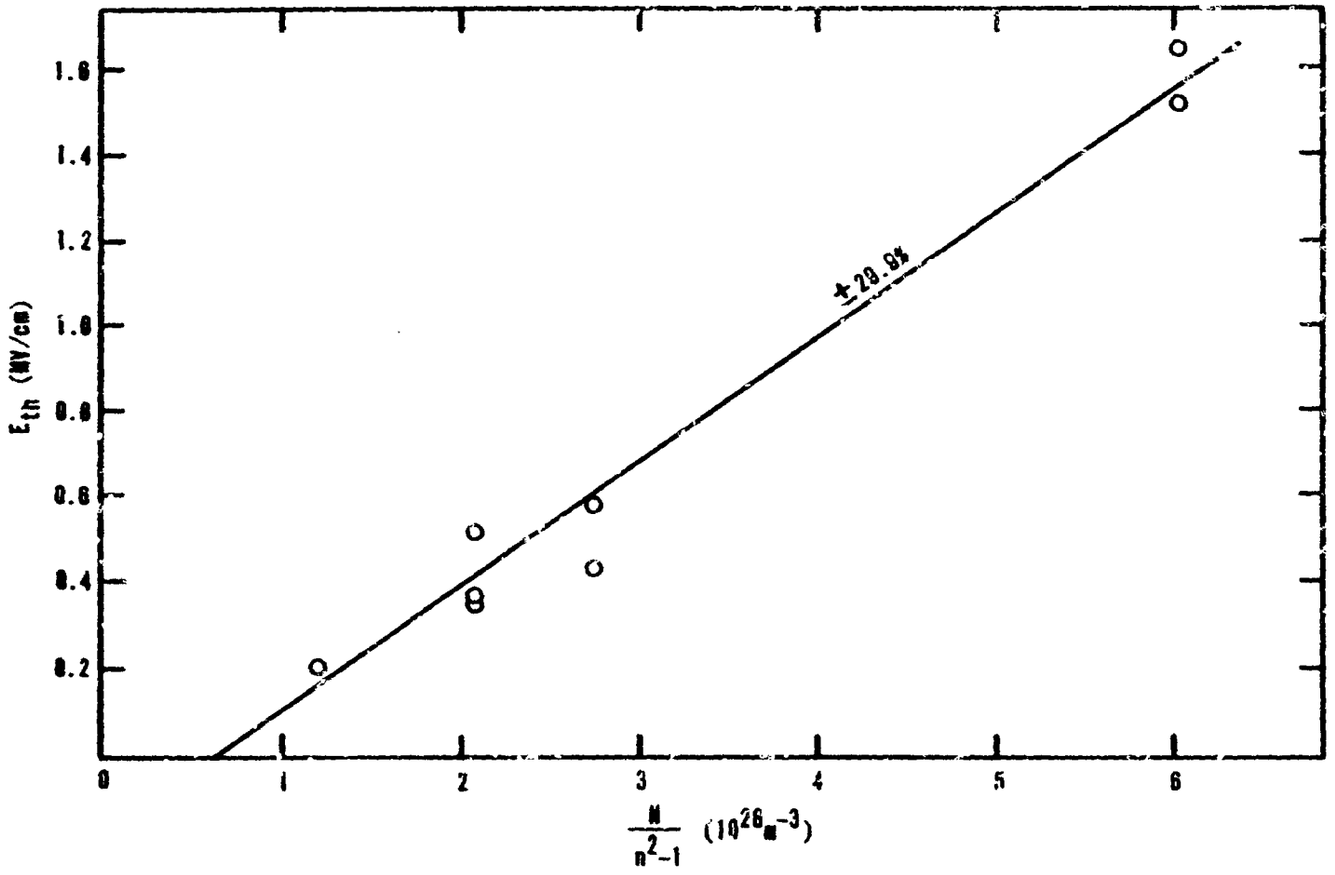

Figure 18. Experimental Threshold Field versus N/n^2-1 for Films of Differing Thickness

These data are plotted in figures 19 and 20. In each case the fit to a least square is very good, being ±7.5 percent in the former and ±7.2 percent in the latter.

The next previously published data considered are those collected by Fradin and co-workers (ref. 17). They damaged the bulk of 11 alkali halides at 1.06 μm. Table 3 is a compilation of the data.

Table 3

BULK DAMAGE THRESHOLDS FOR ALKALI HALIDES WITH 4.7 NSEC PULSES
(adapted from references 16, 17)

Material	Index	Field (MV/cm)	$\frac{N}{n^2-1}$ (10^{28} m^{-3})	$\frac{9.05 \times 10^3}{\sqrt{\sigma_s}(n^2-1)}$ MV/cm
NaI	1.74	1.14	1.46	2.48
NaBr	1.62	1.54	2.31	3.22
NaCl	1.53	2.3	3.32	4.02
NaF	1.32	3.77	10.63	7.99
KI	1.64	0.62	1.32	2.85
KBr	1.54	0.87	2.04	3.64
KCl	1.49	1.31	2.54	4.19
KF	1.36	2.99	6.12	6.51
RbI	1.63	0.92	1.21	2.85
RbBr	1.54	1.27	1.78	3.55
RbCl	1.48	1.54	2.32	4.18

These data are plotted in figures 21 and 22. The least squares fit to the full expression gives a deviation of ±20.1 percent, while the fit to N/n^3-1 is good to ±21.9 percent, the latter being close to the quoted experimental precision of ±20 percent (ref. 17).

Before examining the pulse length dependence of laser-induced damage, it is appropriate to ask whether the processes at 30 psec are the same as the damage processes at 40 nsec. The data collected by Smith (ref. 54) answer this question. Smith determined the threshold electric field for a variety of substances using a 30-psec Nd^{+3} in YAG laser operating at 1.06 μm. The variation of the laser-induced damage threshold as a function of material tested followed the

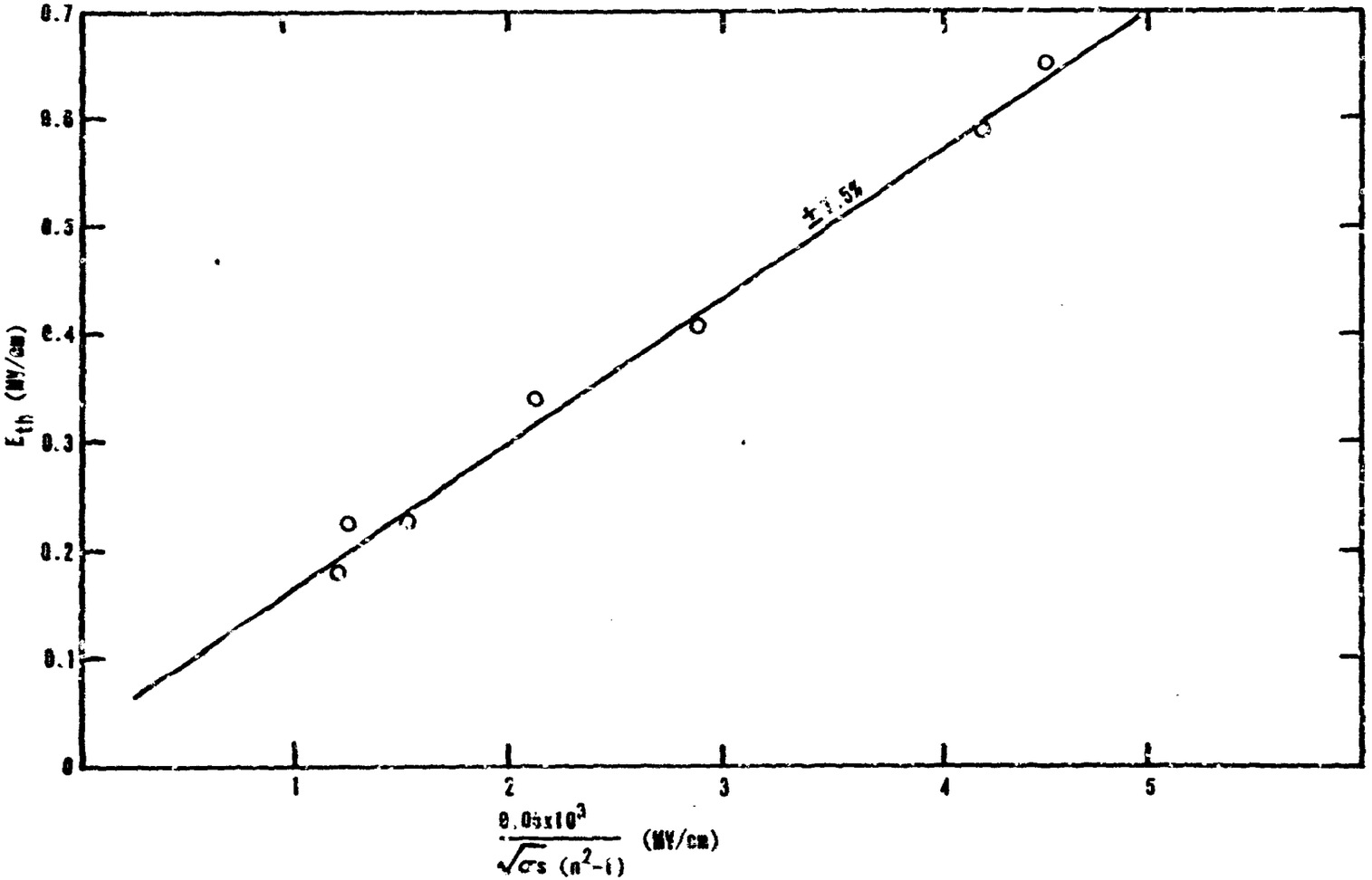

Figure 19. Experimental Threshold Field versus Predicted Field for Vapor-Phase Mixture Films

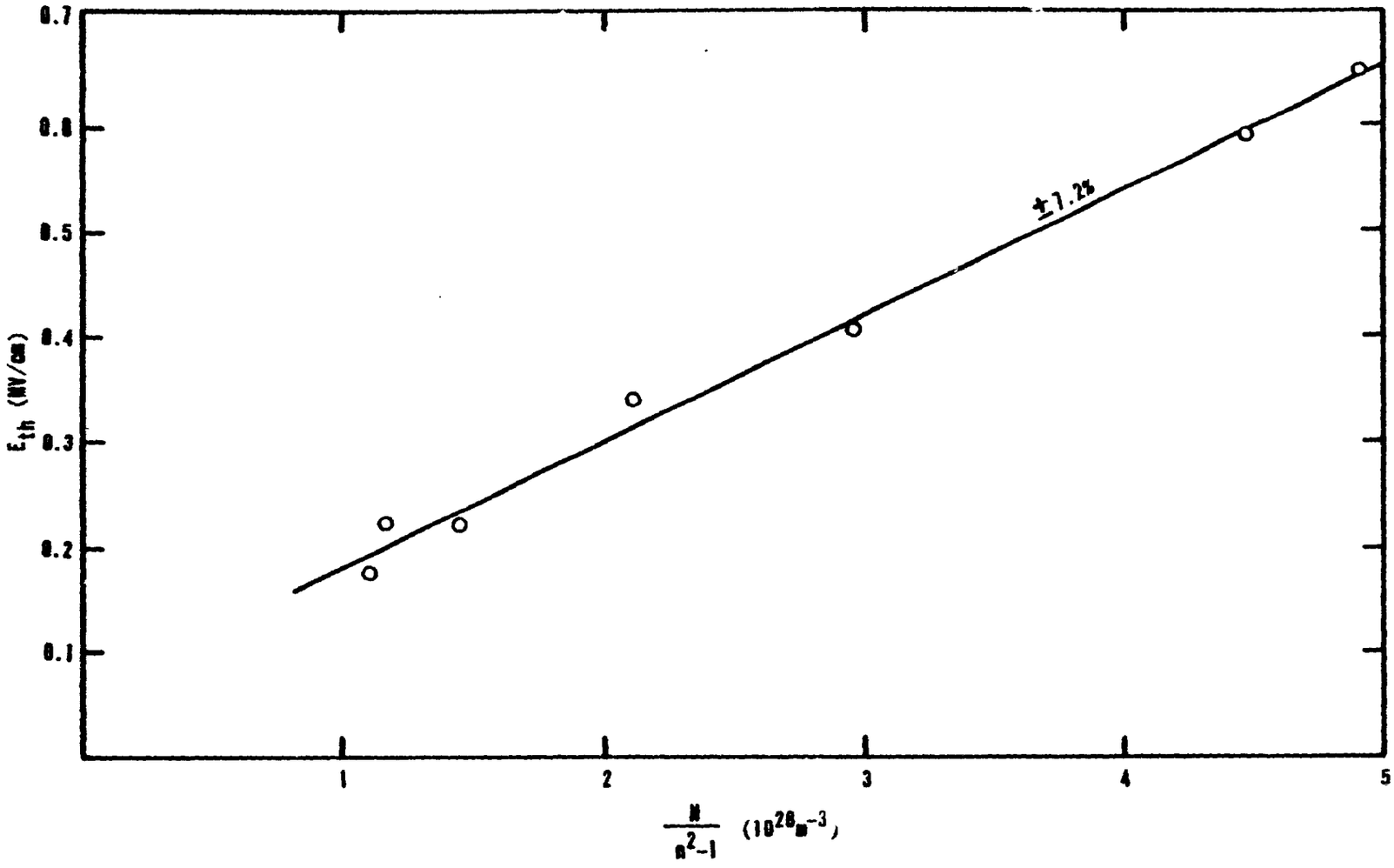

Figure 20. Experimental Threshold Field versus N/n^2-1 for Vapor-Phase Mixture Films

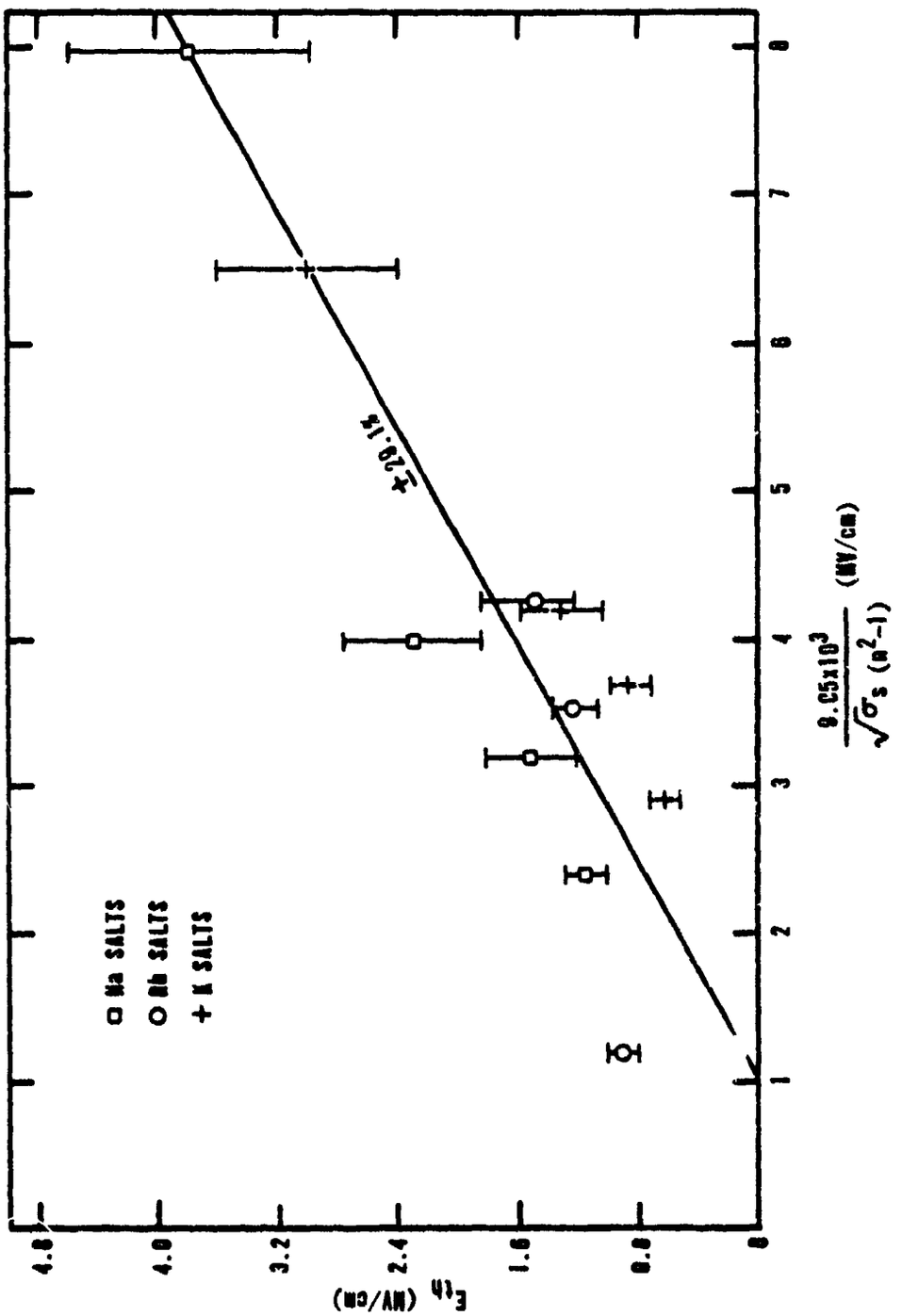

Figure 21. Experimental Bulk Threshold Field versus Predicted Field for Alkali Halides

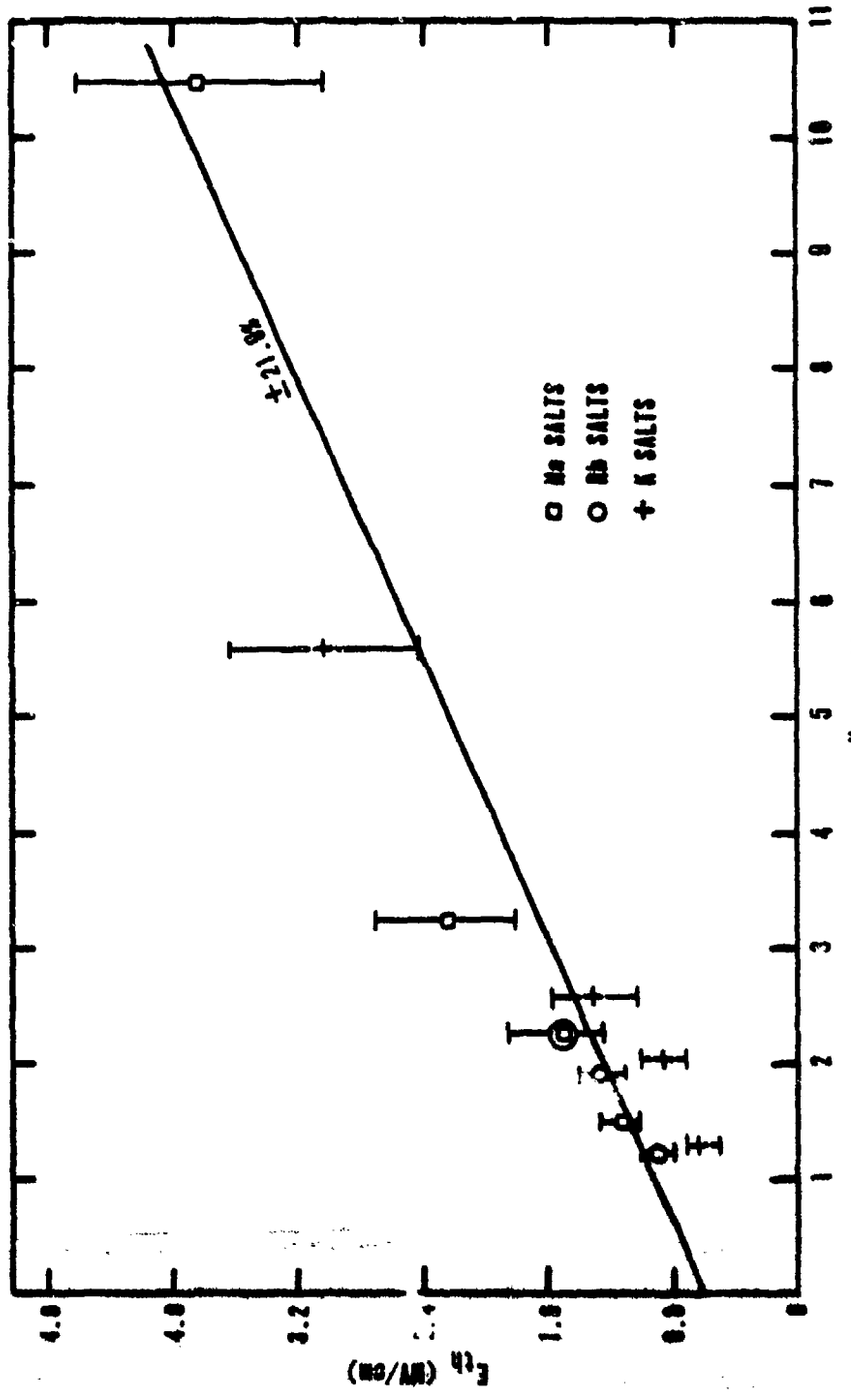

Figure 22. Experimental Bulk Threshold Field versus N/n^2-1 for Alkali Halides

functional form given in equation (62). This is taken as an indication that the damage process does not change in its essential aspects as the pulse duration is shortened from 40 nsec to 30 psec. The essential difference is that the threshold fields are nearly an order of magnitude higher at 30 psec than at 40 nsec. This variation will be tested against the behavior predicted by equation (76).

First consider the material variation of the laser-induced damage threshold at 30 psec pulse duration. Smith's data (ref. 54) are collected in table 4 and presented in figure 23.

Table 4

BULK DAMAGE THRESHOLDS FOR ALKALI HALIDES WITH 30 PSEC PULSES
(adapted from reference 54)

Material	Index	Field (MV/cm)	$\frac{9.05 \times 10^3}{\sqrt{c_s}(n^2-1)}$
NaF	1.32	10.77	7.99
NaCl	1.53	7.34	4.01
NaBr	1.62	5.67	3.22
KF	1.36	8.34	6.31
KCl	1.49	5.86	4.19
KBr	1.54	5.33	3.64
KI	1.64	5.87	2.85
LiF	1.38	12.24	7.04
RbI	1.63	3.40	2.85

The measured field fits the dependence predicted by the final column in table 4 to ±17.4 percent. Thus, the basic damage mechanism does not change for pulse variations between 30 psec and 40 nsec.

As the next topic in the review of previously published data consider the pulse length dependence predicted by equation (76). These data collected by Smith (ref. 54) and Fradin (ref. 17) can be compared because they used the same equipment to perform their experiments. The data are presented in table 5 and figure 24. Table 5 lists the threshold damage field for each material at the specified pulse durations. The NaCl data are presented in figure 24. The least square fit indicates a dependence of threshold field versus pulse length as E_{th} = Const $t_p^{-0.257}$ which compares favorably with E_{th} = Const $t_p^{-0.25}$ predicted by equation (76). The data fit the line to ±8.5 percent which is remarkably good.

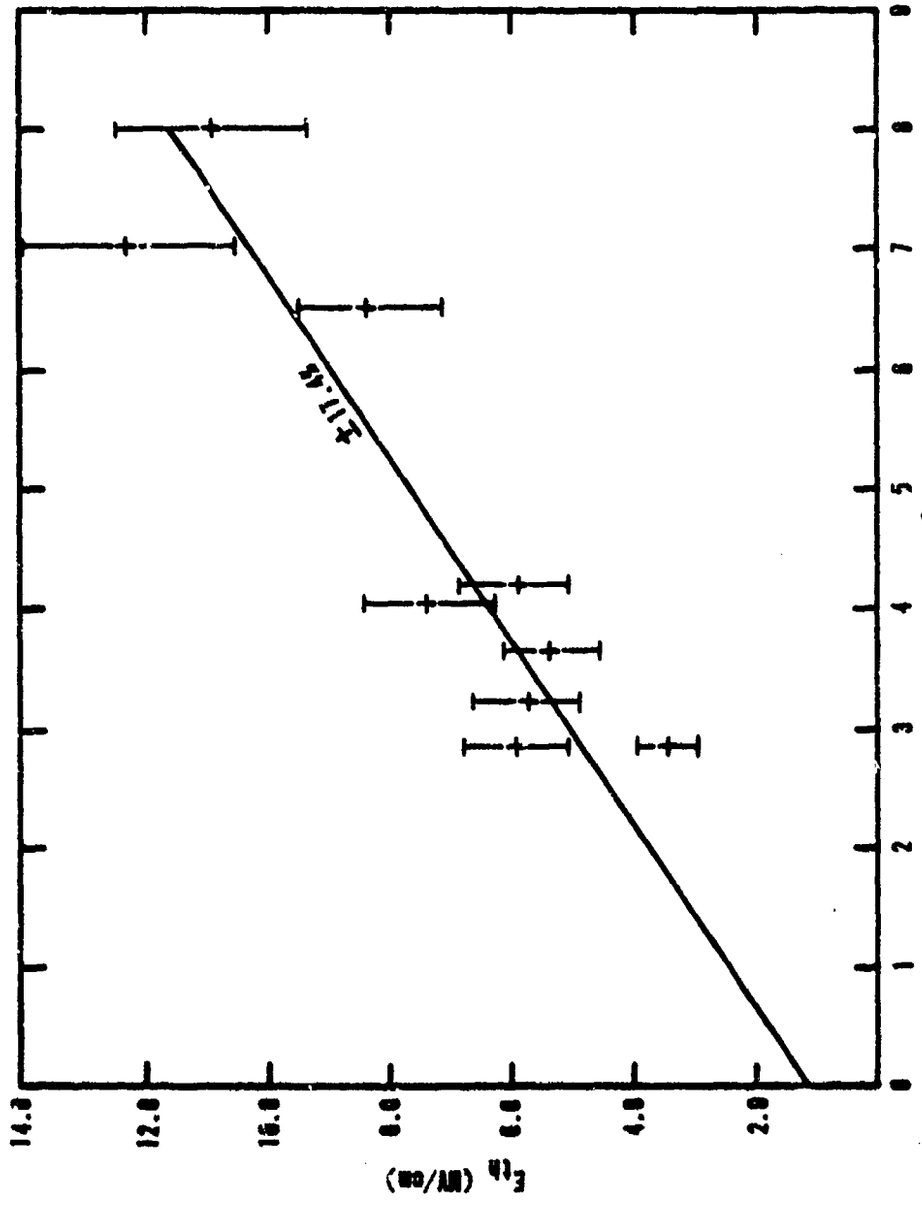

Figure 23. Experimental Bulk Threshold Field versus Predicted Field for Alkali Halides with 30-psec Pulses

Table 5

BULK DAMAGE THRESHOLDS FOR FIVE ALKALI HALIDES AND FUSED SILICA
(adapted from references 16, 17, 54)

	10.3 nsec	4.7 nsec	300 psec	30 psec	15 psec
NaCl	2.1 (MV/cm)	2.3	4.7	7.34	12.4
NaF		3.77		10.77	
NaBr		1.54		5.67	
KF		2.99		8.34	
RbI		0.92		3.40	
Fused Silica		5.2		11.68	

As the final comparison between the theory and previously published results consider the spot size dependence reported by DeShazer et al., (ref. 55). They damaged the surface of single crystal rutile (TiO_2). The focused spot size was varied from 50 μm to 200 μm by using a selection of lenses with various focal lengths. The data are presented in figure 25 as a plot of threshold intensity versus inverse spot size. The agreement between the experimental points and the relationship predicted by equation (78) is 11.1 percent over this range of spot sizes.

6. RESULTS OF THE CURRENT STUDY

a. Thin Films

Surfaces of optical materials do not exhibit damage thresholds as high as their bulk values. To the author's knowledge there has been only one report which claimed that the surface and bulk threshold of a material were measured to be the same (ref. 16). It was shown (ref. 9) that clean optical surfaces exhibited higher damage thresholds than do dirty surfaces. In fact, a piece of dust on an optical surface can absorb laser radiation, and the resulting temperature rise is sufficient to cause localized damage. It was also shown (ref. 56) that particular polishing compounds containing material which is highly absorbent at the laser wavelength will lower the damage threshold. Specifically, jeweler's rouge (iron oxide) lowers the surface threshold for 1.06-μm laser wavelength even though the iron oxide is not present in sufficient quantity to be indicated by Auger spectroscopy. However, even if these two problems of dirt and particulate inclusions are scrupulously avoided, there still remains the problem of surface roughness. A major portion of an effort parallel to the one reported here (ref. 50) was concerned with the evaluation of surface

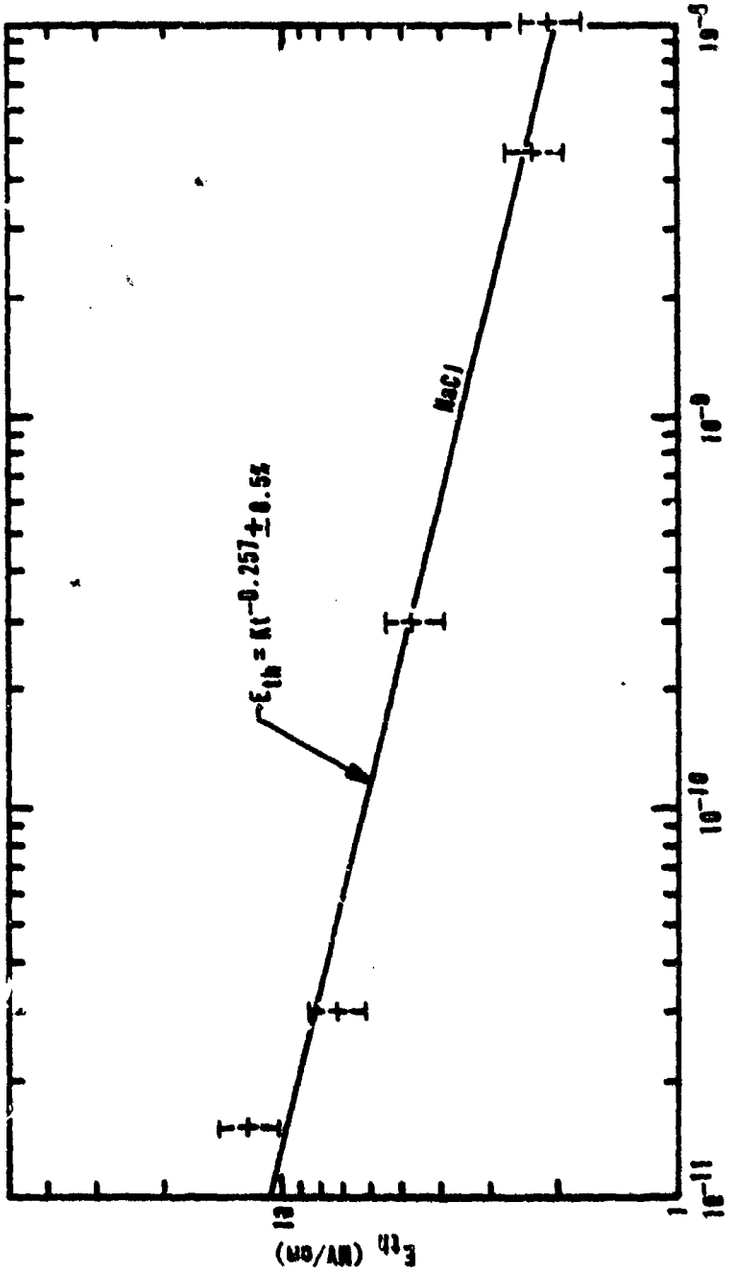

Figure 24. Experimental Bulk Threshold Field for NaCl versus Laser Pulse Duration

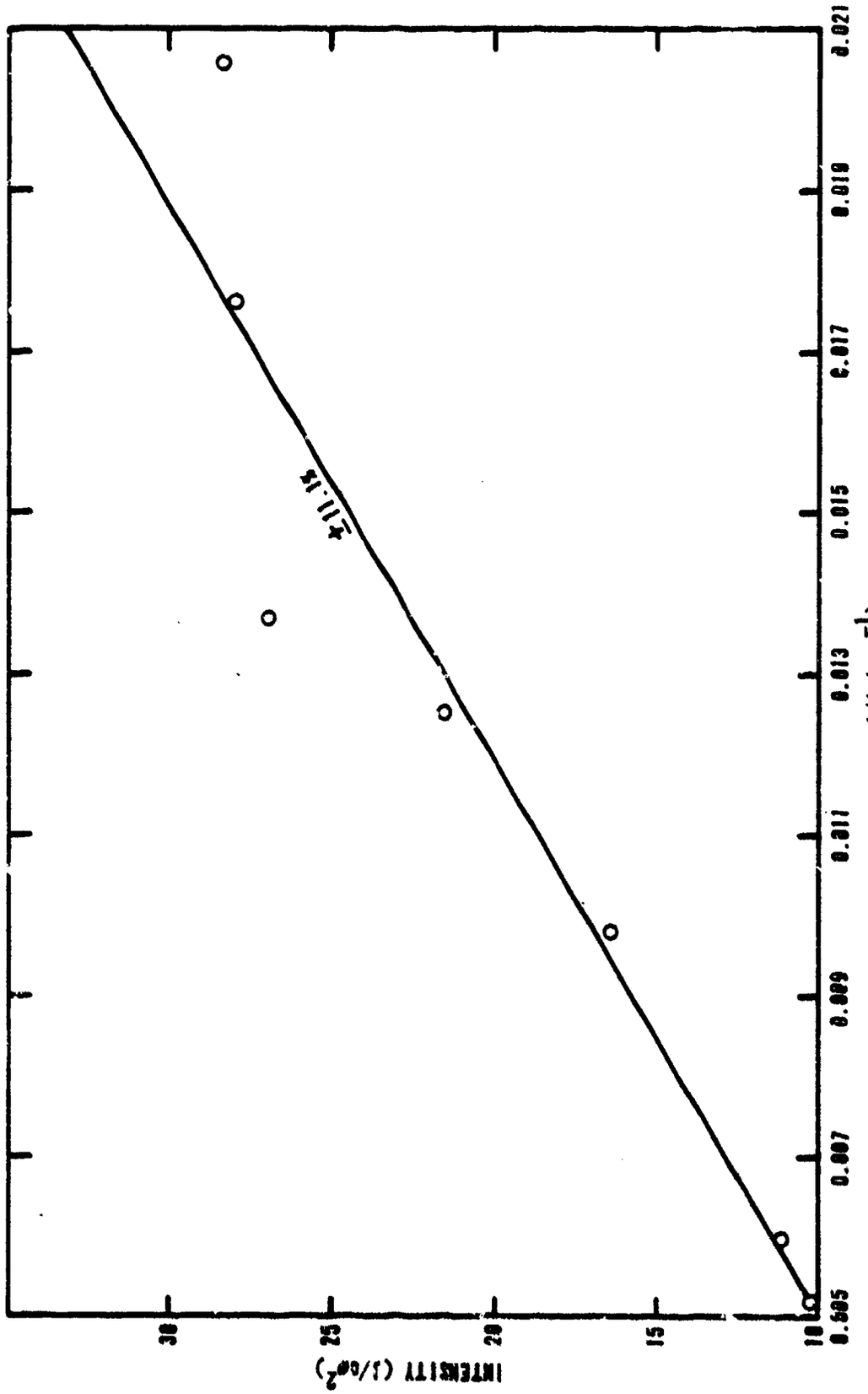

Figure 25. Threshold Intensity versus Focused Spot Size for TiO_2

roughness as it affects surface thresholds to laser-induced damage. In that study a series of fused silica samples with root mean square surface roughness varying over nearly two decades was prepared in triplicate. One of each roughness was left uncoated, one of each roughness was coated with a half wavelength thickness of SiO_2, and one of each roughness was coated with a half wavelength thickness of MgF_2. The results of that study indicated a damage behavior given by

$$\sigma^m E_{th} = \text{constant} \tag{82}$$

for the three experiments. The value of m was 0.61 for the uncoated samples, 0.455 for the MgF_2 coated samples, and 0.42 for the SiO_2 coated samples. So that the intrinsic strength of several optical surfaces can be compared, it is necessary to eliminate the confusing effects of varying surface roughnesses. This can be done by using equation (82) to compare the threshold breakdown fields at a standard roughness. To do so, let σ_k be a standard surface roughness for a particular set of samples. Then if σ_i is the surface roughness of the i^{th} sample in the set, the threshold field for sample i, if it were to have the standard roughness σ_k, is given by

$$E^i_{th}(\sigma_k) = \left(\frac{\sigma_i}{\sigma_k}\right)^m E^i_{th}(\sigma_i) \tag{83}$$

In that which follows, m is taken as 0.5, the average of the experimentally determined values. For the thin film data to be presented, σ_k was arbitrarily taken as 9.8 Å rms, the roughness of the PrF_3 coated sample, while for the bare surfaces a σ_k of 13.5 Å rms is used, it being the MgF_2 roughness.

The thin-film data are presented in table 6 and figures 26 and 27. Again the threshold field is plotted against both N/n^2-1 and $9.05\times10^3/\sqrt{\sigma_s}(n^2-1)$.

The films marked with an asterisk proved inhomogeneous in their spectral reflectivity curves. As such, they are expected to behave in less than an ideal manner. Figure 26 is a plot of $\sqrt{\sigma}\,E_{th}$ versus $9.05\times10^3/\sqrt{\sigma_s}(n^2-1)$. The three inhomogeneous films are indicated by plus signs to mark their positions. All three fell below a least squares fit made without their inclusion. The performance of LiF and MgF_2 in the bare surface data to follow will be particularly revelatory in line with the contention that both LiF and MgF_2 should exhibit considerably higher damage thresholds than did their half-wave films. A similar

Table 6

ROUGHNESS CORRECTED THRESHOLDS FOR 10 HALF-WAVE FILMS ON FOUR SUBSTRATES

Material	Index	σ(Å)	$\sigma^{0.5}$Field (MV/cm)	$\frac{N}{n^2-1}$ ($10^{28}m^{-3}$)	$\frac{9.05\times10^3}{\sqrt{\sigma_s(n^2-1)}}$ (MV/cm)
LiF* on FS	1.38	12.34	0.578	13.356	7.04
MgF_2* on FS	1.377	17.08	1.15	9.705	6.72
SiO_2 on FS	1.449	17.4	1.18	6.02	5.24
SiO_2 on BK-7	1.449	20.8	1.09	6.02	5.24
BaF_2* on FS	1.45	12.3	0.554	4.515	4.98
ThF$_4$ on FS	1.49	12.3	0.990	5.045	4.66
CeF_3 on FS	1.55	12.9	0.71	4.636	4.09
PrF_3 on FS	1.62	9.8	0.906	6.216	3.80
Al_2O_3 on Sapphire	1.754	15.9	0.556	5.58	3.00
ZrO_2 on FS	2.0	15.1	0.48	2.688	1.98
ZnSe on ZnSe	2.40	31.5	0.207	0.95	1.13

study of BaF_2 was not possible due to the lack of a bulk sample of BaF_2. The fit is very good for the points considered (i.e., all but the t ee inhomogeneous films), having an average error of ±12.2 percent.

Figure 27 is a plot of the roughness-corrected threshold field versus N/n^2-1. Here the fit is not quite so good at ±19.4 percent; however, the general trend is still apparent.

From both figures an experimental justification can be seen for the use of the roughness to obtain "equivalent" surfaces. From the raw data the uncorrected threshold fields for the SiO_2 films on fused silica and BK-7 were 0.892 and 0.757 MV/cm, respectively, on surfaces with 17.4 and 20.8 Å rms roughnesses. The correction for surface roughness reconciled the two figures to within 8 percent which is within the experimental accuracy.

The fact that a material is in film form usually relegates its threshold to a value below that of a bare surface of the same material. Films suffer from problems in adhesion, different mechanical and crystallographic properties from the bulk material, fusions, residual stress, and varying degrees of inhomogeneity. Table 7 is a compilation of the ratio of thin-film to bare surface

*Denotes inhomogeneous films, FS = fused silica

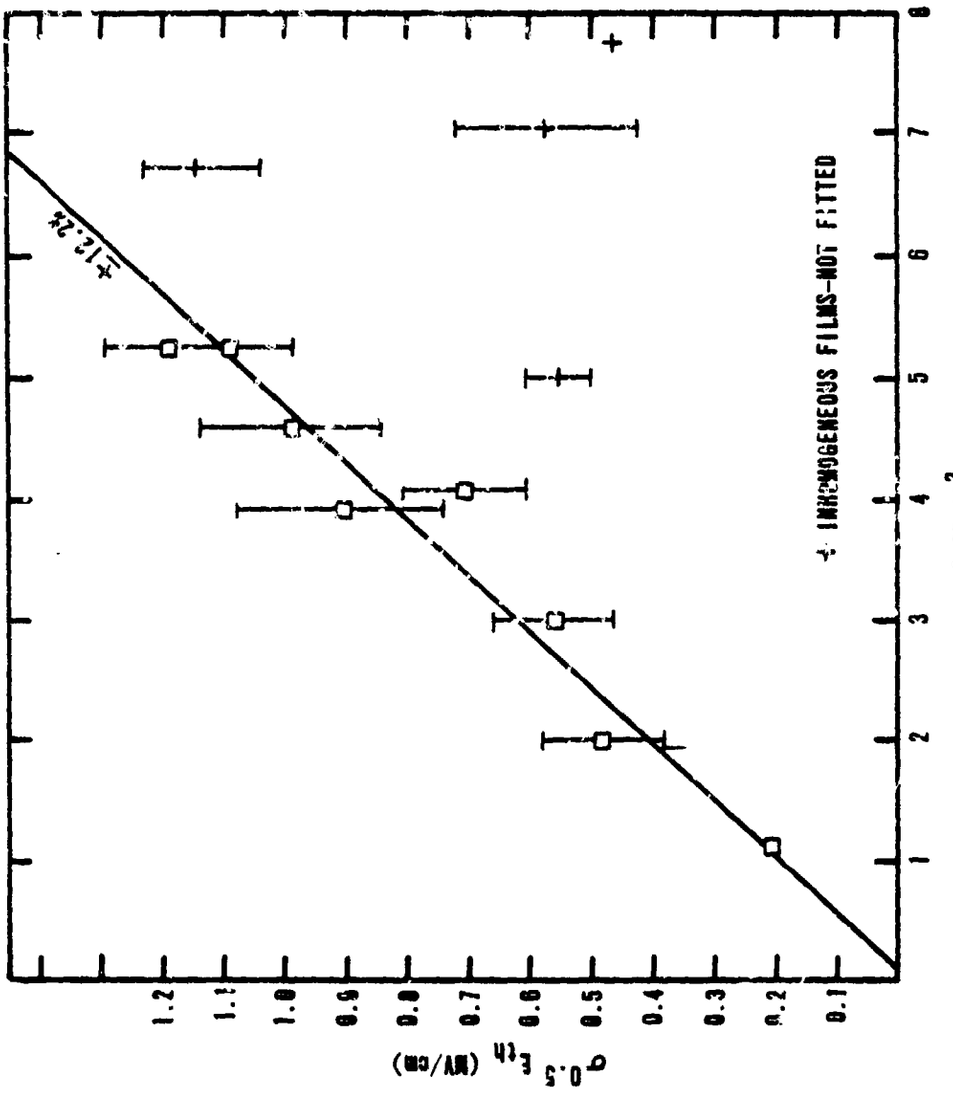

Figure 26. Roughness Corrected Threshold Field versus Predicted Field for Half-Wave Films

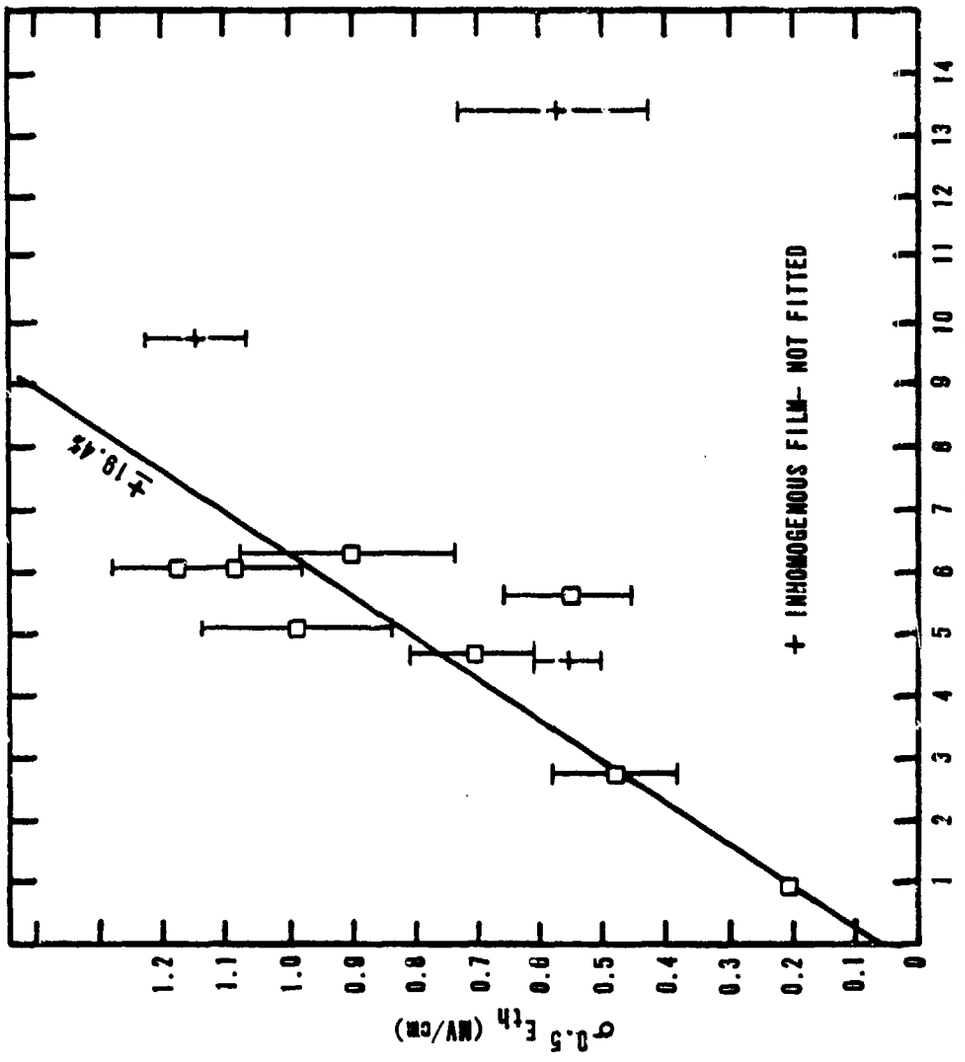

Figure 27. Roughness Corrected Threshold Field versus N/n^2-1 for Half-Wave Films

thresholds observed during this investigation. Both the thin-film and surface thresholds have been corrected for roughness to an equivalent 13.5 Å rms surface.

Table 7

RATIO OF THIN-FILM TO BARE SURFACE THRESHOLD

Material	Bare surface threshold	Film threshold	Ratio
SiO_2 on FS	2.09	0.96	0.459
LiF on FS	3.09	0.49	0.159
MgF_2 on FS	2.78	0.98	0.159
Al_2O_3 on Sapphire	1.09	0.47	0.43
ZnSe on ZnSe	0.142	0.176	1.26

The inhomogeneous films on LiF and MgF_2 exhibit the lowest ratios. The ZnSe film is interesting in that it has a higher threshold than the bare ZnSe surface. This result if not completely unexpected due to the difficulty in producing clear, unbanded, homogeneous bulk ZnSe (ref. 57). Even though one's first thought would be to never place a dielectric coating on a material since films exhibit lower thresholds than uncoated surfaces, there are good reasons for doing so. An antireflective coating can consist of a single material a quarter wavelength thick, with index n_a, placed on a surface with refractive index n_b in which $n_a = \sqrt{n_b}$. Thus SiO_2 with index 1.449 would make a quarter-wave antireflective coating for a material with index 2.1. A typical threshold for a material with n = 2.1 is about 0.7 MV/cm for a 12.5 Å rms surface finish. Thus, SiO_2 with an experimental thin-film threshold of 0.96 MV/cm could be used successfully an an antireflective coating and may in fact increase the damage threshold of the system since the maximum field will be at the air-film interface. The same comments hold, of course, for any two materials in the proper ratio, although many antireflective coatings are placed on materials with such low index that a suitable material is not available with the proper index to make a quarter-wave antireflective coating. In such cases multilayer antireflective coatings are used. To show that the weakest layer in a multilayer coating will fail when the electric field reaches E_{th}, a series of multilayer films were subjected to laser damage.

Two types of film stacks were tested: alternating even-numbered half-wave layers of ZrO_2 and SiO_2 and alternating odd-numbered half-wave layers of ZrO_2 and SiO_2. The even-numbered series consisted of 2, 6, and 10 layers with the ZrO_2 outermost. The odd-numbered series consisted of 3, 7, 11, and 15 layers; each having ZrO_2 at the inner (i.e., on the fused silica substrate) and outer layers. Table 8 is a compilation of the data gathered on these film stacks.

Table 8

THRESHOLD OF FILM STACKS

Design	Threshold Energy (mj)	Incident Field (MV/cm)	Threshold Field (MV/cm)
g(LH)	9.7	1.03	0.53
$g(LH)^3$	4.53	0.70	0.62
$g(LH)^5$	3.6	0.63	0.60
gH(LH)	3.17	0.59	0.48
$gH(LH)^3$	3.5	0.62	0.58
$gH(LH)^5$	3.78	0.64	0.61
$gH(LH)^7$	4.22	0.68	0.66

Here g denotes the substrate, H the high index film (ZrO_2) and L the low index film (SiO_2). In support of the field viewpoint of laser-induced damage it is the field in the ZrO_2 which is the most nearly constant. The threshold field is 0.58 MV/cm ±10.4 percent while the threshold energy is 4.64 mj ±49 percent and the incident optical field is 0.699 MV/cm ±21.6 percent.

In an attempt to discover the best method of film deposition, MgF_2 films were placed on fused silica substrates by radio frequency sputtering, electron beam heating, and thermal evaporation techniques. The resultant threshold fields are given in table 9.

Table 9

THRESHOLDS FOR MgF_2 FILMS VERSUS DEPOSITION TECHNIQUE

Technique	Threshold Electric Field
Electron Gun	0.737 MV/cm
Thermal Evaporation	0.797 MV/cm
R-F Sputter	0.899 MV/cm

At best the results are inconclusive. The variables involved, both those known and those unsuspected, are not well understood. The technique which works well for one material will not necessarily produce a good film with another material.

The final result to be discussed in thin films was due to a bit of serendipity. A set of thin-film samples of various materials had been prepared by electron beam heating with the angle of incidence of the coating material as the variable. When the data were analyzed they made no sense. True, there were wide variations in surface thresholds, but there was not a clear trend with angle of incidence. The surface roughnesses of the substrates were checked but proved inadequate to resolve the discrepancies. However, while checking the absorption spectra which are routinely run on each coating as a quality control measure, an absorption peak at 1.405 μm was found to vary in direct or inverse proportions with the damage threshold, depending on the film material. A check was made which indicated that the fused silica substrate had not all been supplied to the coating company by the same vendor. In fact, the absorption peak was found to correspond to OH^- absorption and was in direct proportion to the values of OH^- concentration quoted in the vendors' literature (ref. 29). The data presented in table 10 summarize the experimental results. The results are quite interesting, especially in the SiO_2 films. In that material, threshold field varies directly with OH^- concentration in the substrate. This may be because SiO_2 goes onto a substrate not fully oxidized in SiO form. The additional oxidation by the OH^- of the substrate improves the film (ref. 29). Conversely, in the MgF_2 films the additional oxidation by higher OH^- concentration (seen by the lower transmission at 1.4 μm and 2.23 μm) causes the MgF_2 to deposit at least near the surface as MgO interspersed with MgF_2 (ref. 29). The trend is suggested in Al_2O_3 films for improved films by additional oxidation and no clear relationship is evidenced by the ZrO_2 films. A definitive experiment with a controlled set of samples is obviously called for by these preliminary results.

b. Bare Surfaces

A set of 11 uncoated samples was tested. The samples ranged from crystalline materials such as LiF and sapphire to optical glasses such as BK-7 and LASF-6. A wide range of refractive index was of prime concern, and the materials tested met this goal with indexes from 1.377 to 2.485. Surface roughness was specified as best finish and ranged from 13.5 Å rms for MgF_2 to 80 for LiF. The latter was a loan from a group interested in testing bulk

Table 10

DAMAGE THRESHOLDS FOR λ/2 FILMS VERSUS OH^- CONCENTRATION IN SUBSTRATE

Material	Threshold field (MV/cm)	% T @ 1.4 μm (%)	Angle of vapor incidence (deg)
Al_2O_3	0.408	90	20.3
Al_2O_3	0.391	81	29.3
Al_2O_3	0.315	90	42.0
SiO_2	1.24	83	24.96
SiO_2	1.16	85	20.3
SiO_2	0.813	92.5	42
SiO_2	0.681	93	29.3
SiO_2	0.564	94	18.55
MgF_2	0.61	95	20.3
MgF_2	0.50	85	18.55
MgF_2	0.50	85	24.96
MgF_2	0.50	86	29.3
MgF_2	0.50	86	42.0
ZrO_2	0.198	79	20.3
ZrO_2	0.252	80	42.0
ZrO_2	0.251	85	24.96
ZrO_2	0.197	86	29.3
ZrO_2	0.292	87	18.55

properties of LiF and as such no emphasis was placed on obtaining a highly polished surface, although 50 Å rms is about the best that can be achieved on LiF (ref. 58). The surface threshold field has been corrected for roughness so that each value is equivalent to 13.5 Å rms surface. The data are presented in table 11 and figures 28 and 29. These data are plotted in figures 28 and 29. The agreement with equation (62) is generally good with the exception of two of the glasses in figure 28. The calculated fit of ±19.3 percent is near the experimental accuracy. The performance of SF-12 and SF-14 is unexplained. The fit without these points becomes ±9.5 percent. The parameters for these two glasses were calculated from data supplied by the vendor*. The roughness

*Dr. Karl H. Mader, Schott Optical Company.

Table 11

ROUGHNESS CORRECTED SURFACE DAMAGE THRESHOLDS FOR 11 DIELECTRICS

Material	Index	$\sigma^{0.5}$ Field (MV/cm)	$\frac{N}{n^2-1}$ ($10^{28}m^{-3}$)	$\frac{9.05\times10^3}{\sqrt{\sigma_s}(n^2-1)}$ (MV/cm)
LiF	1.38	3.09	13.356	7.04
MgF_2	1.377	2.78	9.705	6.72
SiO_2	1.449	2.09	6.02	5.24
BK-7	1.507	1.80	5.96	4.63
Al_2O_3	1.754	1.09	5.12	3.00
SF-12	1.63	0.75	3.99	3.48
SF-14	1.734	0.61	3.98	2.88
LASF-6	1.933	0.80	5.01	2.19
TiO_2	2.28	0.347	2.29	1.46
ZnS	2.288	0.213	1.194	1.30
ZnSe	2.485	0.142	0.874	1.04

corrected threshold electric field is plotted against N/n^2-1 in figure 29. Here the agreement suffers being only ±28.3 percent.

A final bit of interesting information can be extracted from the study by House (ref. 50). Table 12 compiles these data.

Table 12

BREAKDOWN FIELD VERSUS DISORDER

Material	Disorder (σ)	Threshold field	$\frac{9.05\times10^3}{\sqrt{\sigma}(n^2-1)}$
SiO_2 (Bulk)	2.53 Å	5.2 MV/cm[16]	5.24 MV/cm
SiO_2 (Surface)	19.8 (FECO)	1.73	1.85
SiO_2 (Surface)	42.0 (FECO)	0.987	1.27
SiO_2 (Surface)	140.0 (TIS)	0.359	0.695
SiO_2 (Surface)	773.4 (TIS)	0.322	0.296
SiO_2 (Surface)	926.5 (TIS)	0.240	0.270

This indicates a definite relationship between disorder in the material and the threshold field for laser-induced breakdown. For lack of a better term, disorder was chosen and taken as the average atomic spacing in the bulk, σ_s,

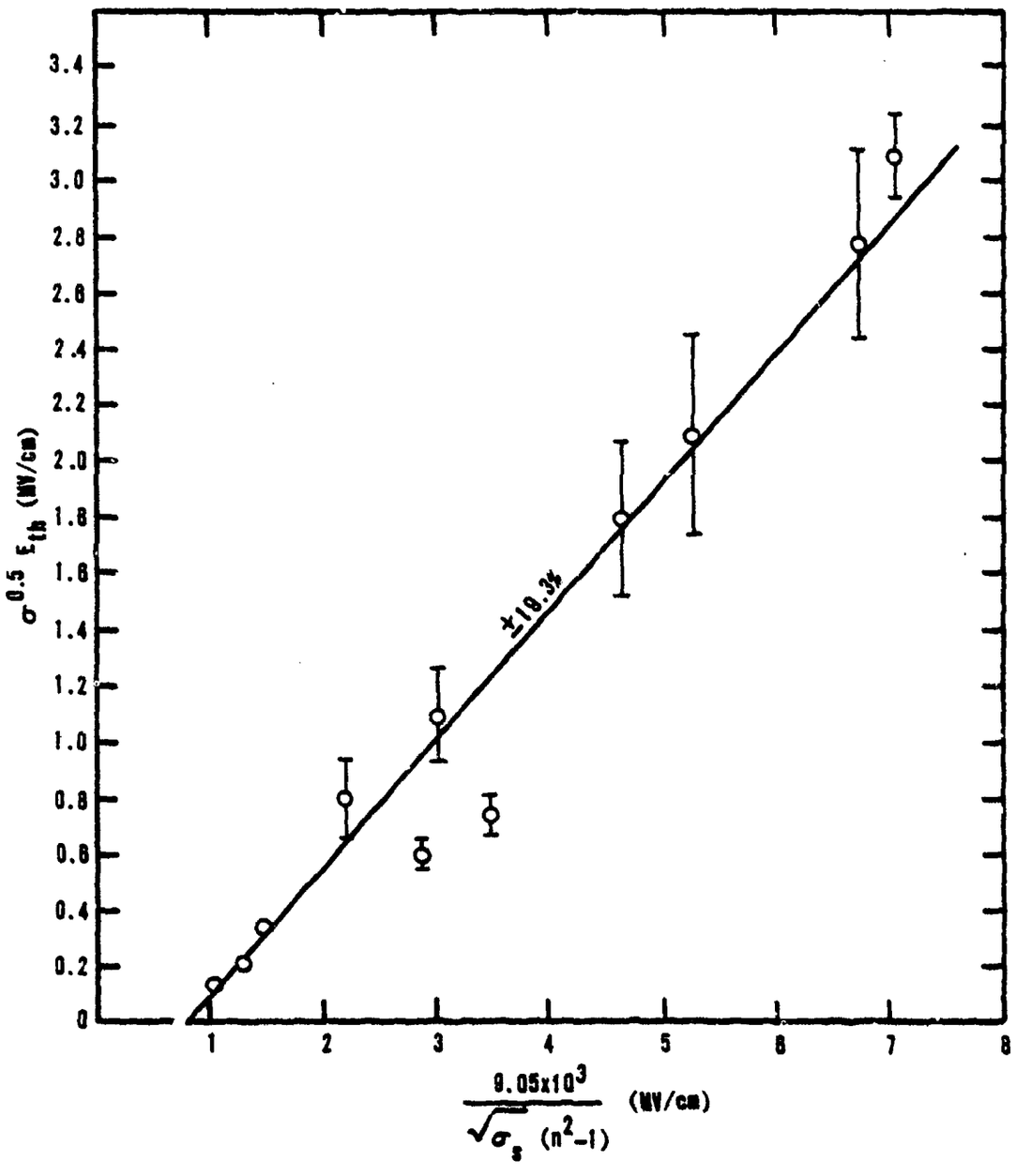

Figure 28. Roughness Corrected Threshold Field versus Predicted Field for 11 Dielectric Materials

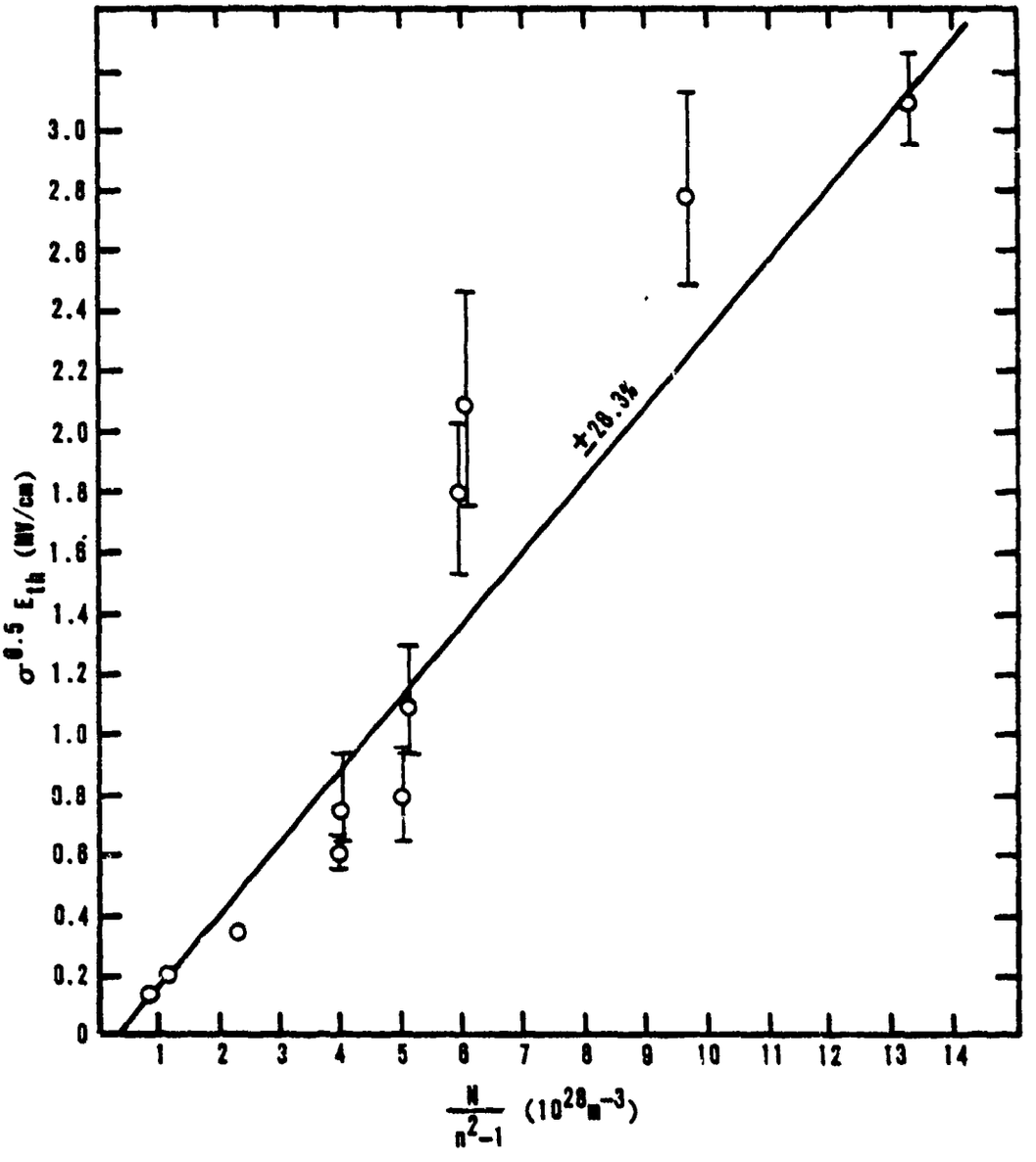

Figure 29. Roughness Corrected Surface Threshold Field versus N/n^2-1 for 11 Dielectric Materials

and the root mean square surface roughness, σ, for those samples damaged on the surface. The values of surface roughness for σ less than 100 Å rms were obtained by FECO interferometry, while those over 100 Å rms were obtained by the method of total integrated scatter. FECO is not effective above 100 Å rms according to Dr. J. Bennett of the Michelson Laboratory at the Naval Weapons Center of China Lake, California (ref. 59). The fields quoted are not corrected for roughness but are the actual measured values. The threshold fields are compared with calculations from equation (62) in the final column, using the disorder in place of σ_s which appears in equation (62). The data fit the predicted dependence to ±21.0 percent over two decades of the variable. The intriguing point, of course, is that the fit of the data is not absurdly bad. Additional calculations are presented in table 13 in which experimentally determined damage fields are used in equation (62) to predict disorders which are compared with measured (surface) or calculated (bulk) values.

Table 13

CALCULATED VERSUS MEASURED DISORDER

Material	Threshold field	Disorder	$\frac{9.05\times10^3}{\sqrt{\sigma}(n^2-1)}$	Calculated disorder
MgF_2 (Surface)	2.78 MV/cm	13.5 Å	2.75 MV/cm	13.2 Å
LiF (Surface)	1.27	80	1.19	62.1
Sapphire (Surface)	0.608	43.0	0.66	51.4
BK-7 (Surface)	1.446	21.0	1.55	24.2
BK-7 (Bulk) (ref. 16)	4.7	2.36	4.63	2.29
LASF-6 (Surface)	0.8	19.94	0.74	17.1
TiO_2 (Surface)	0.285	20.0	0.48	57.2
ZnS (Surface)	0.107	53.56	0.29	399
ZnSe (Surface)	0.116	20.15	0.39	227

Here again the disorder is the average atomic spacing in the bulk and the root mean square roughness for the surface studies. The six cases considered in table 12 and the first six in this table give good agreement between threshold field and the value predicted by using equation (62) with a fit of ±16.2 percent. The calculated disorder is obtained by inserting the measured value of E_{th}, threshold field, into

$$\sqrt{\sigma} = \frac{9.05 \times 10^3}{E_{th}(n^2-1)} \tag{84}$$

SECTION V

CONCLUSIONS

The conclusions for the bare, uncoated optical components is fairly straight-forward. To maximize the power density which can be transmitted through an optical component, one needs to maximize the quantity $\left[\sqrt{\sigma_s}\ (n^2-1)\right]^{-1}$. Other parameters are, of course important but to a lesser degree. For example, linear absorption is generally higher in high index materials (ref. 31). This contention would go a long way toward explaining why the three high index materials (TiO_2, 2.28; ZnS, 2.288; ZnSe, 2.485) showed such poor performance in relation to the threshold fields predicted by equation (62). If laser-induced damage is, in the end, a process of thermal distortion, melting, or crazing, then any mechanism which more effectively couples the laser energy into the lattice affords a means for lowering the damage threshold. One must then conclude that an increase in linear absorption will result in a decrease in damage threshold. This contention is borne out by evidence collected during the course of this study. Several samples of two glass types were supplied with as nearly equal surface finish as possible. The glass types were Owens-Illinois ED-4 and ED-2. The only difference in the two glasses is that ED-4 is undoped and ED-2 is a Nd^{+3} doped laser glass. The refractive indexes are both the same and the number densities are essentially the same. The physical difference is that the doped ED-2 exhibits an increased linear absorption at the laser wavelength of 1.06 μm. The matched pairs of ED-2 and ED-4 were finished in a variety of ways utilizing different conventional polishing and ion polishing techniques. In each matched set the doped ED-2, with a linear absorption coefficient of only 0.001 to 0.002 cm^{-1} (ref. 60), damaged at a lower threshold than did the undoped ED-4 which had lower absorption. Facilities were not available during the course of this study to measure absorption coefficients as low as 0.002 cm^{-1}. The three high index materials in table 13, however, were measured for transmission using a Carey 14 Spectrophotometer and in two of the substances high absorption was found. The TiO_2 had a transmission of 71.2 percent compared to the 71.9 percent expected from a nonabsorbing sample with an index of 2.28. The ZnS had a transmission 46.5 percent compared to the expected value of 71.7 percent and the ZnSe had 50.5 percent compared to the 67 percent for a nonabsorbing material with an index of 2.485. From table 13 one can

compare the ratios of the measured threshold fields to the field predicted by equation (62). For the three materials they are: TiO_2, 0.59; ZnS, 0.37; ZnSe, 0.30. The apparent absorption losses for the three are 0.7 percent, 25.2 percent and 16.5 percent, respectively, although the accuracy of the determination does not allow for much credence in the 0.7 percent value. Thus, the apparent trend is that increasing absorption results in a lower ratio of the observed threshold compared to that predicted by equation (62). That ZnSe does not perform optimally can be inferred from the fact that the ZnSe film exhibited a higher threshold than the uncoated ZnSe surface. Although the study of laser-induced damage is not a sufficiently detailed science to allow direct comparison of results between two separate investigations, the work of DeShazer et al., (ref. 11) suggests strongly that both TiO_2 and ZnS may be stronger in quarter wave-film than the uncoated materials. Intrinsic absorption is not the only mechanism which would explain the anomalously low results for the high index materials. High index materials tend to be mechanically soft. They are generally hard to polish in that the polishing compound scratches and pits the surface. The polishing compound can also easily become imbedded in the material. If a relatively large amount of polishing compound becomes imbedded in the surface, a simple heat absorption mechanism at the particulate inclusions could lower the threshold field.

Aside from the high index materials the equation

$$E_{th} = \frac{9.05 \times 10^3}{\sqrt{\sigma}\ (n^2 - 1)} \tag{85}$$

adequately describes the observed electric field threshold for laser-induced damage to various optical surfaces. It also appears to be predictive of the electric field threshold for laser-induced bulk damage to transparent dielectrics. Before this statement can be made conclusive, a large number of other materials needs to be tested against the predicted behavior.

Finally, consider the threshold fields for the bulk of dielectric materials. From figures 21 and 23, it is apparent that the relative values for bulk threshold fields follows the dependence suggested by equation (62). It is also clear that the damage processes are essentially the same at 30 psec and 10 nsec. The difference in the absolute values of the field between 15 psec and 10 nsec can be explained by considerations of thermal heating of the plasma and lattice.

Thus, the proposed model explains the essential variations of threshold field as a function of material and surface properties (both on the surface and in the bulk) and as a function of laser pulse length.

The general conclusion for thin films is the same as that for bare surfaces. As long as a thin film accurately models the bulk material, equation (62) can be used to predict relative electric field thresholds between different film materials. The major problem involved in attempting to predict thin-film thresholds is the large number of variables involved in the coating process. Residual gas pressures in coating chambers, temperature of the substrate, deposition rate, deposition technique, and condition of the substrate are all important considerations in thin-film coatings. The deposition of thin films appears to be as much an art as it is a science.

The major specific conclusion about thin films is that the roughness of the substrate is just as important in determining thin-film thresholds as bare surface thresholds. No longer can surface or thin-film thresholds be given proper credence unless the surface roughness is also stated.

Specific material properties, such as free radical (OH^-) concentration, has been shown to be important in some thin-film systems. A factor of 2.2 in electric-field threshold obtained by apparently varying only the type of fused silica used as substrate is most important in thin-film technology.

The determining factor in laser-induced damage is the optical electric field. Multilayer thin-film systems can be increased in damage resistance by utilizing this fact. Optical systems can be designed to minimize electric-field amplitudes at weak points in the systems.

The proposed model does not deviate strongly from the observed behavior. Electron avalanche was not considered nor is it apparently necessary to describe laser-induced damage of optical components. Direct local-field generation of free electrons can account for the observed dependence of threshold fields on refractive index, number density, and surface roughness. It is seen that no separate mechanism need be postulated for surface versus bulk damage since the threshold fields for both are shown to obey the same descriptive relationship.

In conclusion, a simple model of laser-induced damage has led to a predictive formula for threshold electric field which holds for a wide variety of materials in bulk, bare surface, and thin-film form.

REFERENCES

1. Glass, A.J., and Guenther, A.H., Eds., Damage in Laser Glass, ASTM Special Technical Publication 469, 1969.

2. Glass, A.J., and Guenther, A.H., Eds., Damage in Laser Materials, NBS Special Publication 341, 1970.

3. Glass, A.J., and Guenther, A.H., Eds., Damage in Laser Materials: 1971, NBS Special Publication 356, 1971.

4. Glass, A.J., and Guenther, A.H., Eds., Laser Induced Damage in Optical Materials: 1972, NBS Special Publication 372, 1972.

5. Glass, A.J., and Guenther, A.H., Eds., Laser Induced Damage in Optical Materials: 1973, NBS Special Publication 387, 1973.

6. Glass, A.J., and Guenther, A.H., Eds., Laser Induced Damage in Optical Materials: 1974, NBS Special Publication 414, 1974.

7. Glass, A.J., and Guenther, A.H., Eds., Laser Induced Damage in Optical Materials: 1975, To be Published.

8. Crisp, M.D., Boling, N.L., and Dube', G., Applied Physics Letters, 21, 364, 1972.

9. Giuliano, Concetto, R., and Hess, L.D., NBS Special Publication 341, p. 76, 1970.

10. Boling, N.L., and Dube', G., NBS Special Publication 372, p. 40, 1972.

11. DeShazer, Larry G., Leung, Kang M., Newnam, Brian E., and Alyassini, Nabil, Study of Laser-Irradiated Thin Films, University of Southern California, Los Angeles, California, 1973.

12. Newnam, Brian E and DeShazer, L.G., NBS Special Publication 372, p.123 1972.

13. Turner, A. Francis, NBS Special Publication 356, p. 119, 1971.

14. Austin, R. Russel, Michaud, Raymond C., Guenter, Arthur H., Putman, Joseph M., and Harniman, Richard, NBS Special Publication 372, p. 135, 1972.

15. Boling, N.L., Dube', G., and Crisp, M.D., NBS Special Publication 387, p. 69, 1973.

16. Fradin, David W., Laser Induced Damage in Solids, Harvard University, Cambridge, Mass., 1973.

17. Fradin, D.W., Yablonovitch, Eli, and Bass, Michael, Applied Optics, 12, No. 4, 700, April 1973.

18. Bloembergen, N., Applied Optics, 12, No. 4, 661, April 1973.

19. Fradin, David W., and Bass, Michael, NBS Special Publication 387, p. 225, 1973.

20. Bliss, E.S., and Milam, D., NBS Special Publication 372, p. 108, 1972.

21. Goodman, J.W., Introduction to Fourier Optics, McGraw-Hill, New York, 145, 1968.

22. Edwards, David F., She, D.Y., Draggoo, V.G., Broberg, T.W., and McAllister, G.L., NBS Special Publication 356, p. 24, 1971.

23. Boling, N.L., and Dube', G., Damage Threshold Studies of Glass Laser Materials, Final Technical Report, Owens-Illinois, Inc., Toledo, Ohio, 1974.

24. Owyoung, A., NBS Special Publication 387, p. 11, 1973.

25. Siegman, A.E., An Introduction to Lasers and Masers, McGraw-Hill, New York, 1971.

26. Longhurst, R.S., Geometrical and Physical Optics, Jarrold and Sons, Ltd., Norwich, England, 1967.

27. Holland, L., The Properties of Glass Surfaces, Chapman and Hall, London, 1966.

28. Porteus, J.O., J. Opt. Soc. of America, 53, No. 12, 1394, Dec. 1963.

29. Austin, R. Russel, Perkin-Elmer Optical Corp. Private Communication.

30. Loomis, John S., Computing the Optical Properties of Multilayer Coatings, AFWL-TR-75-202, Air Force Weapons Laboratory, Kirtland AFB, NM, 1975.

31. Guenther, Arthur H., Air Force Weapons Laboratory, Kirtland AFB, New Mexico, Private Communication.

32. von Hippel, A., Journal of Applied Physics, 8, 815, Dec. 1937.

33. Seitz, Frederick, Physical Review, 76, No. 9, 1376, Nov. 1949.

34. Frolich, H., Proc. Roy. Soc., 160, 230, 1937.

35. Birks, J.B., and Hart, J., Eds., in Progress in Dielectrics, III (Stratton, R., Frolich and Paranjape) John Wiley and Sons, Inc., New York, 235, 1961.

36. Pines, D., Phys. Rev., 92, 626, 1953.

37. Raether, Heinz, Electron Avalanches and Breakdown in Gases, Butterworths, Washington, 1964.

38. Meek, J.M., and Craggs, J.D., Electrical Breakdown of Gases, Oxford at the Clarendon Press, 62, 1953.

39. Kittel, Charles, Introduction to Solid State Physics, John Wiley and Sons, New York, 1966.

40. Bloembergen, Nicolaas, IEEE Journal of Quantum Electronics, QE-10, No. 3, 375, Mar 1974.

41. Bass, Michael, and Barrett, Harrison, H., Applied Optics, 12, No. 4, 690, April 1973.

42. Sparks, M., To Be Published in 1975 Damage Symposium.

43. David, C., Avizonis, P.V., Weichel, H., Bruce, C., and Pyatt, K.D., IEEE Journal of Quantum Electronics, QE-2, No. 9, 493, Sep 1966.

44. Guenther, A.H., and Pendleton, W.K., Laser Interaction and Related Plasma Phenomena, Schwarz, H. and Hora, H. Eds., Plenum Publishing Co., New York, 97, 1972.

45. Alyassini, Nabil, and Parks, Joel H., to be published in 1975 Damage Symposium.

46. Milam, D., Bradbury, R.A., Ricard, R.H., and Bass, M., to be published in 1975 Damage Symposium

47. Yablonovitch, Eli, and Bloembergen, N., Physical Review Letters, 29, No. 14, 907, 2 Oct 1972.

48. Jackson, John David, Classical Electrodynamics, John Wiley and Sons, Inc., New York, 119, 1963.

49. Wunsch, Donald C., Doctoral Dissertation submitted to New Mexico State University, Las Cruces, New Mexico, 64, 1969.

50. House, R.A., Doctoral Dissertation to be submitted to Air Force Institute of Technology, Wright-Patterson AFB, Ohio, 1975.

51. Johnston, Tudor Wyatt, and Dawson, John M., The Physics of Fluids, 16, No. 5, 722, May 1973.

52. Fauquignon, C., and Floux, F., The Physics of Fluids, 13, No. 2., 386, Feb 1970.

53. Boland, B.C., Irons, F.E., and McWhirter, R.W.P., A Spectroscopic Study of the Plasma Generated by a Laser from Polyethylene, U.K. Atomic Energy Authority, Abingdon Berkshire, 1968.

54. Smith, Walter Lee, To be published in 1975 Damage Symposium.

55. DeShazer, L.G., Newnam, B.E., and Leung, K.M., NBS Special Publication 387, 114, 1973.

56. Putman, Joseph, Master Thesis Submitted to Air Force Institute of Technology, Wright-Patterson AFB, Ohio, 1972.

57. Boling, N.L., Ringlion, J.A., and Dube', G., NBS Special Publication 414, p. 119, 1974.

58. Braunstein, M., Laser Window Surface Finishing and Coating Technology, ARPA Contract F19628-73-C-0234, 1973.

59. Bennett, J.M., Naval Weapons Center, China Lake, Calif., Private Communication.

60. Boling, N.L., Owens-Illinois Corp., Toledo, Ohio, Private Communication.